ABSTRACT

Title of Document:	SEQUENCE MODELING OF RAFT POLYMERIZATIONS WITH THE METHOD OF MOMENTS
	Amin Zargar, Master of Science in Chemical and Biomolecular Engineering, May 2008
Directed By:	Dr. Francis Joseph Schork, Chair of Chemical and Biomolecular Engineering, Department of Chemical and Biomolecular Engineering

Attempts to model the sequence structure of copolymers consisted of probabilistic functions that were incomplete and inaccurate. A novel technique to track sequence parameters is developed that determines not only copolymer composition, but sequence distribution as well. RAFT polymerizations are simulated with two independent and concurrent models to track MWD, conversion, copolymer composition, and sequence characteristics. Batch polymerizations are simulated with varying reactor conditions as a proof-of-concept to illustrate the power of the sequence model to track the composition of the polymer. Series of CSTR and PFR reactors with varying reactor conditions are then presented as applications to iteratively fine-tune copolymers with predetermined sequence and compositional structure.

SEQUENCE MODELING OF RAFT POLYMERIZATIONS WITH METHOD OF MOMENTS

By

Amin Zargar

Thesis submitted to the Faculty of the Graduate School of the
University of Maryland, College Park, in partial fulfillment
of the requirements for the degree of
Master of Science in
Chemical and Biomolecular
Engineering
2008

Advisory Committee:
Professor F. Joseph Schork, Chair
Professor Sheryl Ehrman
Professor Srinivasa Raghavan

Dedication

This work is dedicated to my family: my parents, who never wavered in their support, my brothers, who always looked out for me, and my little sister, who always believed in me.

Acknowledgements

I would like to thank my advisor, Dr. Joseph Schork, for his guidance, knowledge, and warmth. His constant encouragement was as needed as his ideas and suggestions. The path we took over this past year was bumpy, but he always helped me refocus as I often "lost the forest for the trees."

I would also like to acknowledge Dr. Clifford Henderson from my alma mater of the Georgia Institute of Technology. I would not be where I am today without him, and more than all of his considerable aid, the example he has set has provided me a goal which I continually strive to achieve.

My transition to the University of Maryland mid-year would have been much more difficult without the help and kindness of Kathleen Lopresti. Throughout my time at Maryland, she constantly helped me, laughed with me, and lent a sympathetic ear. The faculty in the chemical engineering department has been wonderfully receptive and friendly, and beyond helping me realize my immediate goals, they have illuminated my long-term goals. On a personal level, I would like to thank my friends for providing perspective when I would get caught up with the seemingly never-ending grind involved in producing this work.

Table of Contents

List of Figures

Nomenclature

A = Monomer of A

B = Monomer of B

T = RAFT agent

R* = Radical from Initiator or Leaving agent

P = Polymer chain with terminal unit A

Q = Polymer chain with terminal unit B

TP = Polymer chain with terminal unit A bound to RAFT agent

TQ = Polymer chain with terminal unit B bound to RAFT agent

L^* = End sequence of A

O^* = End sequence of B

L = Internal sequence of A

O = Internal sequence of B

f = Efficiency of initiator

I = Initiator

M = Dead Chain

n = Specific number of monomers in polymer chain

r = Total number of monomers in polymer chain

s = Total number of monomers in sequence chain

g = Specific Number of monomers in sequence chain

Chapter 1: Introduction and Background

Background on Controlled Radical Polymerization

Conventional radical polymerization (RP) accounts for 50% of the production of polymers due to its capability to produce high MW structures in a head to tail format [1]. However, radical polymerization cannot produce polymers with a controlled architecture. The average life of a polymerizing free radical is 1 second, which constitutes 1000 acts of propagation with a frequency of 1 millisecond. Therefore, the life of a propagating chain is too short for any meaningful manipulation of reactor conditions in a conventional free radical polymerization. Controlled living polymerization has shown the potential to revolutionize the polymer science field with NMP (nitroxide mediated polymerization), ATRP (atom transfer free radical polymerization), and RAFT (reversible addition-fragmentation chain transfer polymerization), producing controlled, uniform polymers. [2].

Michael Szwarc's discovery of "living" anionic polymerization allowed much greater control of polymerization[3]. Due to the severe restrictions in reactor conditions and the limited number of compatible monomers this truly "living" polymerization did not lead to widespread industrial use. Hence, the extension to living radical chains was much more promising [4].

A chain is in the activated state for the same amount of time in conventional RP, as in CRP, but the whole propagation process now takes much more slowly, allowing ample time to manipulate the polymerizing environment, and thus, the molecular architecture. The lifetime of a growing chain goes from 1 second in RP, to

over an hour in CRP [1]. A chain spends most of its lifetime in the dormant state, with a ratio of living to dead less than 10^{-5} with the transient lifetime of an activated polymer chain between .1-10 millisecond [5]. Polymerization is obviously much slower in CRP, and while RP consists almost exclusively of dead polymers, less than 10% of CRP consists of dead polymers.

All controlled radical polymerizations consist of initiation, propagation, dormancy, and termination [1]. In controlled free radical polymerization (CRP), the dormant polymer chains are activated by chemical stimuli, photochemical effect, or a thermal effect [5]. The slow propagation is caused by "living" polymers being essentially trapped in an activation/deactivation cycle with the retarding agent (i.e. RAFT, ATRP, and NMP). CRP allows the propagating radical to become trapped in this process. Ideally, the dormant chains cannot terminate, but can only deactivate. A dynamic equilibrium between dormant and propagating chains exists in all CRP whether by an activation/deactivation cycle as in NMP or ATRP, or degenerative transfer process as in RAFT[1].

The first form of CRP discovered was Nitroxide-Mediated Polymerization (NMP) in 1985 by Solomon et al. [6]. However, it was the work of Georges et al. [7] in 1993, that the world realized the possibilities of this new free-radical polymerization [8]. This was the beginning of CRP where control in NMP is accomplished between dormant alkoxyamines and propagating radicals as shown in Scheme 1.

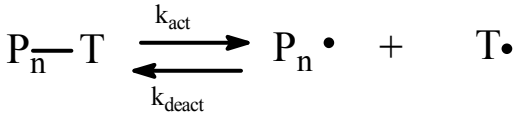

Scheme 1: Reversible termination[8]

This exchange between active and dormant states is known as reversible termination. As in all CRP, the lifetime of the propagating chain in each cycle is so short that a few monomers are added each cycle, hence the analogy of a "living" polymer.

The second form of CRP discovered was Atom Transfer Radical Polymerization (ATRP) in 1995 by Matyjaszewski et al. [9-11], and Sawamoto et al [12-14]who utilized different metal complexes. ATRP also belongs to the reversible termination class of living polymerizations, whose mechanism can also be described by Mechanism 1[8]. ATRP consists of a metal that can increase its oxidation state and coordination sphere, a complexing ligand, and a counterion that can bond (covalently or ionically) to the metal sphere. Metal complexes of copper and ruthenium are the most common, but nickel, palladium and iron have also been used [15-17]. When the bond is broken, the oxidation state of the metal may increase, and the radical becomes trapped in a bond with it.

The most recent form of CRP, and the method that used in this work is RAFT. In 1998, Rizzardo et al.[18-20] published this new polymerization technique involving Reversible Addition-Fragmentation chain Transfer that produced polymers with low polydispersity. The mechanism is detailed in Scheme 2[8].

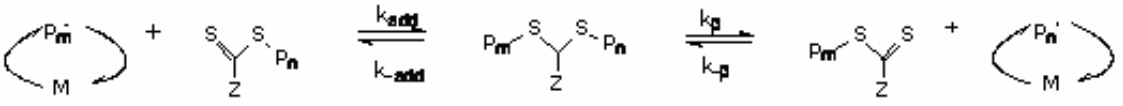

Scheme 2: Mechanism of RAFT transfer[8]

The RAFT process uses a dithioester to deactivate the radical, and induce dormancy. [21] The macro-radical intermediate that is shown in Scheme 2 is unstable and undergoes reversible β-scission in either direction [22]. As detailed in the scheme, RAFT transfer is where a dormant chain T—P reacts with a living chain P^1 to produce a dormant chain T—P^1 with a living chain P which proceeds via the short-lived intermediate state.

In RAFT transfer, the concentration of transfer agents is much higher than initiator, and fast exchange is required to maintain a controlled MW, low polydispersity, and chain architecture [1]. When two radical chains do terminate together, there is a further accumulation of T, which results in even fewer free radicals. Consequently, the concentration of radical chains and termination progressively decrease with time [1]. Since propagation is 1^{st} order and bimolecular termination is 2^{nd} order with respect to radical concentration, the "living" character of CRP lies in reducing the amount of radical concentration through deactivation to greatly decrease bimolecular termination. The creation of well-defined macromolecular structures with defined block, comb, and star copolymers and low polydispersity requires fast initiation with slow propagation [1] .

Introduction to the Sequence model

With the rate constants of all the reactions, and details of experimental conditions such as concentration of reactants (and temperature), it is possible to simulate the whole process of a CRP run and predict the characteristics of the polymer with accuracy, in principle[5]. The method of population balances to produce moment equations for mathematical modeling has been performed by others,

notably Wang et al.[23] to reduce composition drift where they used the Mayo-Lewis equation to determine copolymer composition[24].

These models have all determined molecular weight distribution (MWD), conversion, and copolymer composition. However, population balances have not been used to determine sequence distributions in copolymers. The development of probabilistic models has been the only method of quantifying sequence structure. [25]. The probabilistic functions developed in Ray could be expanded for RAFT copolymers to give a probabilistic representation of each state (dormant, propagating with monomer A, monomer B, etc.) at every degree of polymerization[25]. This provides a nebulous portrayal of the overall polymer and is convenient only with constant probabilities (i.e. monomer composition does not decrease during polymerization). Also, these probabilistic models must be specially done for each sequences as well as MWD, conversion, and other parameters. These probabilistic models can provide only averages, while population balances can be taken to higher moments to provide much more information about the state of the copolymer.

With CRP moving into the commercial scale, gradient copolymers in addition to block copolymers and uniform composition copolymers have been synthesized for their unique characteristics. Gradient copolymers possess properties of both block copolymer and copolymers with uniform composition average. With the advances in CRP enabling unique sequence synthesis, further study is being performed to understand the effects of sequence distribution on polymer properties[26, 27].

The model developed in this work consists of two independent subdivisions: the “chain” model determines MWD, conversion and copolymer composition, while

the novel “sequence” model determines the distribution of sequences. The chain model actually simulates the changes in the copolymer while the sequence model merely tracks sequence structure.

In Chapter 2, the chain and sequence models are developed from reactions to mass balances. With mathematical manipulations, the moment equations are derived to complete the chain and sequence models. These moment equations were the model that was simulated using MATLAB©, with kinetic parameters taken from the literature as the rate constants. Batch polymerizations are simulated in Chapter 3 to illustrate the power of the sequence model to determine sequence distributions. This composition drift produced different quantifiable levels of gradient copolymers. Shot-polymerizations are then simulated to fine-tune copolymers by varying reactor conditions to produce a copolymer with different sequence and compositional segments, which is a common technique[28]. With the sequence model outputs of active and inactive sequences, geometric inferences were made to provide a cartoon snapshot of a ‘typical’ co polymer.

Chapter 4 simulates CSTR and PFR reactors standalone and in series. CSTR reactors produce polymer segments with no composition drift which is evident from various parameters, notably from the equivalence of active and inactive sequences from the sequence model. However, shorter chains are produced, with less conversion, and higher polydispersity. PFR reactors produce longer chains, with higher conversion, and lower polydispersity, but there is composition drifty. The combination of these various configurations allows control of molecular architecture. The combination of these two reactors allows their strengths to complement to

iteratively form copolymers with lower polydispersity, constant copolymer compositions, and a set sequence structure. Chapter 5 will summarize the work presented in the thesis as well as comment on future applications.

Chapter 2: Development of Models

In this chapter, a mathematical model will be developed based on the method of moments to characterize polymers in controlled free radical polymerization. The overall structure of the simulation is split into two independent models run concurrently. One sub-group, hereafter referred to as the "chain model," determines the molecular weight properties of the polymer (e.g. NACL, WACL, polydispersity, etc.). Using population balances, the chain model will determine these properties using moment equations, as has been done in other works [23]. The other sub-group, hereafter referred to as the "sequence model," determines the compositional properties of the polymer (e.g. copolymer composition, ending sequences, etc.). The sequence model is wholly original, and is the first model to use moment equations to not only determine copolymer composition, but also a sequence distribution. Together, these two models provide a description of the molecular architecture of the copolymer.

Before the models are introduced, a declaration of the simplifying assumptions that were made should be stated. These simplifications do not detract from the primarily goal of this work: to illustrate the power of the sequence model for compositional analysis, and to demonstrate the potential to design the molecular architecture in controlled radical polymerization by the use of continuous reactor configurations. The premise of the sequence model can be extended to account for these assumptions, but this work does not require them. For the sake of simplicity, the penultimate effect is ignored (only the terminal unit affects the kinetic rate constant)[23]. Correspondingly, despite the effect the degree of polymerization has on

the propagation, transfer, and termination rate constants, as well as reactivity ratios[2, 29-31], it is also neglected. While in some processes, the macro-radical intermediate formed during RAFT transfer, (P-T-P), may be stable enough to retard polymerization[31-33], initiate new chains [1], and terminate[34, 35], with a maximum manipulated lifetime of 1 second [36], it has not been considered in our model. Lastly, branching has also been disregarded.

Reactions of the Chain Model

The "chain model" will be presented first. There are five stages of RAFT polymerization: initiation, RAFT initiation, RAFT transfer, propagation, and termination. The reactions in the first stage, initiation are shown in Figure 1.

Initiation

(1) $I \xrightarrow{kd,f} 2\,R^*$ (2) $R^* + A \xrightarrow{ki1} P_1$ (3) $R^* + B \xrightarrow{ki2} Q_1$

Figure 1: Initiation of Chain model

The initiator, I, breaks down with an efficiency, f, to form two radical species, R*. These radical species can react with an 'A' or 'B' monomer, to initiate a polymer chain. A 'P' chain is a polymer that has an 'A' monomer as its terminal unit; likewise, a 'Q' chain is a polymer that has a 'B' monomer as its terminal unit. The subscript represents the degree of polymerization. As has been stated, to obtain a monodisperse polymerization, a fast initiation step is highly desirable.

Following initiation of the polymer chains, the next step in the living cycle of the polymer can be RAFT transfer initiation, RAFT transfer, or propagation. These three steps will be presented in that order for ease of comprehension. The reactions in RAFT initiation are presented in Figure 2.

RAFT Transfer Initiation

$$(4)\quad T + P_n \underset{kr11}{\overset{kr12}{\leftrightarrow}} R^* + TP_n \qquad (5)\quad T + Q_n \underset{kr21}{\overset{kr22}{\leftrightarrow}} R^* + TQ_n$$

Figure 2: Raft transfer initiation reactions of chain model

The subscript 'n' signifies any number chain length. With high ratio of RAFT agent, T, to initiator, most polymer chains will be dormant at any given time. The leaving group of the RAFT agent is assumed to have the same reactivity as the radical formed from the initiator [22]. These leaving groups are capable of initiating a new polymer chains, thereby aiding in the goal of a fast initiation step.

A high ratio of transfer to propagation is the most important requirement to obtain low polydispersity [5]. Figure 3 illustrates the reactions involved in RAFT transfer between two polymers.

RAFT Transfer

$$(6)\quad P_n + TQ_r \underset{kraft32}{\overset{kraft31}{\leftrightarrow}} TP_n + Q_r \qquad (7)\quad Q_r + TQ_n \underset{kraft42}{\overset{kraft41}{\leftrightarrow}} TQ_r + Q_n$$

$$(8)\quad Q_n + TP_r \underset{kraft62}{\overset{kraft61}{\leftrightarrow}} TQ_n + P_r \qquad (9)\quad P_r + TP_n \underset{kraft52}{\overset{kraft51}{\leftrightarrow}} TP_r + P_n$$

Figure 3: Raft transfer reactions of chain model

The subscript, 'r', signifies all degrees of polymerization: a polymer chain of a certain length 'n' can react with a polymer chain of any length, 'r'. In RAFT transfer, a living polymer reacts with a dormant polymer; the living polymer becomes dormant and the dormant polymer becomes living. This is known as reversible chain transfer, and it is essential for monodispersity for it ensures all of the chains propagate at the same rate, statistically. Reactions 6 and 8 are identical: they have been artificially

separated for ease of comprehension as in Reaction 6 the 'P' chain is the polymer of interest while in Reaction 8 the 'Q' chain is the polymer of interest.

The reactions in the propagation step are shown in Figure 4.

Propagation

(10) $P_n + A \xrightarrow{kp1} P_{n+1}$ (11) $P_n + B \xrightarrow{kp2} Q_{n+1}$

(12) $Q_n + A \xrightarrow{kp3} P_{n+1}$ (13) $Q_n + B \xrightarrow{kp4} Q_{n+1}$

(14) $P_{n-1} + A \xrightarrow{kp5} P_n$ (15) $P_{n-1} + B \xrightarrow{kp6} Q_n$

(16) $Q_{n-1} + A \xrightarrow{kp7} P_n$ (17) $Q_{n-1} + B \xrightarrow{kp8} Q_n$

Figure 4: Propogation reactions of chain model

Reactions 10-13 illustrate the polymer of the length of interest, 'n', propagating with a monomer to one monomeric unit above the length of interest. Reactions 14-17 show the formation of the polymer of the length of interest, 'n', from a polymer with a length of interest one monomeric unit below.

The final step in the life cycle of a polymer is termination. The termination reactions are shown in Figure 5.

Termination

(18) $P_n + Q_r \xrightarrow{ktc1} M_{(r+n)}$ (19) $P_n + Q_r \xrightarrow{ktd1} M_n + M_r$

(20) $P_n + P_r \xrightarrow{ktc2} M_{(n+r)}$ (21) $P_n + P_r \xrightarrow{ktd2} M_n + M_r$

(22) $Q_n + Q_r \xrightarrow{ktc3} M_{(n+r)}$ (23) $Q_n + Q_r \xrightarrow{ktd3} M_n + M_r$

(24) $Q_n + P_r \xrightarrow{ktc4} M_{(r+n)}$ (25) $Q_n + P_r \xrightarrow{ktd4} M_n + M_r$

Figure 5: Termination reactions of chain model

'M' represents a dead chain. The termination reactions that are shown occur when two polymer chains react. A termination by combination reaction occurs when the two polymer chains react to form one dead chain that is a combination of the length of the two polymer chains as in Reactions 18, 20, 22, and 24. The other kind of termination reaction is by disproportionation, when the two polymer chains react to form two dead chains that are the same length as the two living chains. Since most chains are dormant at any given time, and since both mechanisms of termination are bimolecular, the rate of termination is severely suppressed, relative to free radical polymerization. A termination reaction between a polymer chain and a radical formed from initiator or RAFT leaving group has been ignored as in other simulations[22, 23].

Reactions of the Sequence Model

The sequence model is set up to track the distribution of lengths of sequences of A and B monomers, for both active and inactive sequences. An active sequence can be polymerized further, while a inactive sequence cannot. Essentially, an active sequence is a sequence at the end of a polymer, while an inactive sequence is an internal sequence, which provides revealing information about the geometry of the polymer. However, end sequences on dead chains are inactive, and are hence modeled as internal. While this is technically incorrect, since the ratio of dead to living sequences is very low, modeling end sequences of dead chains as internal does not have a significant effect on the accuracy of the geometric model.

The sequence model is run concurrently with the chain model, but they are completely independent. As with the classic chain model, the sequence model has

five stages in its life cycle: initiation, RAFT initiation, RAFT transfer, propagation, and termination. This mimicking is intentional, as the sequence model can only be accurate if it simulates the same polymerization process, but merely tracks different parameters. Only the active sequences have these five stages. Since branching has not been considered, inactive sequences only have a formation step through cross-propagation and termination. Figure 6 shows the reactions involved in the initiation of active sequences.

Initiation

(26) $I \xrightarrow{kd,f} 2\,R^*$ (27) $R^* + A \xrightarrow{ki1} L_1^*$ (28) $R^* + A \xrightarrow{ki2} O_1^*$

Figure 6: Initiation reactions of sequence model

As in the initiation of the classic model, a free radical and a monomer react. L* signifies a sequence of monomer 'A' at the end of polymer, while O* is a sequence of monomer 'A' at the end of polymer. The subscript represents the number of monomers in that sequence.

These end sequences can also become dormant when an active sequence reacts with a RAFT agent. These reactions are shown in Figure 7.

RAFT Transfer Initiation

(29) $L_g^* + T \underset{kr11}{\overset{kr12}{\leftrightarrow}} TL^*_g + R^*$ (30) $O_g^* + T \underset{kr21}{\overset{kr22}{\leftrightarrow}} TO^*_g + R^*$

Figure 7: RAFT transfer initiation reactions of sequence model

In Reactions 29 and 30, the subscript g represents any end sequence of a specific length. As we stated earlier, since only the ultimate effect is considered, the internal chains do not affect the rate of RAFT initiation. The free radical that is emitted from the RAFT agent will also react with monomer A to initiate a sequence, just as in the classic model.

RAFT transfer between active sequences proceeds in the same manner as with active chains. Figure 8 shows the reactions in degenerative chain transfer

RAFT Transfer

(31) $L^*_g + TO^*_s \underset{kraft32}{\overset{kraft31}{\leftrightarrow}} TL^*_g + O^*_s$ (32) $O^*_g + TO^*_s \underset{kraft42}{\overset{kraft41}{\leftrightarrow}} TO^*_g + O^*_s$

(33) $L^*_g + TL^*_s \underset{kraft52}{\overset{kraft51}{\leftrightarrow}} TL^*_g + L^*_s$ (34) $O^*_g + TL^*_s \underset{kraft62}{\overset{kraft61}{\leftrightarrow}} TO^*_g + L^*_s$

Figure 8: RAFT transfer reactions of sequence model

The subscript, 's', represents all of the possible lengths of that active sequence: an active sequence of a certain length, 'g' can react with a polymer chain of any length, 's'. Reactions 31 and 34 are equivalent, but once again, they have been separated for ease of comprehension. In Reaction 31, the 'L*' is the specific sequence of interest, while in Reaction 34 the 'O*' is the specific sequence of interest.

The propagation of the active sequences is shown in Figure 9.

Propagation

(35) $L_g^* + A \xrightarrow{kp1} L_{g+1}^*$ (36) $L_g^* + B \xrightarrow{kp2} O_1$ (37) $L_{g-1}^* + A \xrightarrow{kp5} L_g^*$

(38) $O_g^* + A \xrightarrow{kp3} L_1^*$ (39) $O_g^* + B \xrightarrow{kp4} O_{g+1}^*$ (40) $O_{g-1}^* + B \xrightarrow{kp8} O_g^*$

Figure 9: Propogation reactions of sequence model

Reactions 35 and 39 are the elongation of the active sequence one monomeric unit beyond the length of interest, 'g', while Reactions 37 and 40 are the formation of the active sequence, 'g', from sequences one monomeric unit below. Reaction 36 and 38 are the cross-propagation reactions. These reactions are essentially an initiation of the monomer that the polymer reacts with.

Terminations of sequences are by combination and disproportionation. Figure 10 illustrates the termination reactions of the sequence model

Termination

(41) $L_g^* + L^*_s \xrightarrow{ktc1} L_{g+s}$

(42) $L_g^* + L^*_s \xrightarrow{ktd1} L_g + L_s$

(43) $L_g^* + O^*_s \xrightarrow{ktc2} L_{g+s}$

(44) $L_g^* + O^*_s \xrightarrow{ktd2} L_g + O_s$

(45) $O_g^* + O^*_s \xrightarrow{ktc3} O_{g+s}$

(46) $O_g^* + O_s^* \xrightarrow{ktd3} O_g + O_s$

(47) $O_g^* + L^*_s \xrightarrow{ktc4} O_{g+s}$

(48) $O_g^* + L_s^* \xrightarrow{ktd4} O_g + L_s$

Figure 10: Termination reactions of sequence model

When the active sequences react in a termination, inactive sequences are formed. Reactions 43 and 44 are identical to Reactions 47 and 48, but they are presented separately for ease of comprehension: in Reactions 43 and 44 the 'L' sequence is of interest while in Reactions 47 and 48 the 'O' sequence is of interest.

The formation of the inactive sequences for both A and B sequences are illustrated in Figure 11.

Inactive Sequences for A

(49) $L_g^* + B \xrightarrow{kp2} L_g$

(50) $L^*_{g\text{-}s} + L^*_s \xrightarrow{ktc1} L_g$

(51) $L_g^* + L^*_s \xrightarrow{ktd1} L_g$

(52) $L^*_g + O^*_s \xrightarrow{ktc2} L_g$

(53) $L_g^* + O^*_s \xrightarrow{ktd2} L_g$

Inactive Sequence for B

(54) $O_g^* + A \xrightarrow{kp3} O_g$

(54) $O^*_{g\text{-}s} + O_s^* \xrightarrow{ktc3} O_g$

(55) $O_g^* + O_s^* \xrightarrow{ktd3} O_g$

(56) $O^*_g + L_s^* \xrightarrow{ktc4} O_g$

(57) $O_g^* + L_s^* \xrightarrow{ktd4} O_g$

Figure 11: Formation reactions of sequence model

'L' signifies an internal sequence of monomer 'A', while 'O' is an internal sequence of monomer 'B'. As mentioned earlier, the cross propagation reactions act not only as initiators of the opposite sequence, but as the formation of a inactive sequence. Reactions 49 and 54 are cross propagations that are identical to Reactions 36 and 38 with the inactive sequences as the sequences of interest. Similarly, Reactions 50-53 and Reactions 54-57 are identical to Reactions 41-44 and Reactions 45-48, respectively. Once again, the difference only lies in the sequence of interest. Reactions 52 and 56 are combination reactions, but with different sequences, they are demarcated without further manipulation. Reactions 54 and 50, however, are the combination of the same sequence that can result in one inactive sequence, so additional manipulation will be required in the moment equations.

With the mechanistic steps of both the chain model and the sequence model now determined, the mass balance reactions can be developed.

Mass Balance of the Chain Model

For the 'P', 'Q', and 'M' chains, the overall mass balance was determined from the addition of the mass balance of the initial chain (P_1, Q_1, and M_1) and the mass balance of any other chain (P_n, Q_n, and M_n). The mass balances of the chain model are shown in Figure 12. A more detailed breakdown is in the Appendix.

$$\frac{dP_1}{dt} + \frac{dP_n}{dt} = k_{i1}[R^*][A] + k_{r11}[R^*][TP_n] - k_{r12}[T][P_n] - k_{raft31}\left(\sum_{r=0}^{\infty} TQ_r\right)[P_n]$$
$$+ k_{raft32}\left(\sum_{r=0}^{\infty} Q_r\right)[TP_n] + k_{raft51}\left(\sum_{r=0}^{\infty} P_r\right)[TP_n] - k_{raft52}\left(\sum_{r=0}^{\infty} TP_r\right)[P_n]$$
$$- k_{p1}[A][P_n] - k_{p2}[B][P_n] + k_{p5}[A][P_{n-1}] + k_{p7}[A][Q_{n-1}]$$
$$- k_{tcc1}\left(\sum_{r=0}^{\infty} Q_r\right)[P_n] - k_{td1}\left(\sum_{r=0}^{\infty} Q_r\right)[P_n] - k_{tc2}\left(\sum_{r=0}^{\infty} P_r\right)[P_n] - k_{td2}\left(\sum_{r=0}^{\infty} P_r\right)[P_n]$$

$$\frac{dQ_n}{dt} + \frac{dQ_1}{dt} = k_{i2}[R^*][B] + k_{r21}[R^*][TQ_n] - k_{r22}[T][Q_n] - k_{raft61}\left(\sum_{r=0}^{\infty} TP_r\right)[Q_n]$$
$$+ k_{raft62}\left(\sum_{r=0}^{\infty} P_r\right)[TQ_n] + k_{raft41}\left(\sum_{r=0}^{\infty} Q_r\right)[TQ_n] - k_{raft42}\left(\sum_{r=0}^{\infty} TQ_r\right)[Q_n]$$
$$- k_{p3}[A][Q_n] - k_{p4}[B][Q_n] + k_{p6}[B][P_{n-1}] + k_{p8}[B][Q_{n-1}]$$
$$- k_{tc4}\left(\sum_{r=0}^{\infty} P_r\right)[Q_n] - k_{td4}\left(\sum_{r=0}^{\infty} P_r\right)[Q_n] - k_{tc3}\left(\sum_{r=0}^{\infty} Q_r\right)[Q_n] - k_{td3}\left(\sum_{r=0}^{\infty} Q_r\right)[Q_n]$$

$$\frac{dTP_n}{dt} = -k_{r11}[R^*][TP_n] + k_{r12}[T][P_n] + k_{raft31}\left(\sum_{r=0}^{\infty} TQ_r\right)[P_n] - k_{raft32}\left(\sum_{r=0}^{\infty} Q_r\right)[TP_n]$$
$$- k_{raft51}\left(\sum_{r=0}^{\infty} P_r\right)[TP_n] + k_{raft52}\left(\sum_{r=0}^{\infty} TP_r\right)[P_n]$$

$$\frac{dTQ_n}{dt} = -k_{r21}[R^*][TQ_n] + k_{r22}[T][Q_n] - k_{raft41}\left(\sum_{r=0}^{\infty} Q_r\right)[TQ_n] + k_{raft42}\left(\sum_{r=0}^{\infty} TQ_r\right)[Q_n]$$
$$+ k_{raft61}\left(\sum_{r=0}^{\infty} TP_r\right)[Q_n] - k_{raft62}\left(\sum_{r=0}^{\infty} P_r\right)[TQ_n]$$

$$\frac{dM_1}{dt} + \frac{dM_n}{dt} = \tfrac{1}{2} k_{tc1}\left(\sum_{a=0}^{n} P_a Q_{n-a}\right) + \tfrac{1}{2} k_{tc4}\left(\sum_{a=0}^{n} P_a Q_{n-a}\right) + \tfrac{1}{2} k_{tc2}\left(\sum_{a=0}^{n} P_a P_{n-a}\right)$$

$$+ \tfrac{1}{2}\, k_{tc3}\left(\sum_{a=0}^{n} Q_a Q_{n-a}\right) + k_{td1}\left(\sum_{r=0}^{\infty} Q_r\right)[P_n] + k_{td2}\left(\sum_{r=0}^{\infty} P_r\right)[P_n]$$

$$+ k_{td3}\left(\sum_{r=0}^{\infty} Q_r\right)[Q_n] + k_{td4}\left(\sum_{r=0}^{\infty} P_r\right)[Q_n]$$

Figure 12: Mass balances of major components of chain model

Mass Balance of the Sequence Model

The mass balances of the sequence model were developed in the same manner as in the chain model and are shown in Figure 13. A more detailed breakdown is in the Appendix.

$$\frac{dL_1^*}{dt} + \frac{dL_g^*}{dt} = k_{i1}[R^*][A] - k_{p1}[A][L_g^*] - k_{p2}[B][L_g^*] + k_{p5}[A][L_{g\text{-}1}^*] - k_{r11}[T][L_g^*]$$
$$+ k_{r12}[TL_g^*][R^*] - k_{raft51}[TL_s^*][L_g^*] + k_{raft52}[TL_g^*][L_s^*] - k_{raft31}[TO_s^*][L_g^*]$$
$$+ k_{raft32}[TL_g^*][O_s^*] - k_{tc1}\left(\sum_{s=0}^{\infty} L_s^*\right)[L_g^*] - k_{td1}\left(\sum_{s=0}^{\infty} L_s^*\right)[L_g^*] - k_{tc2}\left(\sum_{s=0}^{\infty} O_s^*\right)[L_g^*]$$
$$- k_{tc2}\left(\sum_{s=0}^{\infty} O_s^*\right)[L_g^*]$$

$$\frac{dO_1^*}{dt} + \frac{dO_g^*}{dt} = k_{i2}[R^*][B] - k_{p3}[A][O_g^*] - k_{p4}[B][O_g^*] + k_{p8}[B][O_{g\text{-}1}^*] - k_{r11}[T][O_g^*]$$
$$+ k_{r12}[TO_g^*][R^*] - k_{raft41}[TO_s^*][O_g^*] + k_{raft42}[TO_g^*][O_s^*] - k_{raft31}[TL_s^*][O_g^*]$$
$$+ k_{raft32}[TO_g^*][L_s^*] - k_{tc4}\left(\sum_{s=0}^{\infty} L_s^*\right)[O_g^*] - k_{td4}\left(\sum_{s=0}^{\infty} L_s^*\right)[O_g^*] - k_{tc3}\left(\sum_{s=0}^{\infty} O_s^*\right)[O_g^*]$$
$$- k_{td3}\left(\sum_{s=0}^{\infty} O_s^*\right)[O_g^*]$$

$$\frac{dTL_g^*}{dt} = k_{r11}[T][L_g^*] - k_{r12}[TL_g^*][R^*] + k_{raft51}[TL_s^*][L_g^*] - k_{raft52}[TL_g^*][L_s^*]$$
$$+ k_{raft31}[TO_s^*][L_g^*] - k_{raft32}[TL_g^*][O_s^*]$$

$$\frac{dTO_g^*}{dt} = k_{r11}[T][O_g^*] - k_{r12}[TO_g^*][R^*] + k_{raft41}[TO_s^*][O_g^*] - k_{raft42}[TO_g^*][O_s^*]$$
$$+ k_{raft31}[TL_s^*][O_g^*] - k_{raft32}[TO_g^*][L_s^*]$$

Inactive Sequences

$$\frac{dL_g}{dt} = k_{p2}\,[B]\,[L_g^*] - k_{tc1}\left(\sum_{s=0}^{\infty} L_s^* L_{g-s}^*\right) - k_{td1}\left(\sum_{s=0}^{\infty} L_s^*\right)\,[L_g^*] - k_{tc2}\left(\sum_{s=0}^{\infty} O_s^*\right)\,[L_g^*]$$

$$- k_{td2}\left(\sum_{s=0}^{\infty} O_s^*\right)\,[L_g^*]$$

$$\frac{dO_g}{dt} = k_{p3}\,[A]\,[O_g^*] - k_{tc4}\left(\sum_{s=0}^{\infty} L_s^*\right)\,[O_g^*] - k_{td4}\left(\sum_{s=0}^{\infty} L_s^*\right)\,[O_g^*] - k_{tc3}\left(\sum_{s=0}^{\infty} O_s^* O_{g-s}^*\right)$$

$$- k_{td3}\left(\sum_{s=0}^{\infty} O_s^*\right)\,[O_g^*]$$

Figure 13: Mass balances of major components of sequence model

Definition of Moments

Both the molecular weight distribution and the various sequence distributions will be described by the method of moments. Moment equations were developed for each of the polymer chains of interest. The definitions of the moment equations for the chain model are shown in Figure 14.

Chain Model

Propagating Radical Chains:

$$Y_i^a = \sum_{n=0}^{\infty} n^i [P_n] \qquad Y_i^b = \sum_{n=0}^{\infty} n^i [Q_n]$$

Dormant Chains:

$$Z_i^a = \sum_{n=0}^{\infty} n^i [TP_n] \qquad Z_i^b = \sum_{n=0}^{\infty} n^i [TQ_n]$$

Dead Chains:

$$D_i^a = \sum_{n=0}^{\infty} n^i [M_n]$$

Figure 14: Moment definitions of chain model

The order of the moment, 'i', is represented as the subscript of each of the moments, with the superscript indicating a 'P' or 'Q' chain. The definitions of the moment equations for the sequence model are shown in Figure 15.

Sequence Model

Inactive Chains:

$$\overline{S}_i^a = \sum_{g=1}^{\infty} g^i [L_g] \qquad \overline{S}_i^b = \sum_{g=1}^{\infty} g^i [O_g]$$

Active Chains:

$$S_i^a = \sum_{g=1}^{\infty} g^i [L_g^*] \qquad S_i^b = \sum_{g=1}^{\infty} g^i [O_g^*]$$

$$T_i^a = \sum_{g=1}^{\infty} g^i [TL_g^*] \qquad T_i^b = \sum_{g=1}^{\infty} g^i [TO_g^*]$$

Figure 15: Moment definitions of sequence model

These definitions are needed to develop the moment balances that are derived from the mass balances that were developed earlier.

Moment Equations for the Chain Model

The moment equations for the chain model were developed by multiplying both the left hand and right hand sides of the mass balances listed above by $\sum_{n=0}^{\infty} n^i$.

The following equation shows the derivation of the left-hand side of the moment equation:

$$\frac{dY_i^a}{dt} = \sum_{n=0}^{\infty} n^i \left(\frac{dP_n}{dt} \right) = \sum_{n=0}^{\infty} n^i \left(\frac{dP_1}{dt} + \frac{dP_n}{dt} \right).$$

The terms on the right hand side are straight-forward, with the exception of the propagation reactions that form the polymer with the length of interest (Reactions 14-17). The manipulation of those terms is shown below Figures 16 and 17.

$$\sum_{n=1}^{\infty} n^i P_{n-1} = \sum_{n=1}^{\infty} (n+1)^i P_n$$

i =0	i =1	i =2
$\sum_{n=1}^{\infty} P_n = Y_0^a$	$\sum_{n=1}^{\infty} (n+1) P_n = Y_1^a + Y_0^a$	$\sum_{n=1}^{\infty} (n+1)^2 P_n = Y_2^a + 2 * Y_1^a + Y_0^a$

Figure 16: Moment equivalencies of 'P' chain

$\sum_{n=1}^{\infty} n^i Q_{n-1} = \sum_{n=1}^{\infty} (n+1)^i Q_n$		
i =0	i =1	i =2
$\sum_{n=1}^{\infty} Q_n = Y_0^b$	$\sum_{n=1}^{\infty} (n+1) Q_n = Y_1^b + Y_0^b$	$\sum_{n=1}^{\infty} (n+1)^2 Q_n = Y_2^b + 2 * Y_1^b + Y_0^b$

Figure 17: Moment equivalencies of 'Q' chain

The only other terms that require manipulation are the termination by combination reactions. The manipulation of these mass balances into moment equations is shown below:

$$\left(\sum_{n=0}^{\infty}\sum_{c=0}^{n} n^i P_c P_{n-c}\right) = \left(\sum_{n=0}^{\infty}\sum_{c=0}^{n} [c+(n-c)]^i P_c P_{n-c}\right) = \sum_{m=0}^{i}\left(\frac{i}{m}\right)\sum_{n=0}^{\infty}\sum_{c=0}^{n} c^m P_c (n-c)^{i-m} P_{n-c}$$

$$= \sum_{m=0}^{i}\left(\frac{i}{m}\right)\sum_{n=0}^{\infty} n^m P_n \sum_{c=0}^{\infty} c^{i-m} P_c = \sum_{m=0}^{i}\left(\frac{i}{m}\right) Y_i^a Y_{i-m}^a$$

where

$\left(\frac{i}{m}\right) = \frac{i!}{m!(i-m)!}$. The breakdown of each moment by the order is shown in Figure 18.

<u>i = 0</u>

m = 0: $Y_0^a Y_0^b$

<u>i = 1</u>

m = 0: $(1)(1) Y_0^a Y_1^b$ m = 1: $(1)(1) Y_1^a Y_0^b$

<u>i = 2</u>

m = 0: $(1)(1) Y_0^a Y_2^b$ m = 1: $(2)(1) Y_1^a Y_1^b$ m = 2: $(1)(1) Y_2^a Y_0^b$

Figure 18: Termination by combination moment equivalencies

With these mathematical manipulations, the moment equations can be easily determined from the mass balances, which are shown in Figure 19.

$$\frac{dY_i^a}{dt} = \sum_{n=0}^{\infty} n^i \left(\frac{dP_n}{dt} \right) = \sum_{n=0}^{\infty} n^i \left(\frac{dP_1}{dt} + \frac{dP_n}{dt} \right)$$

$$\frac{dY_0^a}{dt} = k_{i1}[R^*][A] + k_{r11}[R^*][Z_0^a] - k_{r12}[T][Y_0^a] - k_{raft31}[Z_0^b][Y_0^a]$$

$$+ k_{raft32}[Y_0^b][Z_0^a] + k_{raft51}[Y_0^a][Z_0^a] - k_{raft52}[Z_0^a][Y_0^a] - k_{p1}[A][Y_0^a]$$

$$- k_{p2}[B][Y_0^a] + k_{p5}[A][Y_0^a] + k_{p7}[A][Y_0^b] - k_{tc1}[Y_0^b][Y_0^a] - k_{td1}[Y_0^b][Y_0^a]$$

$$- k_{tc2}[Y_0^a][Y_0^a] - k_{td2}[Y_0^a][Y_0^a]$$

$$\frac{dY_1^a}{dt} = k_{i1}[R^*][A] + k_{r11}[R^*][Z_1^a] - k_{r12}[T][Y_1^a] - k_{raft31}[Z_0^b][Y_1^a]$$

$$+ k_{raft32}[Y_0^b][Z_1^a] + k_{raft51}[Y_0^a][Z_1^a] - k_{raft52}[Z_0^a][Y_1^a] - k_{p1}[A][Y_1^a]$$

$$- k_{p2}[B][Y_1^a] + k_{p5}[A][Y_1^a + Y_0^a] + k_{p7}[A][Y_1^b + Y_0^b] - k_{tc1}[Y_0^b][Y_1^a]$$

$$- k_{td1}[Y_0^b][Y_1^a] - k_{tc2}[Y_0^a][Y_1^a] - k_{td2}[Y_0^a][Y_1^a]$$

$$\frac{dY_2^a}{dt} = k_{i1}[R^*][A] + k_{r11}[R^*][Z_2^a] - k_{r12}[T][Y_2^a] - k_{raft31}[Z_0^b][Y_2^a]$$

$$+ k_{raft32}[Y_0^b][Z_2^a] + k_{raft51}[Y_0^a][Z_2^a] - k_{raft52}[Z_0^a][Y_2^a] - k_{p1}[A][Y_2^a]$$

$$- k_{p2}[B][Y_2^a] + k_{p5}[A][Y_2^a + 2*Y_1^a + Y_0^a] + k_{p7}[A][Y_2^b + 2*Y_1^b + Y_0^b]$$

$$- k_{tc1}[Y_0^b][Y_2^a] - k_{td1}[Y_0^b][Y_2^a] - k_{tc2}[Y_0^a][Y_2^a] - k_{td2}[Y_0^a][Y_2^a]$$

$$\frac{dY_i^b}{dt} = \sum_{n=0}^{\infty} n^i \left(\frac{dQ_n}{dt} \right) = \sum_{n=0}^{\infty} n^i \left(\frac{dQ_1}{dt} + \frac{dQ_n}{dt} \right)$$

$$\frac{dY_0^b}{dt} = k_{i2}[R^*][B] + k_{r21}[R^*][Z_0^b] - k_{r22}[T][Y_0^b] - k_{raft61}[Z_0^a][Y_0^b]$$

$$+ k_{raft62}[Y_0^a][Z_0^b] + k_{raft41}[Y_0^b][Z_0^b] - k_{raft42}[Z_0^b][Y_0^b] - k_{p3}[A][Y_0^b]$$

$$- k_{p4}[B][Y_0^b] + k_{p6}[B][Y_0^a] + k_{p8}[B][Y_0^b] - k_{tc4}[Y_0^a][Y_0^b] - k_{td4}[Y_0^a][Y_0^b]$$

$$- k_{tc3}[Y_0^b][Y_0^b] - k_{td3}[Y_0^b][Y_0^b]$$

$$\frac{dY_1^b}{dt} = k_{i2}[R^*][B] + k_{r21}[R^*][Z_1^b] - k_{r22}[T][Y_1^b] - k_{raft61}[Z_0^a][Y_1^b]$$

$$+ k_{raft62}[Y_0^a][Z_1^b] + k_{raft41}[Y_0^b][Z_1^b] - k_{raft42}[Z_0^b][Y_1^b] - k_{p3}[A][Y_1^b]$$

$$- k_{p4}[B][Y_1^b] + k_{p6}[B][Y_1^a + Y_0^a] + k_{p8}[B][Y_1^b + Y_0^b] - k_{tc4}[Y_0^a][Y_1^b]$$

$$- k_{td4}[Y_0^a][Y_1^b] - k_{tc3}[Y_0^b][Y_1^b] - k_{td3}[Y_0^b][Y_1^b]$$

$$\frac{dY_2^b}{dt} = k_{i2}[R^*][B] + k_{r21}[R^*][Z_2^b] - k_{r22}[T][Y_2^b] - k_{raft61}[Z_0^a][Y_2^b]$$

$$+ k_{raft62}[Y_0^a][Z_2^b] + k_{raft41}[Y_0^b][Z_2^b] - k_{raft42}[Z_0^b][Y_2^b] - k_{p3}[A][Y_2^b]$$

$$- k_{p4}[B][Y_2^b] + k_{p6}[B][Y_2^a + 2*Y_1^a + Y_0^a] + k_{p8}[B][Y_2^b + 2*Y_1^b + Y_0^b]$$

$$- k_{tc4}[Y_0^a][Y_2^b] - k_{td4}[Y_0^a][Y_2^b] - k_{tc3}[Y_0^b][Y_2^b] - k_{td3}[Y_0^b][Y_2^b]$$

$$\frac{dZ_i^a}{dt} = \sum_{n=0}^{\infty} n^i \left(\frac{dTP_n}{dt} \right)$$

$$\frac{dZ_i^a}{dt} = -k_{r11}[R^*][Z_i^a] + k_{r12}[T][Y_i^a] + k_{raft31}[Z_0^b][Y_i^a] - k_{raft32}[Y_0^b][Z_i^a]$$

$$- k_{raft51}[Y_0^a][Z_i^a] + k_{raft52}[Z_0^a][Y_i^a]$$

$$\frac{dZ_i^b}{dt} = \sum_{n=0}^{\infty} n^i \left(\frac{dTQ_n}{dt} \right)$$

$$\frac{dZ_i^b}{dt} = -k_{r21}[R^*][Z_i^b] + k_{r22}[T][Y_i^b] - k_{raft41}[Y_0^b][Z_i^b] + k_{raft42}[Z_0^b][Y_i^b]$$

$$+ k_{raft61}[Z_0^a][Y_i^b] - k_{raft62}[Y_0^a][Z_i^b]$$

$$\frac{dD_i}{dt} = \sum_{n=0}^{\infty} n^i \left(\frac{dM_n}{dt} \right)$$

$$\frac{dD_0}{dt} = ½\, k_{tc1}[Y_0^a][Y_0^b] + ½\, k_{tc4}[Y_0^a][Y_0^b] + ½\, k_{tc2}[Y_0^a][Y_0^a] + ½\, k_{tc3}[Y_0^b][Y_0^b]$$

$$+ k_{td1}[Y_0^b][Y_0^a] + k_{td2}[Y_0^a][Y_0^a] + k_{td3}[Y_0^b][Y_0^b] + k_{td4}[Y_0^a][Y_0^b]$$

$$\frac{dD_1}{dt} = ½\, k_{tc1}[Y_0^a Y_1^b + Y_1^a Y_0^b] + ½\, k_{tc4}[Y_0^a Y_1^b + Y_1^a Y_0^b] + ½\, k_{tc2}[Y_0^a Y_1^a + Y_1^a Y_0^a]$$

$$+ ½\, k_{tc3}[Y_0^b Y_1^b + Y_1^b Y_0^b] + k_{td1}[Y_0^b][Y_1^a] + k_{td2}[Y_0^a][Y_1^a]$$

$$+ k_{td3}[Y_0^b][Y_1^b] + k_{td4}[Y_0^a][Y_1^b]$$

$$\frac{dD_2}{dt} = ½\, k_{tc1}[Y_0^a Y_2^b + 2*Y_1^a Y_1^b + Y_2^a Y_0^b] + ½\, k_{tc4}[Y_0^a Y_2^b + 2*Y_1^a Y_1^b + Y_2^a Y_0^b]$$

$$+ ½\, k_{tc2}[Y_0^a Y_2^a + 2*Y_1^a Y_1^a + Y_2^a Y_0^a] + ½\, k_{tc3}[Y_0^b Y_2^b + 2*Y_1^b Y_1^b + Y_2^b Y_0^b]$$

$$+ k_{td1}[Y_0^b][Y_2^a] + k_{td2}[Y_0^a][Y_2^a] + k_{td3}[Y_0^b][Y_2^b] + k_{td4}[Y_0^a][Y_2^b]$$

Figure 19: Moment equatinos of major components of sequence model

Moment Equations for the Sequence Model

The moment equations of the sequence model were developed from the sequence mass balances akin to the chain model and are shown in Figure 20. A more detailed breakdown is in the Appendix.

$$\frac{dS_i^a}{dt} = \sum_{g=0}^{\infty} g^i \left(\frac{dL_g^*}{dt} \right) = \sum_{g=1}^{\infty} g^i \left(\frac{dL_1^*}{dt} + \frac{dL_{g+1}^*}{dt} \right)$$

$$\frac{dS_0^a}{dt} = k_{i1}[R^*][A] - k_{p1}[A]\left(S_0^a\right) - k_{p2}[B]\left(S_0^a\right) + k_{p5}[A]\left(S_0^a\right) - k_{r11}[T]\left(S_0^a\right)$$

$$+ k_{r12}\left(T_0^a\right)[R^*] - k_{raft51}\left(T_0^a\right)\left(S_0^a\right) + k_{raft52}\left(S_0^a\right)\left(T_0^a\right) - k_{raft31}\left(T_0^b\right)\left(S_0^a\right)$$

$$+ k_{raft32}\left(S_0^b\right)\left(T_0^a\right) - k_{tc1}\left(S_0^a\right)\left(S_0^a\right) - k_{td1}\left(S_0^a\right)\left(S_0^a\right) - k_{tc2}\left(S_0^b\right)\left(S_0^a\right) - k_{tc2}\left(S_0^b\right)\left(S_0^a\right)$$

$$\frac{dS_1^a}{dt} = k_{i1}[R^*][A] - k_{p1}[A]\left(S_1^a\right) - k_{p2}[B]\left(S_1^a\right) + k_{p5}[A]\left(S_0^a + S_1^a\right) - k_{r11}[T]\left(S_1^a\right)$$

$$+ k_{r12}\left(T_1^a\right)[R^*] - k_{raft51}\left(T_0^a\right)\left(S_1^a\right) + k_{raft52}\left(S_0^a\right)\left(T_1^a\right) - k_{raft31}\left(T_0^b\right)\left(S_1^a\right)$$

$$+ k_{raft32}\left(S_0^b\right)\left(T_1^a\right) - k_{tc1}\left(S_0^a\right)\left(S_1^a\right) - k_{td1}\left(S_0^a\right)\left(S_1^a\right) - k_{tc2}\left(S_0^b\right)\left(S_1^a\right) - k_{tc2}\left(S_0^b\right)\left(S_1^a\right)$$

$$\frac{dS_2^a}{dt} = k_{i1}[R^*][A] - k_{p1}[A]\left(S_2^a\right) - k_{p2}[B]\left(S_2^a\right) + k_{p5}[A]\left(S_0^a + 2S_1^a + S_2^a\right) - k_{r11}[T]\left(S_2^a\right)$$

$$+ k_{r12}\left(T_2^a\right)[R^*] - k_{raft51}\left(T_0^a\right)\left(S_2^a\right) + k_{raft52}\left(S_0^a\right)\left(T_2^a\right) - k_{raft31}\left(T_0^b\right)\left(S_2^a\right)$$

$$+ k_{raft32}\left(S_0^b\right)\left(T_2^a\right) - k_{tc1}\left(S_0^a\right)\left(S_2^a\right) - k_{td1}\left(S_0^a\right)\left(S_2^a\right) - k_{tc2}\left(S_0^b\right)\left(S_2^a\right) - k_{tc2}\left(S_0^b\right)\left(S_2^a\right)$$

$$\frac{dS_i^b}{dt} = \sum_{g=0}^{\infty} g^i\left(\frac{dO_g^*}{dt}\right) = \sum_{g=1}^{\infty} g^i\left(\frac{dO_1^*}{dt} + \frac{dO_{g+1}^*}{dt}\right)$$

$$\frac{dS_0^b}{dt} = k_{i2}[R^*][B] - k_{p3}[A]\left(S_0^b\right) - k_{p4}[B]\left(S_0^b\right) + k_{p8}[B]\left(S_0^b\right) - k_{r21}[T]\left(S_0^b\right)$$

$$+ k_{r22}\left(T_0^b\right)[R^*] - k_{raft41}\left(T_0^b\right)\left(S_0^b\right) + k_{raft42}\left(S_0^b\right)\left(T_0^b\right) - k_{raft61}\left(T_0^a\right)\left(S_0^b\right)$$

$$+ k_{raft62}\left(S_0^a\right)\left(T_0^b\right) - k_{tc4}\left(S_0^a\right)\left(S_0^b\right) - k_{td4}\left(S_0^a\right)\left(S_0^b\right) - k_{tc3}\left(S_0^b\right)\left(S_0^b\right) - k_{td3}\left(S_0^b\right)\left(S_0^b\right)$$

$$\frac{dS_1^b}{dt} = k_{i2}[R^*][B] - k_{p3}[A]\left(S_1^b\right) - k_{p4}[B]\left(S_1^b\right) + k_{p8}[B]\left(S_0^b + S_1^b\right) - k_{r21}[T]\left(S_1^b\right)$$

$$+ k_{r22}\left(T_1^b\right)[R^*] - k_{raft41}\left(T_0^b\right)\left(S_1^b\right) + k_{raft42}\left(S_0^b\right)\left(T_1^b\right) - k_{raft61}\left(T_0^a\right)\left(S_1^b\right)$$

$$+ k_{raft62}\left(S_0^a\right)\left(T_1^b\right) - k_{tc4}\left(S_0^a\right)\left(S_1^b\right) - k_{td4}\left(S_0^a\right)\left(S_1^b\right) - k_{tc3}\left(S_0^b\right)\left(S_1^b\right) - k_{td3}\left(S_0^b\right)\left(S_1^b\right)$$

$$\frac{dS_2^b}{dt} = k_{i2}[R^*][B] - k_{p3}[A]\left(S_2^b\right) - k_{p4}[B]\left(S_2^b\right) + k_{p8}[B]\left(S_0^b + 2S_1^b + S_2^b\right) - k_{r21}[T]\left(S_2^b\right)$$

$$+ k_{r22}\left(T_2^b\right)[R^*] - k_{raft41}\left(T_0^b\right)\left(S_2^b\right) + k_{raft42}\left(S_0^b\right)\left(T_2^b\right) - k_{raft61}\left(T_0^a\right)\left(S_2^b\right)$$

$$+ k_{raft62}\left(S_0^a\right)\left(T_2^b\right) - k_{tc4}\left(S_0^a\right)\left(S_2^b\right) - k_{td4}\left(S_0^a\right)\left(S_2^b\right) - k_{tc3}\left(S_0^b\right)\left(S_2^b\right) - k_{td3}\left(S_0^b\right)\left(S_2^b\right)$$

$$\frac{dT_i^a}{dt} = k_{r11}[T]\left(S_i^a\right) - k_{r12}\left(T_i^a\right)[R^*] + k_{raft51}\left(T_0^a\right)\left(S_i^a\right) - k_{raft52}\left(S_0^a\right)\left(T_i^a\right)$$

$$+ k_{raft31}\left(T_0^b\right)\left(S_i^a\right) - k_{raft32}\left(S_0^b\right)\left(T_i^a\right)$$

$$\frac{dT_i^b}{dt} = k_{r21}[T]\left(S_i^b\right) - k_{r22}\left(T_i^b\right)[R^*] + k_{raft41}\left(T_0^b\right)\left(S_i^b\right) - k_{raft42}\left(S_0^b\right)\left(T_i^b\right)$$

$$+ k_{raft31}\left(T_0^a\right)\left(S_i^b\right) - k_{raft32}\left(S_0^a\right)\left(T_i^b\right)$$

Internal Sequences

$$\frac{d\overline{S}_0^a}{dt} = k_{p2}[B]\left(S_0^a\right) + k_{tc1}\left(S_0^a\right)\left(S_0^a\right) + k_{td1}\left(S_0^a\right)\left(S_0^a\right) + k_{tc2}\left(S_0^b\right)\left(S_0^a\right) + k_{tc2}\left(S_0^b\right)\left(S_0^a\right)$$

$$\frac{d\overline{S}_1^a}{dt} = k_{p2}[B]\left(S_1^a\right) + k_{tc1}\left(\left(S_0^a\right)\left(S_1^a\right) + \left(S_1^a\right)\left(S_0^a\right)\right) + k_{td1}\left(S_0^a\right)\left(S_1^a\right)$$

$$+ k_{tc2}\left(S_0^b\right)\left(S_1^a\right) + k_{tc2}\left(S_0^b\right)\left(S_1^a\right)$$

$$\frac{d\overline{S}_2^a}{dt} = k_{p2}[B]\left(S_2^a\right) + k_{tc1}\left(\left(S_0^a\right)\left(S_2^a\right) + 2*\left(S_1^a\right)\left(S_1^a\right) + \left(S_0^a\right)\left(S_2^a\right)\right)$$

$$+ k_{td1}\left(S_0^a\right)\left(S_2^a\right) + k_{tc2}\left(S_0^b\right)\left(S_2^a\right) + k_{tc2}\left(S_0^b\right)\left(S_2^a\right)$$

$$\frac{d\overline{S}_0^b}{dt} = k_{p3}[A]\left(S_0^b\right) + k_{tc4}\left(S_0^a\right)\left(S_0^b\right) + k_{td4}\left(S_0^a\right)\left(S_0^b\right) + k_{tc3}\left(S_0^b\right)\left(S_0^b\right) + k_{td3}\left(S_0^b\right)\left(S_0^b\right)$$

$$\frac{d\overline{S}_1^b}{dt} = k_{p3}[A]\left(S_1^b\right) + k_{tc4}\left(S_0^a\right)\left(S_1^b\right) + k_{td4}\left(S_0^a\right)\left(S_1^b\right) + k_{tc3}\left(\left(S_0^b\right)\left(S_1^b\right) + \left(S_1^b\right)\left(S_0^b\right)\right)$$

$$+ k_{td3}\left(S_0^b\right)\left(S_1^b\right)$$

$$\frac{d\overline{S}_2^b}{dt} = k_{p3}[A]\left(S_2^b\right) + k_{tc4}\left(S_0^a\right)\left(S_2^b\right) + k_{td4}\left(S_0^a\right)\left(S_2^b\right)$$

$$+ k_{tc3}\left(\left(S_0^b\right)\left(S_2^b\right) + 2*\left(S_1^b\right)\left(S_1^b\right) + \left(S_0^b\right)\left(S_2^b\right)\right) + k_{td3}\left(S_0^b\right)\left(S_2^b\right)$$

Figure 20: Moment equations of major components of sequence model

The chain model and the sequence model can be closed with a mass balance on the minor terms (i.e. monomers A and B, free radicals, initiator, and RAFT agent). The mass balances for those terms are shown below in Figure 21.

$$\frac{dA}{dt} = -k_{i1}[R^*][A] - k_{p1}[Y_0^a][A] - k_{p3}[Y_0^b][A]$$

$$\frac{dB}{dt} = -k_{i2}[R^*][B] - k_{p2}[Y_0^a][B] - k_{p4}[Y_0^b][B]$$

$$\frac{dI}{dt} = -k_d[I]$$

$$\frac{dR^*}{dt} = 2*k_d(f)[I] - ki1[A][R^*] - ki2[B][R^*] - k_{r11}[Z_0^a][R^*] + k_{r12}[Y_0^a][T]$$

$$- k_{r21}[Z_0^b][R^*] + k_{r22}[Y_0^b][T]$$

$$\frac{dT}{dt} = k_{r21}[R^*][Z_0^b] - k_{r22}[T][Y_0^b] + k_{r11}[R^*][Z_0^a] - k_{r12}[T][Y_0^a]$$

Figure 21: Mass balances of minor components

Key Paramters

With the model complete, important parameters can be defined to characterize the simulated polymer. These parameters are defined by both the chain model and the sequence model. The chain model is used to determine the number-average-chain-length, the weight-average-chain-length, conversion, and the polydispersity. In a

purely living system—termination rate constants are set to zero—the chain model can determine the copolymer composition of each monomer, which was also used as a check to the sequence model determined copolymer composition. The derivation of the chain model parameters is shown below.

$$\textbf{\textit{NACL}} = \frac{\sum_{n=0}^{\infty} n(P_n) + \sum_{n=0}^{\infty} n(Q_n) + \sum_{n=0}^{\infty} n(TP_n) + \sum_{n=0}^{\infty} n(TQ_n) + \sum_{n=0}^{\infty} n(D_n)}{\sum_{n=0}^{\infty} (P_n) + \sum_{n=0}^{\infty} (Q_n) + \sum_{n=0}^{\infty} (TP_n) + \sum_{n=0}^{\infty} (TQ_n) + \sum_{n=0}^{\infty} (D_n)}$$

$$= \frac{Y_1^a + Y_1^b + Z_1^a + Z_1^b + D_1^a}{Y_0^a + Y_0^b + Z_0^a + Z_0^b + D_0^a}$$

$$\textbf{\textit{WACL}} = \frac{\sum_{n=0}^{\infty} n^2(P_n) + \sum_{n=0}^{\infty} n^2(Q_n) + \sum_{n=0}^{\infty} n^2(TP_n) + \sum_{n=0}^{\infty} n^2(TQ_n) + \sum_{n=0}^{\infty} n^2(D_n)}{\sum_{n=0}^{\infty} n(P_n) + \sum_{n=0}^{\infty} n(Q_n) + \sum_{n=0}^{\infty} n(TP_n) + \sum_{n=0}^{\infty} n(TQ_n) + \sum_{n=0}^{\infty} n(D_n)}$$

$$= \frac{Y_2^a + Y_2^b + Z_2^a + Z_2^b + D_2^a}{Y_1^a + Y_1^b + Z_1^a + Z_1^b + D_1^a}$$

Polydispersity = WACL / NACL

$$\textbf{\textit{Conversion}} = \frac{\sum_{n=0}^{\infty} n(P_n) + \sum_{n=0}^{\infty} n(Q_n) + \sum_{n=0}^{\infty} n(TP_n) + \sum_{n=0}^{\infty} n(TQ_n) + \sum_{n=0}^{\infty} n(D_n)}{\sum_{n=0}^{\infty} n(P_n) + \sum_{n=0}^{\infty} n(Q_n) + \sum_{n=0}^{\infty} n(TP_n) + \sum_{n=0}^{\infty} n(TQ_n) + \sum_{n=0}^{\infty} n(D_n) + A + B}$$

$$= \frac{Y_1^a + Y_1^b + Z_1^a + Z_1^b + D_1^a}{Y_1^a + Y_1^b + Z_1^a + Z_1^b + D_1^a + A + B}$$

The sequence model is used to determine many parameters about the composition of the polymer. In addition to copolymer composition, the sequence model is used to determine the average ending of A and B monomers in a polymer

chain, the average internal sequence of each monomer and the dispersity of all of the sequences. The copolymer composition of A is determined through the addition of all of the number sequences of A (active, or inactive) divided by all of the number sequences. The dispersity of the sequences indicates the uniformity of each sequence, or all the sequences. The sequence model can also determine the conversion, which was used a cross-check with the chain model determined conversion. The definitions of these parameters are shown below.

Fraction of Copolymer A $= \dfrac{\sum_{g=0}^{\infty} g(L_g) + \sum_{g=0}^{\infty} g(L_g^*)}{\sum_{g=0}^{\infty} g(L_g) + \sum_{g=0}^{\infty} g(L_g^*) + \sum_{g=0}^{\infty} g(O_g) + \sum_{g=0}^{\infty} g(O_g^*)}$

$= \dfrac{\overline{S}_1^a + S_1^a + T_1^a}{\overline{S}_1^a + S_1^a + \overline{S}_1^b + S_1^b + T_1^a + T_1^b}$

Fraction of Copolymer B $= \dfrac{\sum_{g=0}^{\infty} g(O_g) + \sum_{g=0}^{\infty} g(O_g^*)}{\sum_{g=0}^{\infty} g(L_g) + \sum_{g=0}^{\infty} g(L_g^*) + \sum_{g=0}^{\infty} g(O_g) + \sum_{g=0}^{\infty} g(O_g^*)}$

$= \dfrac{\overline{S}_1^b + S_1^b + T_1^b}{\overline{S}_1^a + S_1^a + \overline{S}_1^b + S_1^b + T_1^a + T_1^b}$

Number Average of Active Sequence A $= \dfrac{\sum_{g=0}^{\infty} g(L_g^*) + \sum_{g=0}^{\infty} g(TL_g^*)}{\sum_{g=0}^{\infty} (L_g^*) + \sum_{g=0}^{\infty} (TL_g^*)}$

$= \dfrac{S_1^a + T_1^a}{S_0^a + T_0^a}$

Number Average of Active Sequence B $= \dfrac{\sum_{g=0}^{\infty} g(O_g^*) + \sum_{g=0}^{\infty} g(TO_g^*)}{\sum_{g=0}^{\infty} (O_g^*) + \sum_{g=0}^{\infty} (TO_g^*)}$

$$= \frac{S_1^b + T_1^b}{S_0^b + T_0^b}$$

Number Average of Inactive Sequence A $= \dfrac{\sum_{g=0}^{\infty} g(L_g)}{\sum_{g=0}^{\infty} (L_g)}$

$$= \frac{\overline{S}_1^a}{\overline{S}_0^a}$$

Number Average of Inactive Sequence B $= \dfrac{\sum_{g=0}^{\infty} g(O_g)}{\sum_{g=0}^{\infty} (O_g)}$

$$= \frac{\overline{S}_1^b}{\overline{S}_0^b}$$

NASL $= \dfrac{\sum_{g=0}^{\infty} g(L_g^*) + \sum_{g=0}^{\infty} g(O_g^*) + \sum_{g=0}^{\infty} g(TL_g^*) + \sum_{g=0}^{\infty} g(TO_g^*) + \sum_{g=0}^{\infty} g(L_g) + \sum_{g=0}^{\infty} g(O_g)}{\sum_{g=0}^{\infty} (L_g^*) + \sum_{g=0}^{\infty} (O_g^*) + \sum_{g=0}^{\infty} (TL_g^*) + \sum_{g=0}^{\infty} (TO_g^*) + \sum_{g=0}^{\infty} (L_g) + \sum_{g=0}^{\infty} (O_g)}$

$$= \frac{\overline{S}_1^a + S_1^a + \overline{S}_1^b + S_1^b + T_1^a + T_1^b}{\overline{S}_0^a + S_0^a + \overline{S}_0^b + S_0^b + T_0^a + T_0^b}$$

WASL $= \dfrac{\sum_{g=0}^{\infty} g^2(L_g^*) + \sum_{g=0}^{\infty} g^2(O_g^*) + \sum_{g=0}^{\infty} g^2(TL_g^*) + \sum_{g=0}^{\infty} g^2(TO_g^*) + \sum_{g=0}^{\infty} g^2(L_g) + \sum_{g=0}^{\infty} g^2(O_g)}{\sum_{g=0}^{\infty} g(L_g^*) + \sum_{g=0}^{\infty} g(O_g^*) + \sum_{g=0}^{\infty} g(TL_g^*) + \sum_{g=0}^{\infty} g(TO_g^*) + \sum_{g=0}^{\infty} g(L_g) + \sum_{g=0}^{\infty} g(O_g)}$

$$= \frac{\overline{S}_2^a + S_2^a + \overline{S}_2^b + S_2^b + T_2^a + T_2^b}{\overline{S}_1^a + S_1^a + \overline{S}_1^b + S_1^b + T_1^a + T}$$

Dispersity of Sequences = WASL / NASL

Dispersity of A sequences

$$= \frac{\sum_{g=0}^{\infty} g^2\left(L_g^*\right)+\sum_{g=0}^{\infty} g^2\left(TL_g^*\right)+\sum_{g=0}^{\infty} g^2\left(L_g\right)}{\sum_{g=0}^{\infty} g\left(L_g^*\right)+\sum_{g=0}^{\infty} g\left(TL_g^*\right)+\sum_{g=0}^{\infty} g\left(L_g\right)} \Bigg/ \frac{\sum_{g=0}^{\infty} g\left(L_g^*\right)+\sum_{g=0}^{\infty} g\left(TL_g^*\right)+\sum_{g=0}^{\infty} g\left(L_g\right)}{\sum_{g=0}^{\infty}\left(L_g^*\right)+\sum_{g=0}^{\infty}\left(TL_g^*\right)+\sum_{g=0}^{\infty}\left(L_g\right)}$$

$$= \frac{\overline{S}_2^a + S_2^a + T_2^a}{\overline{S}_1^a + S_1^a + T_1^a} \Bigg/ \frac{\overline{S}_1^a + S_1^a + T_1^a}{\overline{S}_0^a + S_0^a + T_0^a}$$

Dispersity of B sequences

$$= \frac{\sum_{g=0}^{\infty} g^2\left(O_g^*\right)+\sum_{g=0}^{\infty} g^2\left(TO_g^*\right)+\sum_{g=0}^{\infty} g^2\left(O_g\right)}{\sum_{g=0}^{\infty} g\left(O_g^*\right)+\sum_{g=0}^{\infty} g\left(TO_g^*\right)+\sum_{g=0}^{\infty} g\left(O_g\right)} \Bigg/ \frac{\sum_{g=0}^{\infty} g\left(O_g^*\right)+\sum_{g=0}^{\infty} g\left(TO_g^*\right)+\sum_{g=0}^{\infty} g\left(O_g\right)}{\sum_{g=0}^{\infty}\left(O_g^*\right)+\sum_{g=0}^{\infty}\left(TO_g^*\right)+\sum_{g=0}^{\infty}\left(O_g\right)}$$

$$= \frac{\overline{S}_2^b + S_2^b + T_2^b}{\overline{S}_1^b + S_1^b + T_1^b} \Bigg/ \frac{\overline{S}_1^b + S_1^b + T_1^b}{\overline{S}_0^b + S_0^b + T_0^b}$$

The chain and sequence models were run concurrently on MATLAB©. A stiff ordinary differential equation solver, ode15s, was used as the solver. The extensive MATLAB© code is available upon request.

Ratios of living to dead chains were noted to verify the low production of "dead" chains, as well as to validate the simplifying assumption that end sequences on dead chains do not significantly affect the geometric inferences that are taken from the sequence model. A ratio between the end sequences was calculated to determine which end sequence is more prevalent. The average internal sequences reveal the sequence structure, while the dispersity indicates the uniformity of this sequence structure.

With the models developed, simulations were done using varying reactor schemes to produce a controlled molecular architecture. The sequence model predicts

the composition structure of each polymer segment produced from each reactor condition Chapter 3 simulates stand-alone batch reactors and shot-polymerizations producing polymers with different structures. Chapter 4 moves beyond to series of PFR and CSTR reactors producing some polymer segments that have length as well as compositional uniformity.

Chapter 3: Batch Reactors

With the introduction to the model complete, Chapter 3 will simulate five different reactor runs to illustrate the power of the novel sequence model to analyze the composition of polymers. After a brief overview of the kinetic parameters and model, two stand-alone batch reactor runs will be simulated. The goal of these two simulations will be to highlight the affect on 'composition drift' on sequence distribution. The sequence model is the only model derived from population balances that can quantify the degree of compositional drift. In the final section of this chapter, shot-polymerizations will be simulated to produce and quantify the distinct polymer segments that were produced from manipulating reactor conditions.

Kinetic Parameters

The kinetic parameters are taken from Wang et al., with the notable exception of RAFT transfer[23]. The ratio between raft transfer and propagation is kept high because that is the main requirement to keep polydispersity low[5]. There has been much debate on the longevity of the macro-radical intermediate P-T-P and the rate constant of the addition-fragmentation coefficients[36-38]. However, since the characterization of this macro-radical is still in its infancy, and the goal of this work is to demonstrate the usefulness of moments in regards to sequences, the macro-radical lifetime is considered negligible. As developed elsewhere, the reaction constants are considered to be unchanged with or without RAFT agents [22, 23, 37]. Reactivity ratios are changed arbitrarily with common numbers to simulate a variety of copolymers. These reactivity ratios are taken from values obtained from conventional

radical polymerization, which have been found to be similar in RAFT copolymerization[39].

$f = 0.6$	$k_{p,ii} = 10^3$
$k_d = 10^{-5}$	$k_{p,ij}$ = depends on reactivity ratios
$k_{i,i} = 3*10^3$	$k_{tc,i} = 10^7$
$k_{r,ij} = 10^5$	$k_{td,i} = 10^7$
$k_{raft,ij} = 10^5$	

Overview of Models

This model uses the method of moments for RAFT processes that has already been elucidated in other works[22, 23]. While the chain model is used to determine degree of polymerization, conversion, and polydispersity, the sequence model is used concurrently to determine copolymer composition using the novel approach of sequences with population balances. The sequence model tracks "active" and "inactive" sequences. An "active" sequence can polymerize, while an "inactive" sequence cannot. Since branching is not considered in our model for the sake of simplicity, all sequences at the end of chains are considered active and all internal sequences in chains are considered inactive. The notable exception is that all sequences on "dead polymers", including end sequences, are considered inactive. Therefore, the geometry that is suggested by the sequence distribution is skewed, but with a high ratio of living to dead chains, it will be insignificant. Correspondingly, the termination reaction between radicals formed from initiators and living chains has been neglected as in other various works. Beyond illustrating the power of our

technique, an analysis has been done about the structures that can be formed with series of reactors.

Batch Simulations

1st Batch Scenario

In the first scenario, equimolar concentrations (1 M) of A and B are initially charged to the reactor. Reactivity ratios are 0.6 and 0.4, respectively. The amount of initiator is 3% of the total concentration of monomer with a tenfold proportion of RAFT agents. Figure 22 highlights the characteristics of the batch reactor as the reaction progresses.

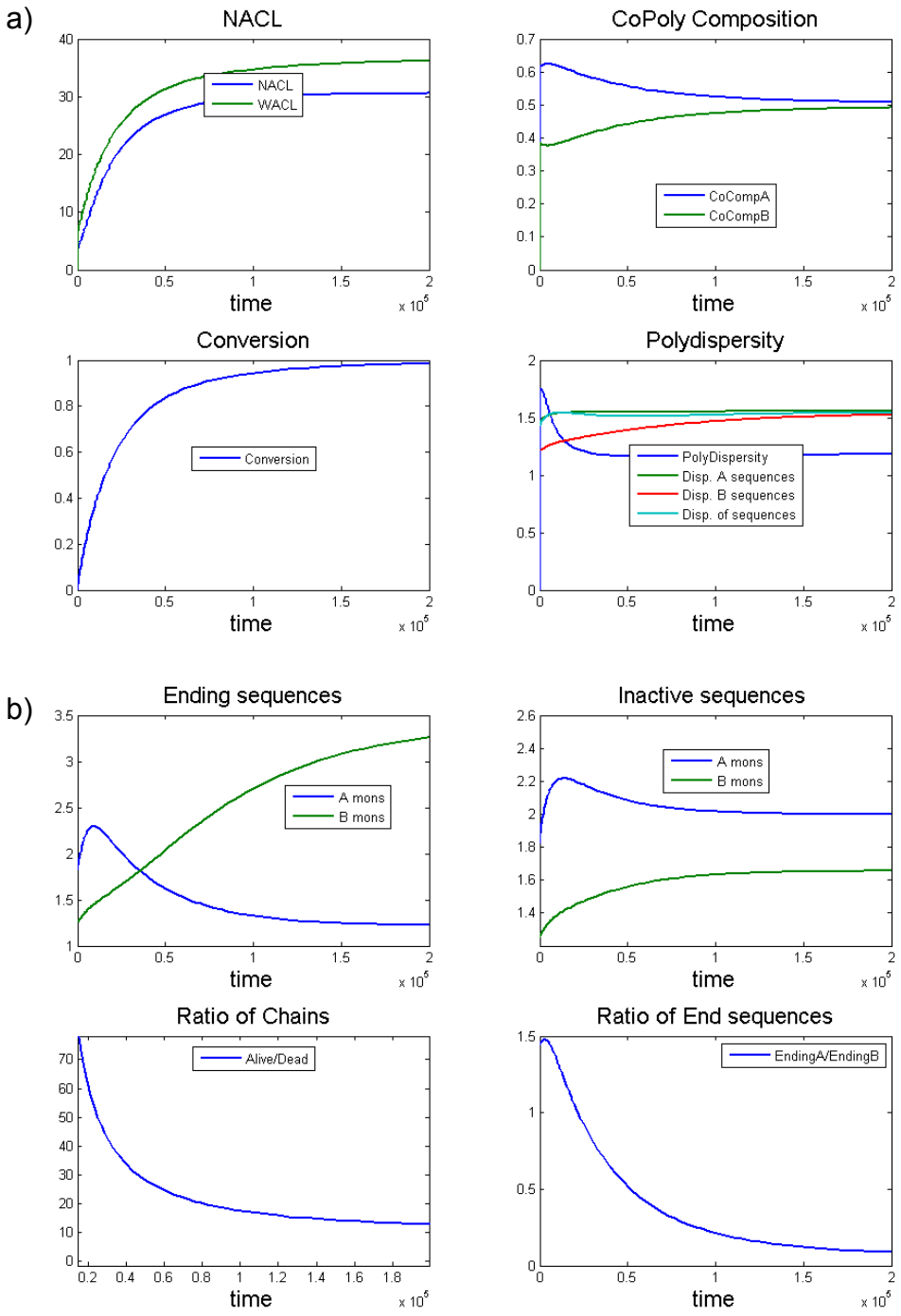

Figure 22: a) NACL, copolymer composition, conversion and dispersity plotted versus time. b) Ending sequences, inactive sequence, ratio of living to dead chains, and ratio of end sequences plotted versus time.

A degree of polymerization of 30.8 is reached with a polydispersity of 1.18. Living chains are much more prevalent at the end of the reaction, justifying the

neglect of the effect of dead chains on the geometric inferences, which are elucidated below. The small amount of dead polymers is the cause of the deviation of the polydispersity from the value of 1 (a purely living system). Using our sequence model, the copolymer composition of 50.8% of monomer A is reached. As Wang has pointed out, different reactivity ratios result in "composition drift" during the course of a reaction [23], which is clearly the case in this reaction. The copolymer composition of A monomer begins at 62.1% at the beginning of the reaction and slowly declines to the final value of 50.8%. There is also a shift in the ratio of end sequences from favoring 'A' to 'B' at the beginning of the polymerization to 10X as many polymers ending in a 'B' sequence to an 'A' sequence. This indicates that "composition drifting" occurs, where more of the B monomer is being added to the polymer at the end of the reaction cycle. This is highlighted by the average ending of a 'B' sequence consisting of over 3 monomer units.

The average inactive sequence of A and B monomers is 2.00 and 1.62 respectively. As the figure shows, while a 50.8% copolymer composition of A would seemingly indicate a repeated series of one A and one B monomer polymerized; in fact, a longer string of A's and B's polymerize. With the average inactive sequence of B's totaling 1.6, every 3rd series of two A and two B monomers, there is a series of two A monomers and 2 B monomers. Since at the start of the reaction, end sequences of 'A' monomers were more prevalent than 'B' monomers, the first sequence is of 'A' monomers with a length of 2.0 from the average end sequence. The dispersities of the sequences are all at approximately 1.5, indicating that the sequences are fairly

uniform. The following graphic in Figure 23 presents the snapshot of the process with a “cartoon” polymer composition inferred from the sequence data.

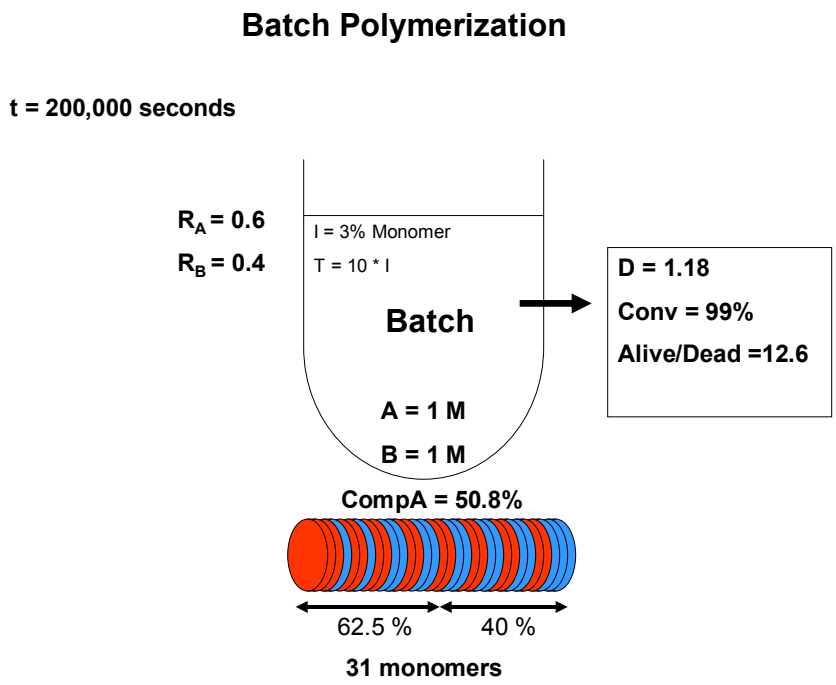

Figure 23: Flow diagram of process with cartoon "snapshot" of simulated polymer

This “typical” polymer is only presented as an approximate representation of the polymerization. In the cartoon, the number of A and B monomers total 16 and 15, respectively, which totals a copolymer composition of 51.6% of ‘A’ monomer. The average internal sequence of A and B of the “typical” polymer is 2.00 and 1.71, respectively. As can be seen, the cartoon illustrates a polymer that is rich in ‘A’ monomer at the head and ‘B’ monomer at the tail. The characteristics of the cartoon and the actual simulated polymer match well, justifying the presentation of the cartoon as a rough snapshot of the polymer segment.

2nd Batch Scenario

In the second batch simulation, 2 and 1 molar concentrations of A and B are initially charged to the reactor, and the reactivity ratios are adjusted to 2 and 0.5,

respectively. Following the addition of initiator as 3% of the total concentration of monomer, and RAFT agents as tenfold the amount of initiator, the polymerization begins, as Figure 24 illustrates.

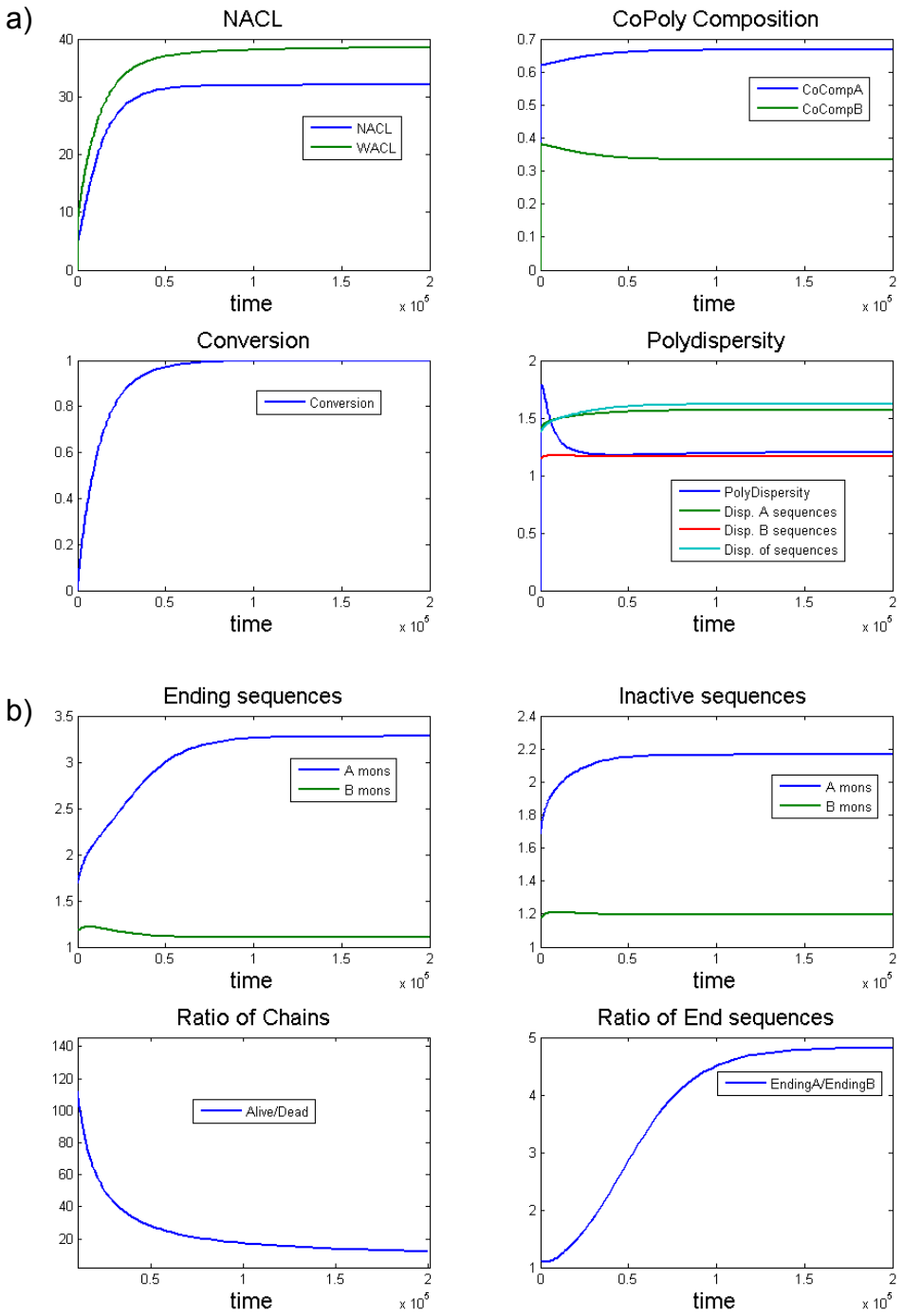

Figure 24: a) NACL, copolymer composition, conversion and dispersity plotted versus time. b) Ending sequences, inactive sequence, ratio of living to dead chains, and ratio of end sequences plotted versus time.

A desirable ratio of 11.6 living to dead polymer chains is determined at the end of the reaction with a low polydispersity of 1.20. While a 67% copolymer composition of ‘A’ would indicate a repeated series of two ‘A’ monomers polymerizing followed by a ‘B’ monomer, due to reactivity ratios, occasionally a longer string of ‘A’ and ‘B’ monomers polymerize. With the average inactive sequence of ‘A’ and ‘B’ totaling 2.18 and 1.2, approximately every fifth series of two ‘A’ and one ‘B’ monomer, there is a series of 3 A monomers and 2 B monomers. Throughout the reaction, the end sequence always favor ‘A’ monomer, with the ratio of ‘A’ to ‘B’ end sequences rising from just above 1 at the beginning of the polymerization to nearly 5 at the end of the polymerization with an average end sequence length of 3.2 monomer units. With twice as many ‘A’ monomers as ‘B’ monomers in the feed, this was expected. With this information, a “typical” polymer can be determined. The dispersities of the ‘A’ and ‘B’ sequences were 1.55 and 1.18, respectively. The higher dispersity of ‘A’ sequences is expected, considering it has a higher concentration and reactivity ratio; this indicates the uniformity of the ‘B’ sequences is higher than the uniformity of the ‘A’ sequences. The following graphic in Figure 25 presents a snapshot of the process.

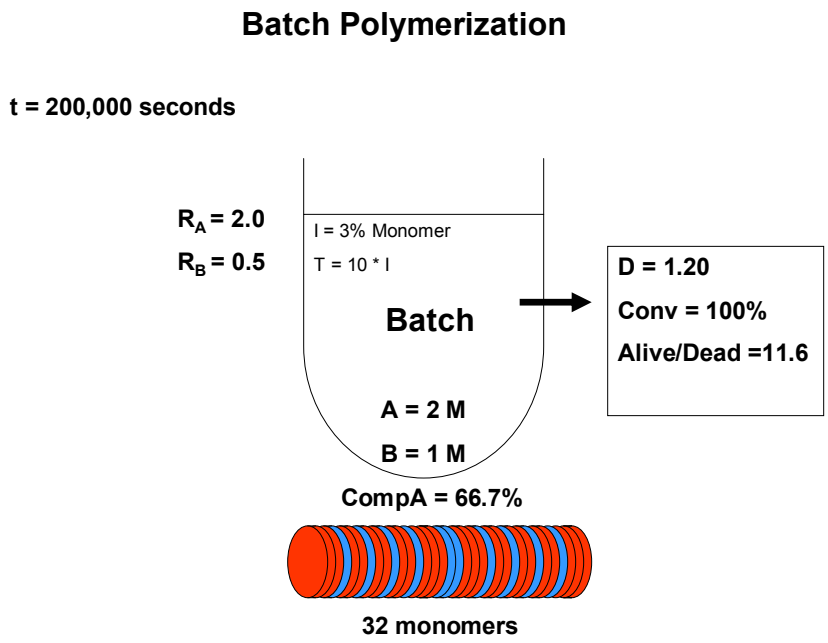

Figure 25: Flow diagram of process with cartoon "snapshot" of simulated polymer

Shot-Polymerizations

Other polymerization scenarios can be performed using a batch reactor. Shot-polymerizations, consist of adding reactants to a batch and allowing it to polymerize for a predetermined period, and then adding more monomer to add to the existing polymer. Semibatch, shot or series of continuous reactors provide the best paths towards fine-tuning the polymer. The final state of the chain model after the first time interval is fed as the initial condition of Reactor 2 in the simulation, plus the additional monomeric feed. Therefore at the end of the second time interval, the molecular weight distribution and conversion simulated by the chain model is of the entire polymer (i.e. both polymer segments). The sequence model, however, is reset after the first time interval to zero, allowing a fresh sequence distribution of the

second polymer segment. Therefore, a complete composition analysis can be done on both polymer segments. If it were desirable, the chain model could have also been reset in regards to these parameters, but more information is directly garnered without it. Three shot-polymerizations with different monomeric properties and feed conditions were simulated below.

1st Shot-Polymerization Scenario

The first series has an initial charge of 3 M and 1 M of A and B monomer, respectively. Reactivity ratios were set at 0.6 and 0.4. Following the addition of initiator as 3% of the total concentration of monomer, and RAFT agents as tenfold the amount of initiator, the polymerization begins, as Figure 26 illustrates.

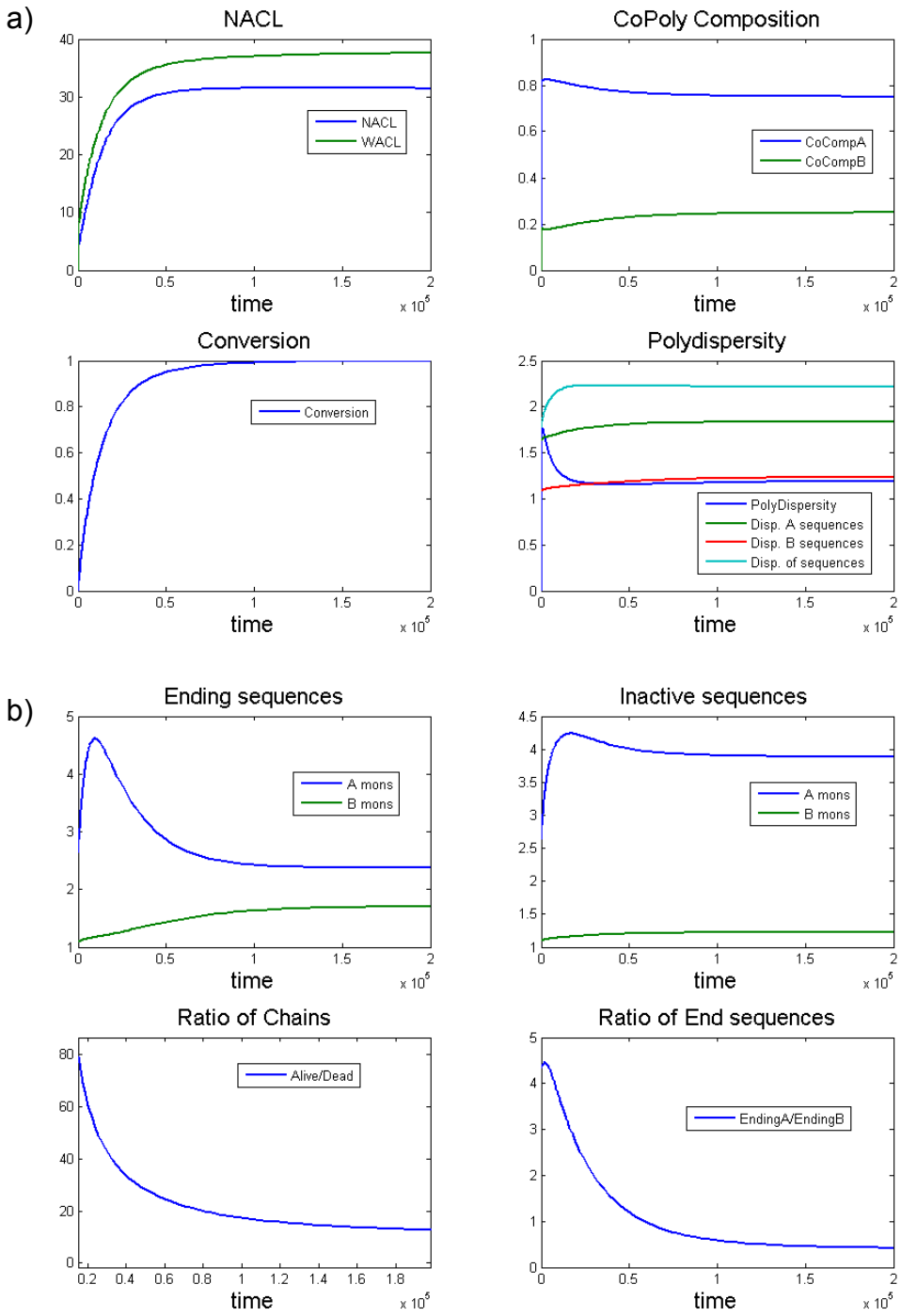

Figure 26: a) NACL, copolymer composition, conversion and dispersity plotted versus time. b) Ending sequences, inactive sequence, ratio of living to dead chains, and ratio of end sequences plotted versus time.

Figure 26 shows that a NACL of 32 with a conversion of 100% is achieved at the end of the first interval. A low polydispersity of 1.20 is obtained with a living to

dead ratio of 12.6. With a 100% conversion and a 3:1 molar feed ratio, the expected copolymer composition of 75% is obtained. The ratio of end sequences initially strongly favored ‘A’ monomers, but at the end of the reaction nearly three times as many chains ended in a sequence of ‘B’ monomers with an average ending close to 2 monomers. Since the feed consisted of 3 times as many ‘A’ monomers, this indicates a great deal of composition drifting. With the average inactive sequence of ‘A’ and ‘B’ totaling 3.81 and 1.21, a clear picture of the polymer at the end of the first batch reactor is formed with a small ‘B’ monomer-rich segment at the tail end of the polymer. The dispersities of the sequences illustrate the lack of sequence uniformity with dispersity of ‘A’ sequences, ‘B’ sequences, and all sequences totaling 1.83, 1.22 and 2.23, respectively. The discrepancy between the low polydispersity and high dispersity of sequences illustrate that although the polymer is very monodisperse in size, its composition is quite irregular. Before the 2nd reactor run commences, 1 M and 3 M concentrations of ‘A’ and ‘B’ are fed to the reactor. The sequence model is reset to determine the characteristics of the next segment of polymerization, which is shown in Figure 27.

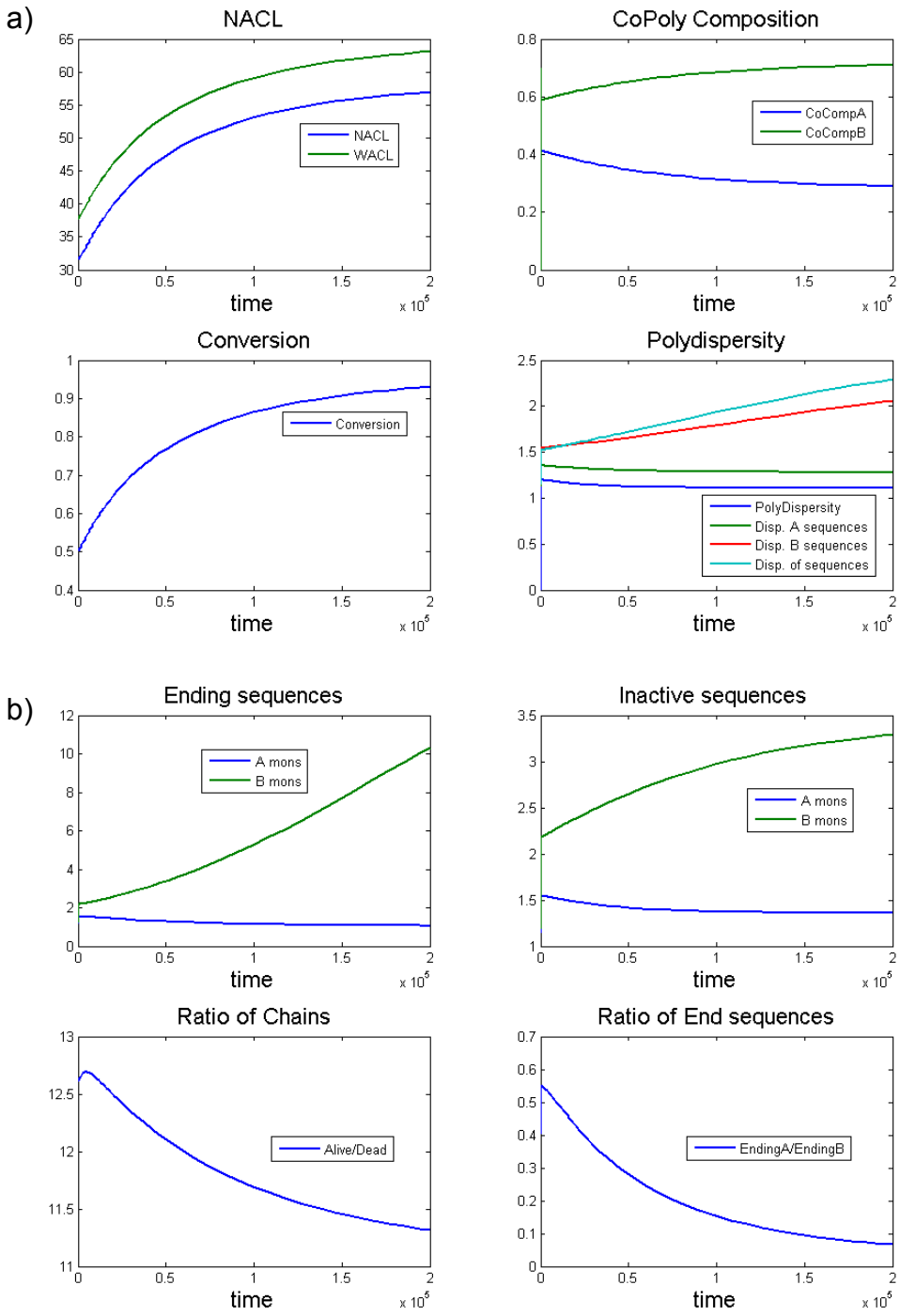

Figure 27: a) NACL, copolymer composition, conversion and dispersity plotted versus time. b) Ending sequences, inactive sequence, ratio of living to dead chains, and ratio of end sequences plotted versus time.

Figure 27 shows that a NACL of 57.2 with a conversion of 93.1% is achieved at the end of the second batch polymerization. Low polydispersity and a high living to

dead ratio are maintained. Composition drifting is even more evident than in the first reactor as the copolymer composition of 'A' monomer in the polymer segment begins at 40.0% and gradually reduces to 29.1% at the end of the polymerization. The ratio of 'A' to 'B' end sequences always favors B, which indicates both the start and end sequence, with the average ending of 'B' over 10 monomers. With the average inactive sequences of 'A' and 'B', a polymer segment that is disproportionately end-heavy in 'B' is determined. Of note, is that because of the very high monomeric ending of 'B', the inactive sequence of 'B' is skewed slightly more. The dispersities of the sequences once again is high for the highly concentrated component with the dispersity of 'A' sequences, 'B' sequences, and all sequences totaling 1.31, 2.02 and 2.27, respectively. With this information, a cartoon snapshot is once again presented in Figure 28 to highlight the aspects of this polymerization.

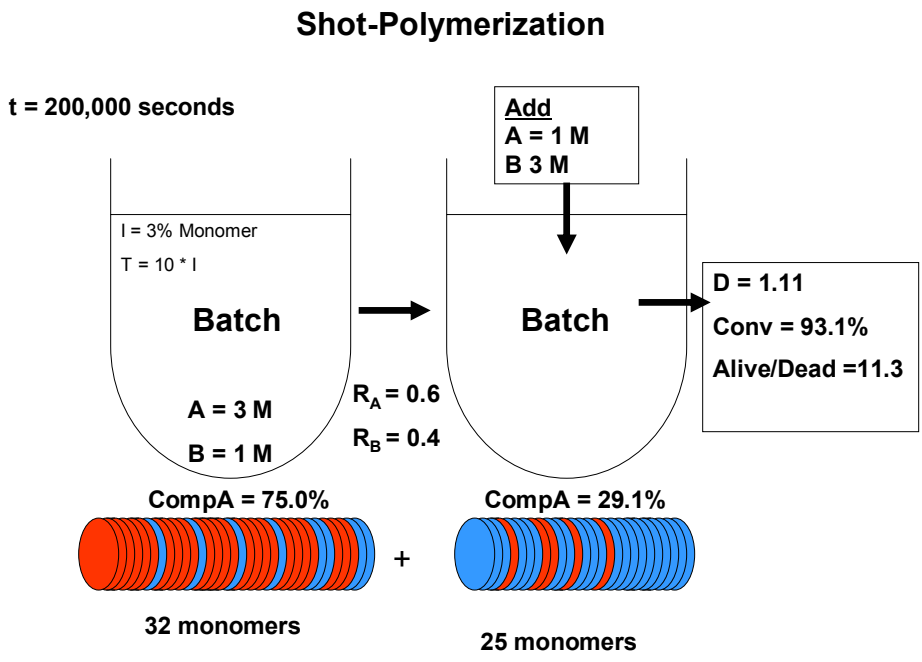

Figure 28: Flow diagram of process with cartoon "snapshot" of simulated polymer

2nd Shot-Polymerization Scenario

The second shot-polymerization that was simulated has an equimolar initial charge of 1M. Reactivity ratios were set at 2.0 and 0.5 for A and B, respectively. Following the addition of initiator as 3% of the total concentration of monomer, and RAFT agents as tenfold the amount of initiator, the polymerization begins, as Figure 29 illustrates.

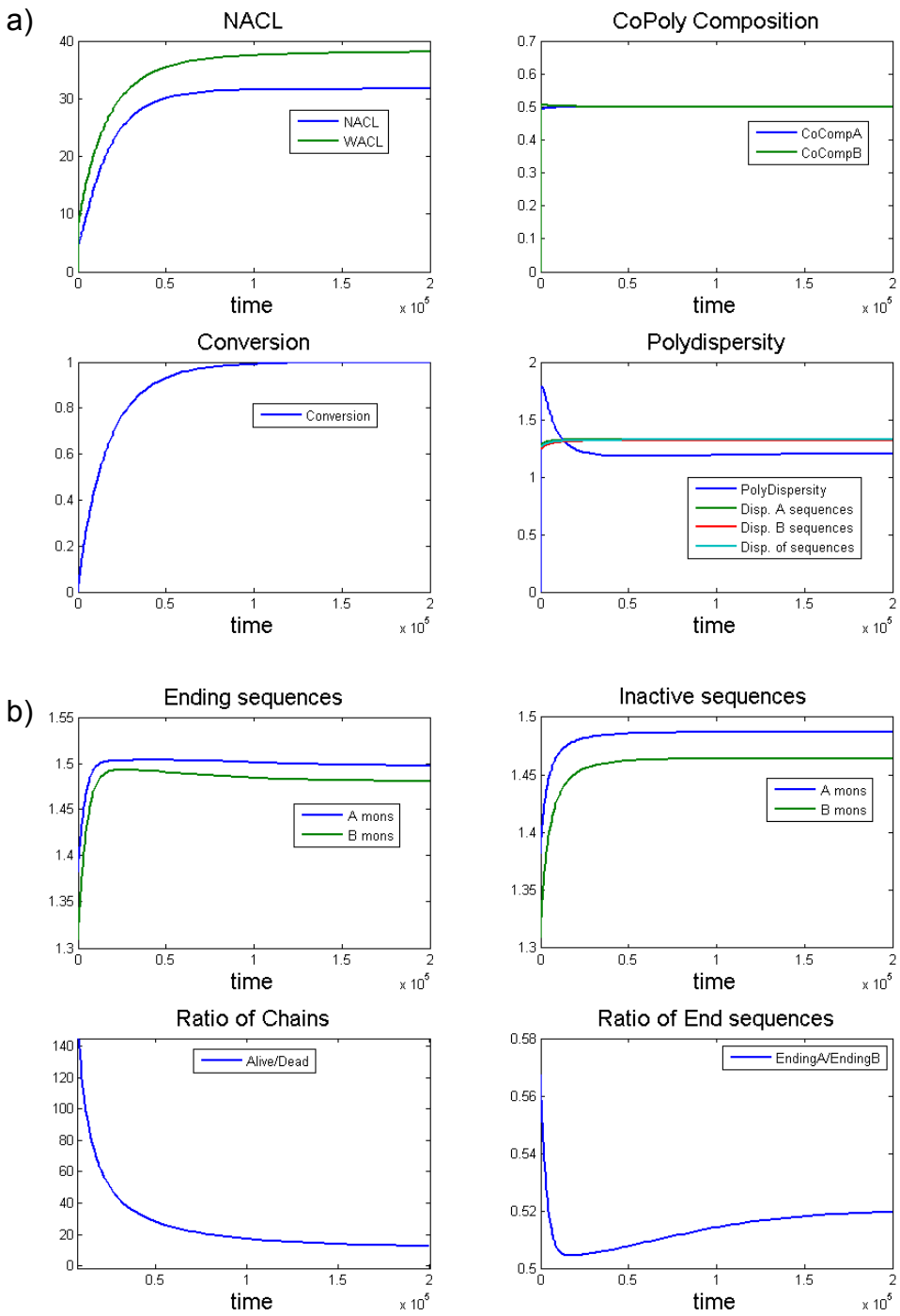

Figure 29: a) NACL, copolymer composition, conversion and dispersity plotted versus time. b) Ending sequences, inactive sequence, ratio of living to dead chains, and ratio of end sequences plotted versus time.

Figure 29 shows that a NACL of 32.1 with a conversion of 100% is achieved at the end of the first reactor. A low polydispersity of 1.20 is obtained with a living to

dead ratio of 12.6. With a 1:1 molar ratio and a 100% conversion, the expected copolymer composition of 50% is obtained. However, further inspection of the sequence analysis shows that the reactivity ratios slightly influenced the sequence structure. The ratio of end sequences strongly favored the less reactive 'B', and the average ending of 'B' was approximately 1.5 monomer units. With the average inactive sequence of 'A' and 'B' totaling 1.49 and 1.46, the influence of the reactivity ratios from the equivalent values of 1.50 is shown. However, composition drift did not occur as the end sequences approximately match the internal sequence values throughout the polymerization. This is due to the very similar reactivity ratios (0.6 and 0.4) and equivalent feeds. The low polydispersity and low dispersity of the sequences illustrate both a uniform size and sequence lengths. Before the 2nd reactor runs, 1 M and 0.25 M concentrations of 'A' and 'B' are fed to the reactor. The sequence model is reset to determine the characteristics of the next segment of polymerization, which is shown in Figure 30.

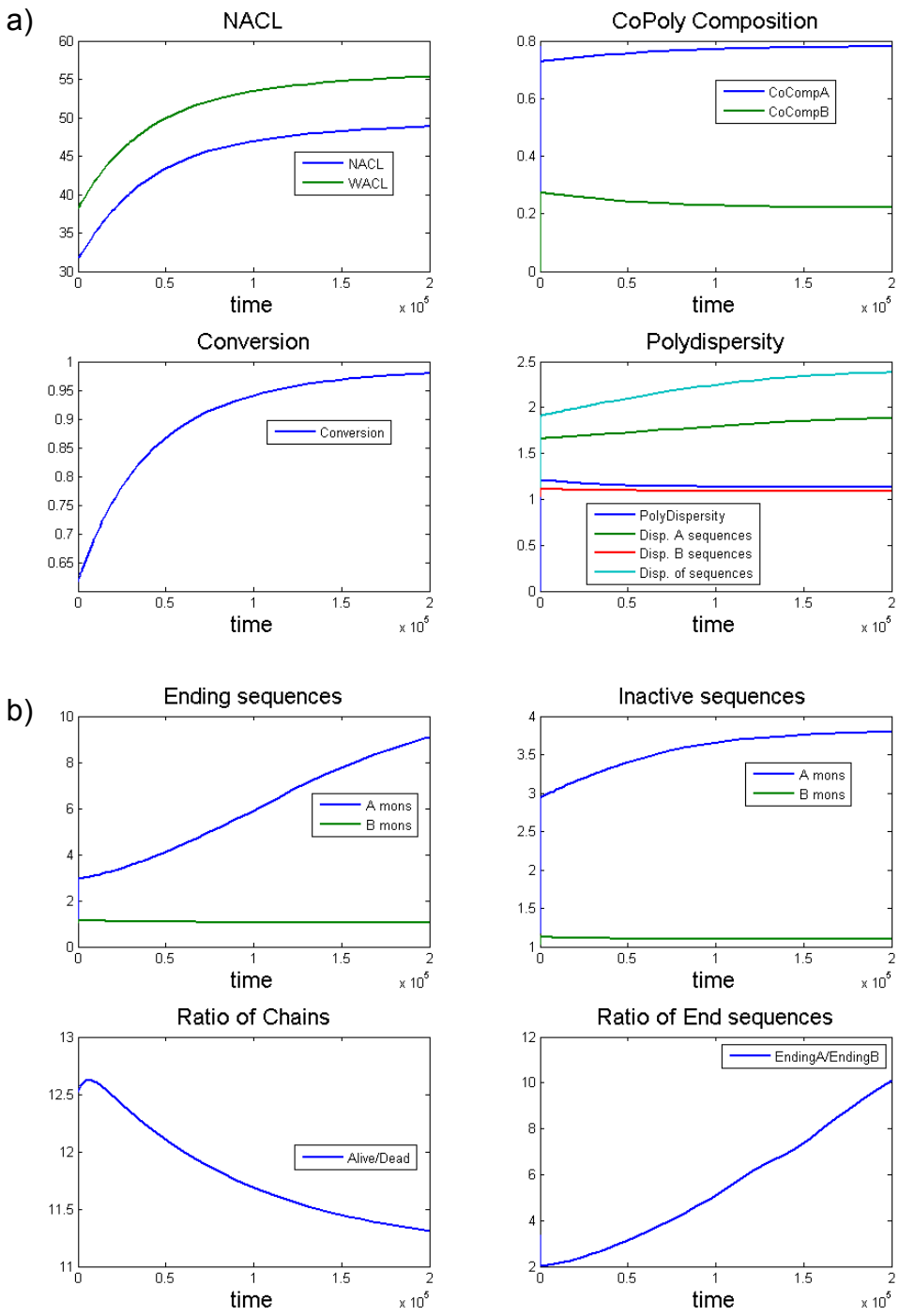

Figure 30: a) NACL, copolymer composition, conversion and dispersity plotted versus time. b) Ending sequences, inactive sequence, ratio of living to dead chains, and ratio of end sequences plotted versus time.

Figure 30 shows that a NACL of 48.8 with a conversion of 98.1% is achieved at the end of the second batch polymerization. Therefore, the polymer has been

elongated by approximately 17 monomers. Low polydispersity and a high living to dead ratio are maintained. However, composition drifting is evident in the 10X ratio of 'A' to 'B' end sequences, with the average end sequence of 'A' approximately 9 monomers. Copolymer composition of 'A' is about 77% at the end of the polymerization, rising from 72% at the beginning, which also indicates composition drifting. With the average inactive sequences of 'A' and 'B', a polymer that is very end-heavy in 'A' is determined. The dispersities of the sequences are much higher at the end of the 2nd time, while the polydispersity decreased slightly. The polymer is more monodisperse in size, but the second polymer segment has a more non-uniform sequence length. With the above information, a cartoon snapshot is once again presented in Figure 31 to highlight the aspects of this polymerization.

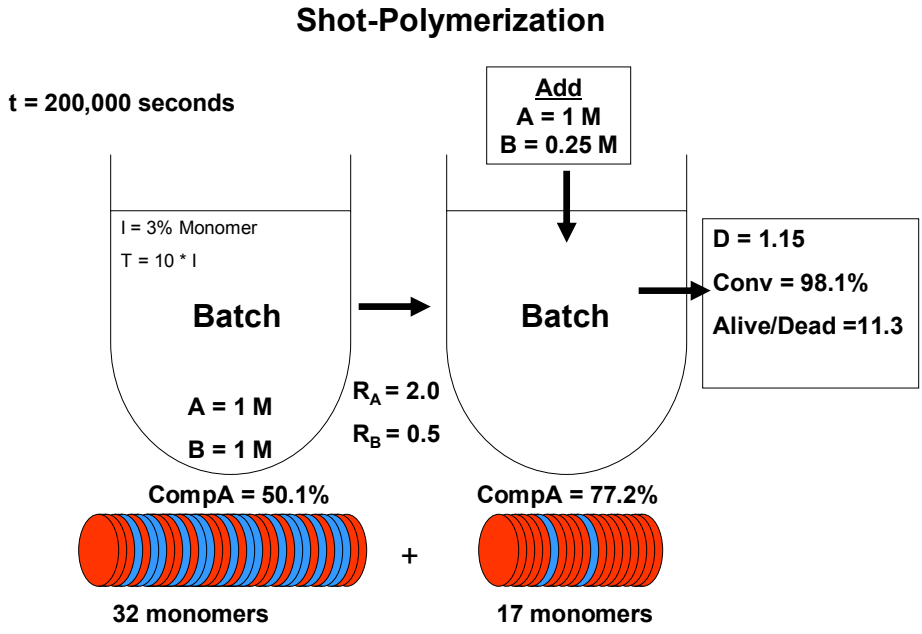

Figure 31: Flow diagram of process with cartoon "snapshot" of simulated polymer

3rd Shot-Polymerization Scenario

The last shot-polymerization is simulated to produce a polymer with a higher degree of polymerization. As such, the RAFT kinetic rate coefficients were reduced by an order of magnitude to 10^4. As in the work of Pinto, RAFT parameters have been changed arbitrarily[40]. Correspondingly, the amount of initiator was reduced to 2% of the total concentration of monomer. Reactivity ratios were set at 2.0 and 0.5 for A and B, respectively. With an initial charge of 3 M and 2 M of A and B, respectively, and RAFT agents as tenfold the amount of initiator, the polymerization begins, as Figure 32 illustrates.

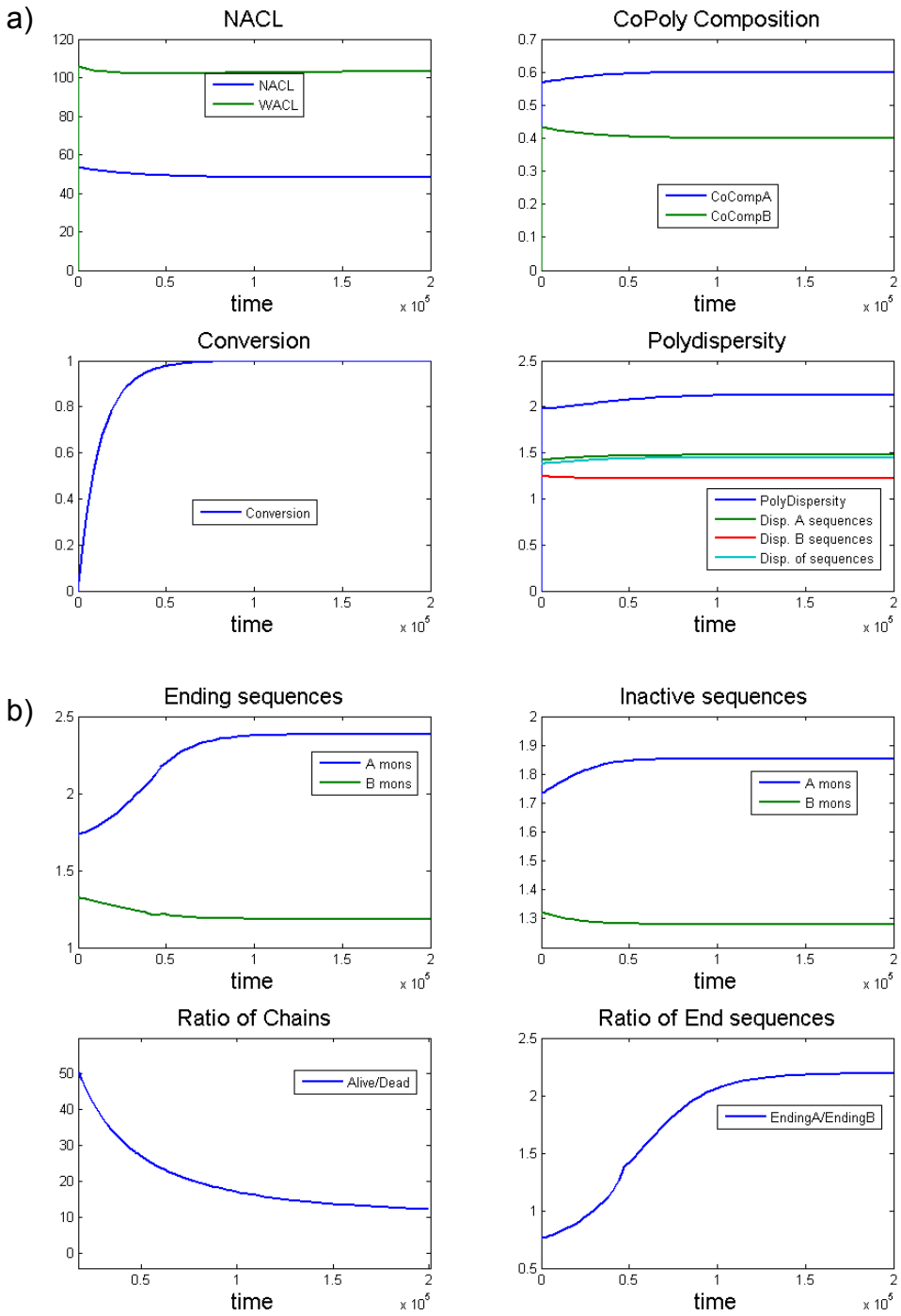

Figure 32: a) NACL, copolymer composition, conversion and dispersity plotted versus time. b) Ending sequences, inactive sequence, ratio of living to dead chains, and ratio of end sequences plotted versus time.

Figure 32 shows that a NACL of 48 with a conversion of 100% is achieved at the end of the first reactor. As expected with a lower rate of RAFT transfer and RAFT

initiation rate constants, polydispersity is considerably higher than previous simulations with a value of 2.10. However, a high living to dead ratio of 12.3 is still maintained. With a 3:2 molar ratio, the expected copolymer composition of 'A' monomer of 60% is obtained with full conversion. However, further inspection of the sequence analysis shows that composition drifting did not produce a simple sequence structure of three 'A' monomers followed by two 'B' monomers. The ratio of end sequences favored B at the beginning of the polymerization while it strongly favored 'A' at the end of the simulation with the average ending of 'A' monomers close to 2.4 monomers. With the average inactive sequence of 'A' and 'B' totaling 1.85 and 1.29, a clear picture of the polymer at the end of the first batch reactor is formed. The dispersities of the sequences illustrate fairly uniform sequence length with dispersity of 'A' sequences, 'B' sequences, and all sequences totaling 1.47, 1.22 and 1.49, respectively. In this simulation, a relatively high polydispersity and low dispersity of sequences is determined to illustrate that although the polymer not very monodisperse, its sequence length is quite regular. Before the 2nd polymerization run, 2 M and 3 M concentrations of 'A' and 'B' are fed to the reactor. The sequence model is reset to determine the characteristics of the next segment of polymerization as shown in Figure 33.

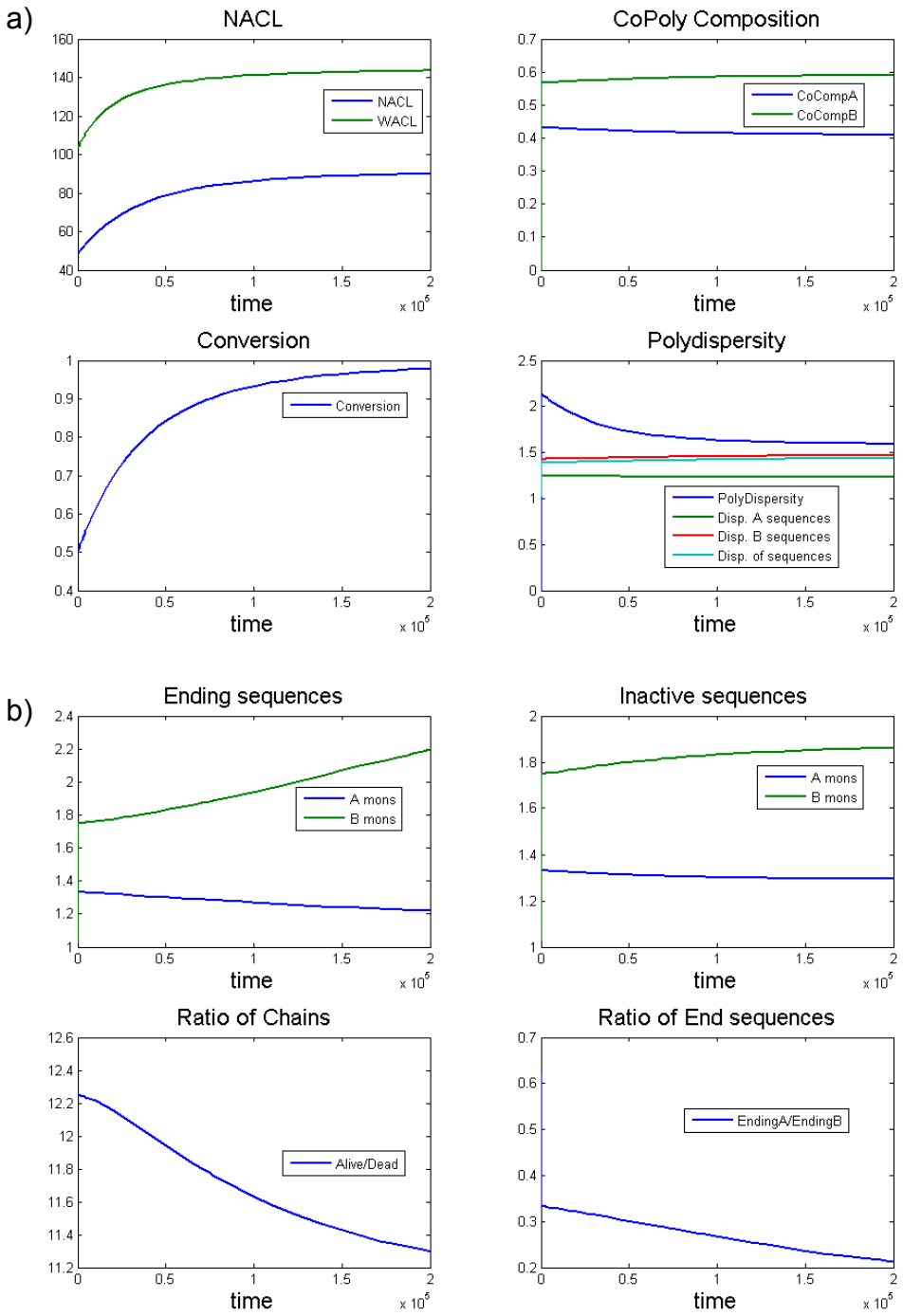

Figure 33: a) NACL, copolymer composition, conversion and dispersity plotted versus time. b) Ending sequences, inactive sequence, ratio of living to dead chains, and ratio of end sequences plotted versus time.

Figure 33 shows that a NACL of 90 with a conversion of 98% is achieved at the end of the second batch reactor. Therefore, the polymer has been elongated by

approximately 42 units. The polydispersity has been lowered to 1.59 and a high living to dead ratio is maintained. The composition of copolymer 'A' in this segment is determined to be the expected 40%. The ratio of 'A' to 'B' end sequences is 0.21 with the average ending of 'B' over 2 monomers. With the average inactive sequences of 'A' and 'B' totaling 1.84 and 1.33, respectively. The dispersities of the sequences and polydispersity are all near the value of 1.5, which illustrate a balance between size uniformity and composition uniformity. With this information, a cartoon snapshot is once again presented in Figure 34 to highlight the aspects of this polymerization.

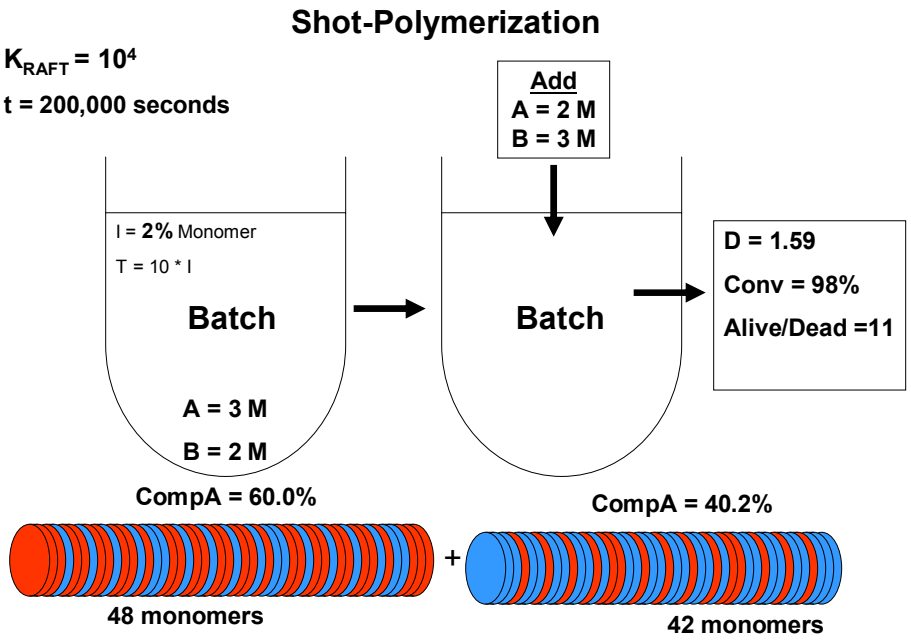

Figure 34: Flow diagram of process with cartoon "snapshot" of simulated polymer

Summary

These examples have illustrated the power of the sequence model when combined with a chain model that can characterize the MWD. The original method of using population balances in regards to sequences has shown revealing information

about copolymer structure that results from composition drift due to reactivity ratios. Shot-polymerizations have been simulated to fine-tune polymers with gradient copolymers produced as well as large block copolymer segments. This manipulation of reactor conditions will be extended in Chapter 4 to series of CSTR and PFR reactors.

Chapter 4: Series of Reactors

In this chapter, CSTR (continuous stirred tank reactor) and PFR (plug flow reactor) are considered in stand-alone, and in series. CSTR and PFR reactors are in widespread use throughout industry and a measure of the efficacy of the sequence model would be incomplete without an analysis of polymerizations with these reactors. Series reactions allow a simple path towards manipulating reactor conditions and feeds to design a specified copolymer. CSTR and PFR reactors are used in concert for they complement each others strengths and weaknesses. CSTR reactors typically have low monomer conversion, but the continuous input of fresh feed at constant concentrations provides a uniform constant copolymer composition. Conversely, PFR reactors (which are essentially batch reactors) have a high conversion, but are susceptible to the same compositional drifting as batch reactors. Hence a series could produce constant uniform polymer segments followed by gradient polymer segments while obtaining a high conversion. Five different scenarios of CSTR and PFR reactors in series are analyzed to produce this controlled architecture.

CSTR Reactors: Stand-alone and in series

1st Scenario

The first scenario is simulated as a proof of concept to illustrate that the chain and sequence models can determine the characteristics of a CSTR. In the first scenario, equimolar concentrations (2.5 M) of 'A' and 'B' are fed to a CSTR. Reactivity ratios are set at 2.0 and 0.5, respectively. The amount of initiator is increased to .5% of the total concentration of monomer with a nine-fold proportion of

RAFT agents. These conditions will highlight this proof-of-concept scenario. Figure 35 shows the characteristics of this CSTR as the reaction progresses.

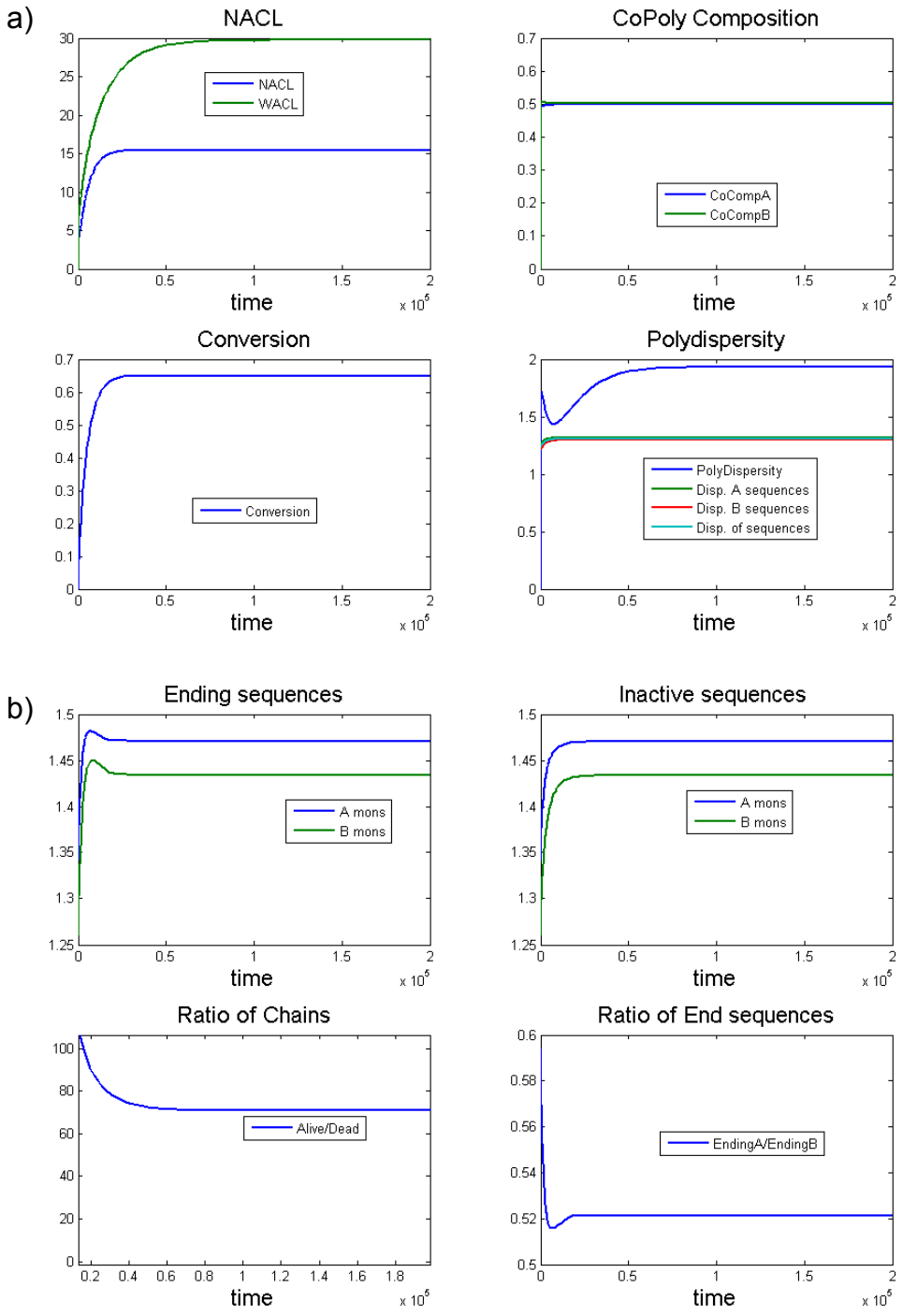

Figure 35: a) NACL, copolymer composition, conversion and dispersity plotted versus time. b) Ending sequences, inactive sequence, ratio of living to dead chains, and ratio of end sequences plotted versus time.

As Figure 35 shows, all characteristics simulated by the chain model reach steady-state at approximately 100,000 seconds, approximately 6.67 times greater than the residence time. However, the copolymer composition reaches a constant value after a short transient period while all aspects of the reactor has not yet reached steady state. This underscores the primary strength of the CSTR: it eliminates composition drifting once steady state is reached. The sequence model highlights the lack of composition drifting by the equivalent average end and internal sequence for each monomer determined by the sequence model. Shortly after the polymerization, the ending and internal sequences of 'A' both reach 1.47 monomers while the ending and internal sequences of 'B' both reach 1.43 monomers. The degree of polymerization in this segment totaled only 15.2, with a conversion of 65.1%. Such low numbers are the nature of CSTR reactors when combined with RAFT agent. A polydispersity of 1.96 is predicted by the chain model with a 50.1% copolymer composition of 'A' monomer. A truly living system should have a polydispersity of 2 in a CSTR due to the residence time distribution[41], but the small amount of dead polymers present in the reactor lowers the polydispersity to 1.96. The dispersities of all of the sequences are at a low value of 1.28, indicating that compositional and sequence uniformity was produced, although predictably, size uniformity was not. A highly favorable aspect of CSTR reactors is the high ratio of living to dead sequences produced: a very high ratio of 72 living to dead polymers is obtained at steady-state. The end sequence of 'B' monomers is favored 3:2 over 'A' monomers with the average end sequence totaling 1.43 monomers. With the above information, the compositional nature of the

polymer segment can be approximated as was done in Chapter 3 to create a "typical" polymer. The snapshot of this CSTR is shown in Figure 36.

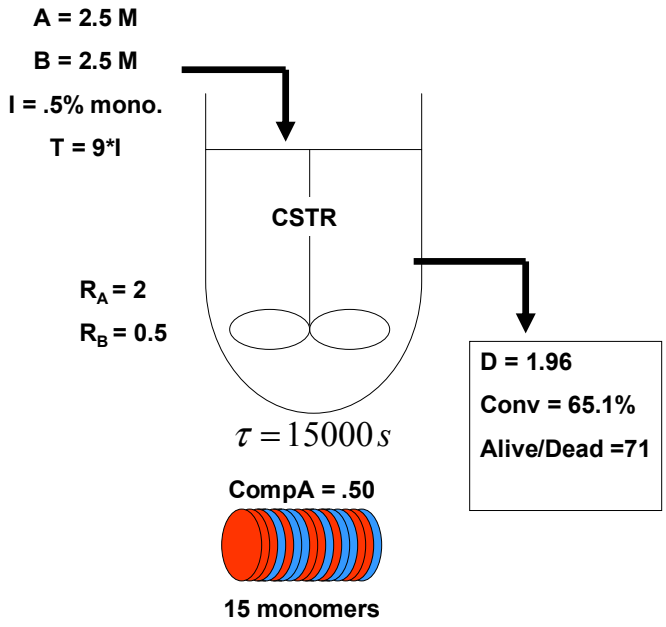

Figure 36: Flow diagram of process with cartoon "snapshot" of simulated polymer

2nd Scenario

The second scenario is a series of two CSTR reactors. While the first scenario was a proof-of-concept, the second is to develop a single polymer that is dominated by one polymer in the first segment, and the other polymer in the second segment. Reactivity ratios are set at 0.6 and 0.4, respectively and the reactor has a residence time of 15000 seconds. The first reactor has a feed of 2.5 M and 1.0 M of 'A' and 'B', respectively. With the same corresponding amounts of initiator and RAFT agent as in the first scenario, the polymerization is simulated. The characteristics of the product of the first reactor as a function of time are shown in Figure 37.

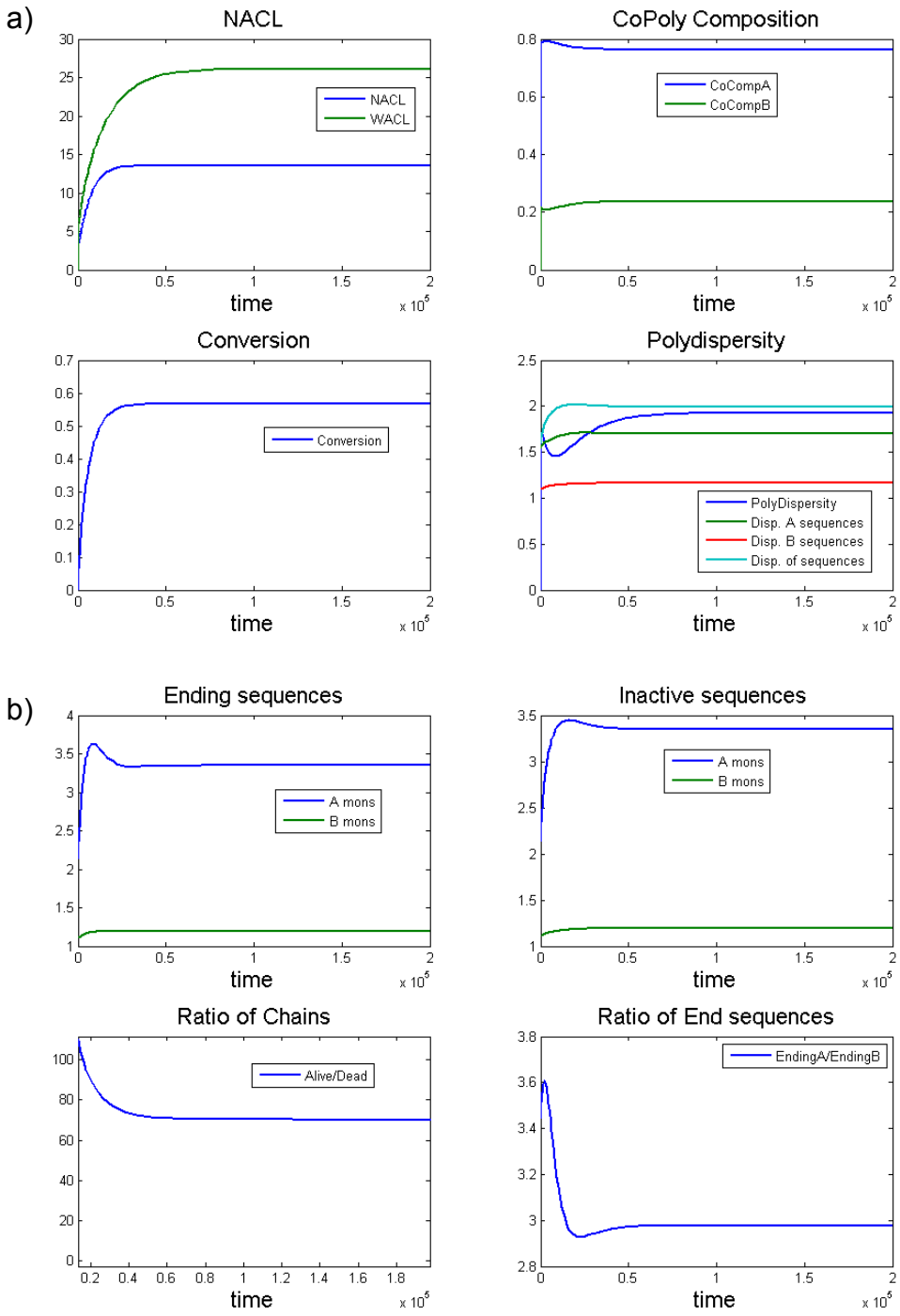

Figure 37:a) NACL, copolymer composition, conversion and dispersity plotted versus time. b) Ending sequences, inactive sequence, ratio of living to dead chains, and ratio of end sequences plotted versus time.

As in the previous scenario, composition drifting is eliminated with the CSTR as Figure 37 shows. This is once again highlighted by the equivalent average end and

internal sequence for each monomer determined by the sequence model. The degree of polymerization in this segment totaled only 14, with a conversion of 57%. Such low numbers are the nature of CSTR reactors when combined with RAFT agent. A polydispersity of 1.91 is predicted by the chain model with a 76% copolymer composition of 'A' monomer. The dispersities of the sequences is also at the high value of 1.99, indicating that neither a high degree of size or sequence uniformity is reached in the first polymer segment. A very high ratio of 71 living to dead polymers is obtained at steady-state. The end sequence of 'A' is favored nearly three-fold over 'B' with the average end sequence greater than 3 monomers. With the average end and internal sequence of 'A' totaling 3.35, and the average end and internal sequence of 'B' totaling 1.25, the compositional nature of the polymer segment can be approximated.

Since steady-state has been reached, the output of the CSTR is fed as a continuous feed to another CSTR. Monomer concentrations of 1 M and 3.5 M of 'A' and 'B' are added to the output stream. The sequence model is reset to determine a fresh analysis of the next polymer segment as shown in Figure 38.

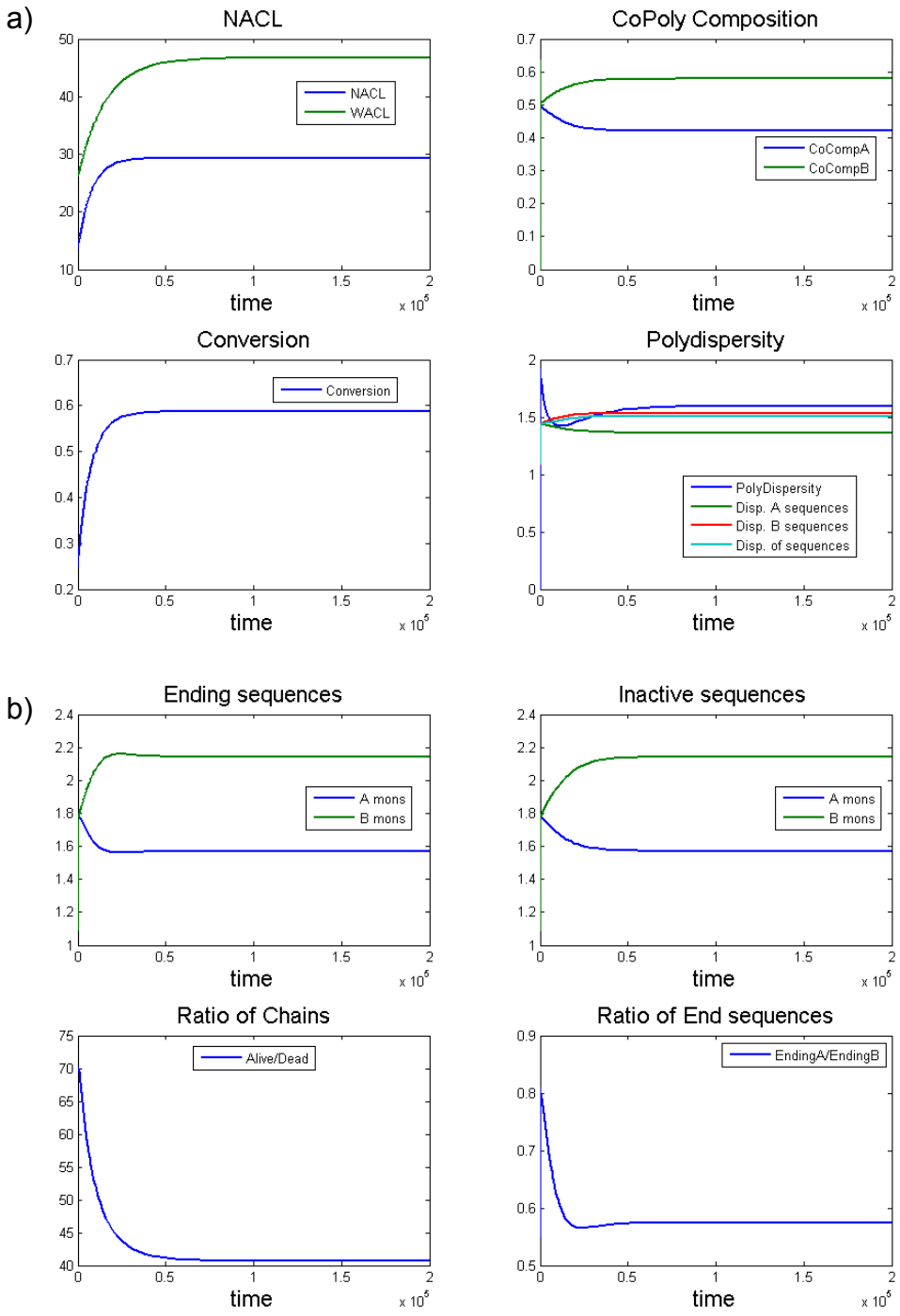

Figure 38: a) NACL, copolymer composition, conversion and dispersity plotted versus time. b) Ending sequences, inactive sequence, ratio of living to dead chains, and ratio of end sequences plotted versus time.

Figure 38 shows that an NACL of 29.1 with a conversion of 58.8% is achieved once the second CSTR reactor reaches steady-state. Therefore, the polymer

has been elongated by approximately 15 units. The polydispersity is lowered to 1.60 and a very high living to dead ratio is maintained. Expectedly, the polydispersity is lowered in a series of CSTR reactors (series of CSTR reactors approach a RTD of a batch reactor) as has been proven theoretically, and experimentally using RAFT by Smulders et al [42]. The ratio of 'A' to 'B' end sequences is 0.58 with the average ending of 'B' over 2 monomer units. Once again, compositional drifting is eliminated at steady state as the ending and internal sequences of A and B are equivalent. The dispersities of the sequences are lower in the second segment than in the first polymer segment, which reveals that the second segment has a more uniform sequence structure. The 41.8% copolymer composition of 'A' monomer highlights an overall polymer that is heavy in 'A' monomer at the head of the polymer and 'B' monomer at the end of the polymer. With this information, a cartoon snapshot is once again presented in Figure 39 to highlight the aspects of this polymerization.

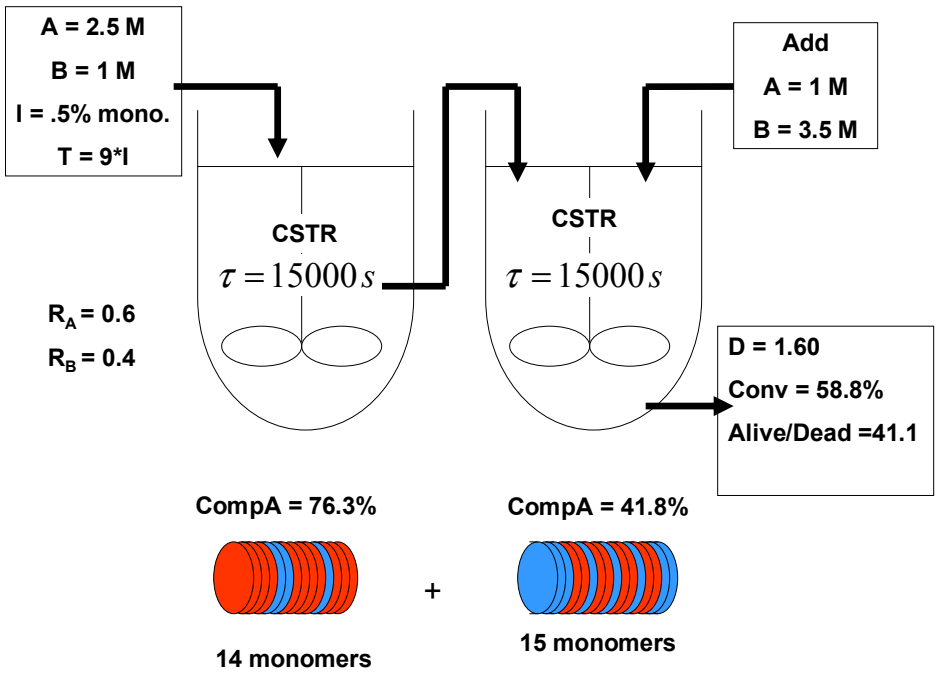

Figure 39: Flow diagram of process with cartoon "snapshot" of simulated polymer

CSTR and PFR Reactors in Series

1st Scenario

The third scenario is a reactor series of a CSTR to a PFR to another CSTR. The PFR is inserted to increase the overall conversion of the process. The goal of this simulation is to combine block copolymer segments with gradient segments and to use PFRs in concert with CSTRs to augment overall conversion in balance with compositional uniformity. Reactivity ratios are set at 2.0 and 0.5, respectively and each reactor has a residence time of 15000 seconds. The first CSTR reactor has a feed of purely 'A' monomer at a concentration of 2.5 M—the simulation inputs a negligible concentration of 'B' monomer to maintain numeric stability. With the same corresponding amounts of initiator and RAFT agent as in the previous scenarios, the polymerization is simulated. The characteristics of the simulation as a function of time are shown in Figure 40.

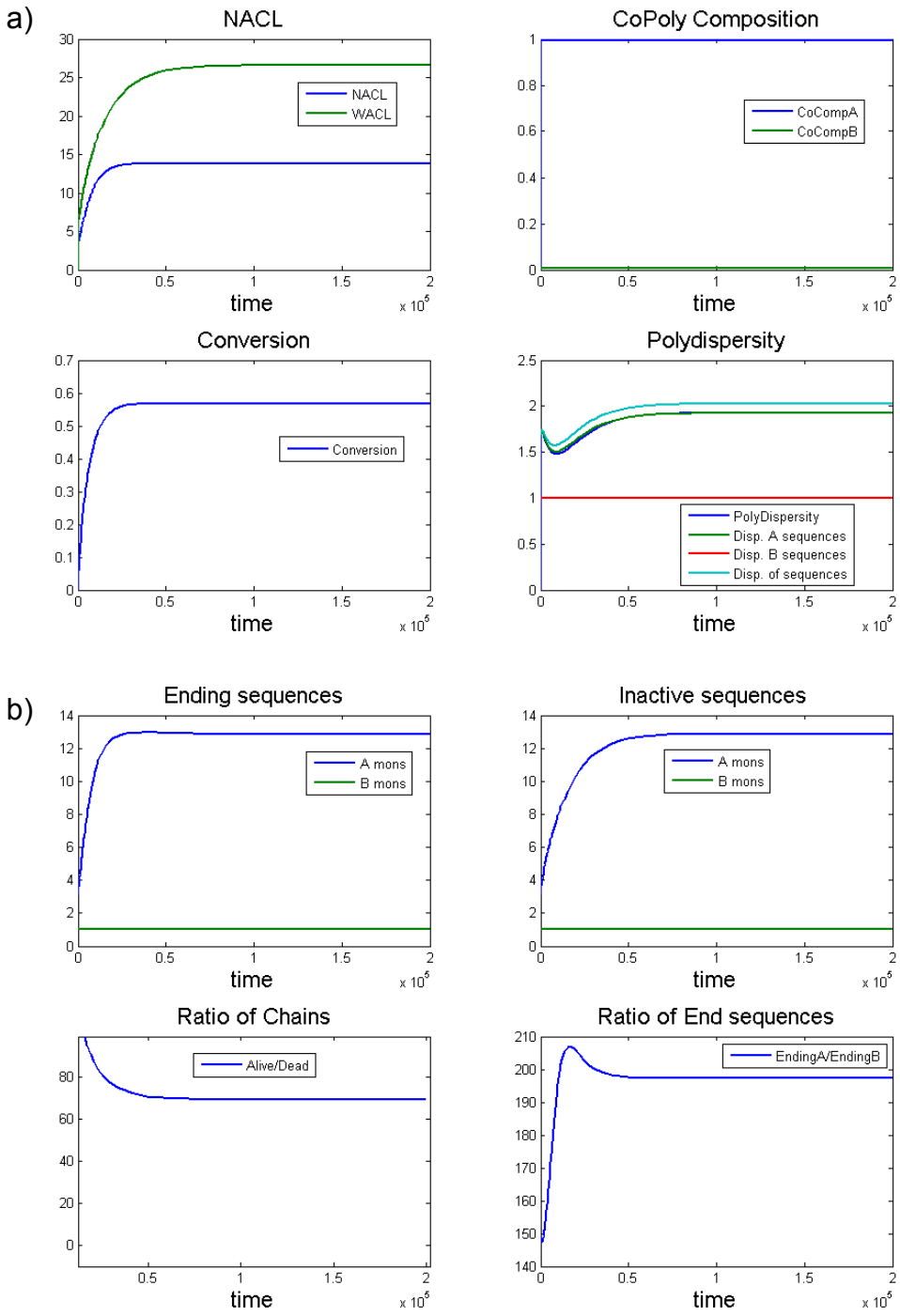

Figure 40:a) NACL, copolymer composition, conversion and dispersity plotted versus time. b) Ending sequences, inactive sequence, ratio of living to dead chains, and ratio of end sequences plotted versus time.

The degree of polymerization in this first segment totaled only 13, with a conversion of 57%. A polydispersity of 1.91 is predicted by the chain model with the

dispersities of the sequences at almost the same value, indicating neither a high degree of size or composition uniformity. A very high ratio of 69 living to dead polymers is obtained at steady-state. The copolymer composition is nearly 100%; therefore a close examination of the sequence model is unnecessary. However, it should be noted that the average end sequence of 'A' monomers and internal sequence (noting that in this case, internal sequences are all "inactive" dead polymers) totals nearly 13, which corresponds to the chain models simulation of an NACL of 13. Since steady-state has been reached, the output of the CSTR is fed as continuous feed to a PFR, which has a residence time of 15000 seconds. In addition, equimolar concentrations (2.5 M) of 'A' and 'B' are added to the feed stream. The sequence model is reset to determine a fresh analysis of the next polymer segment as shown in Figure 41.

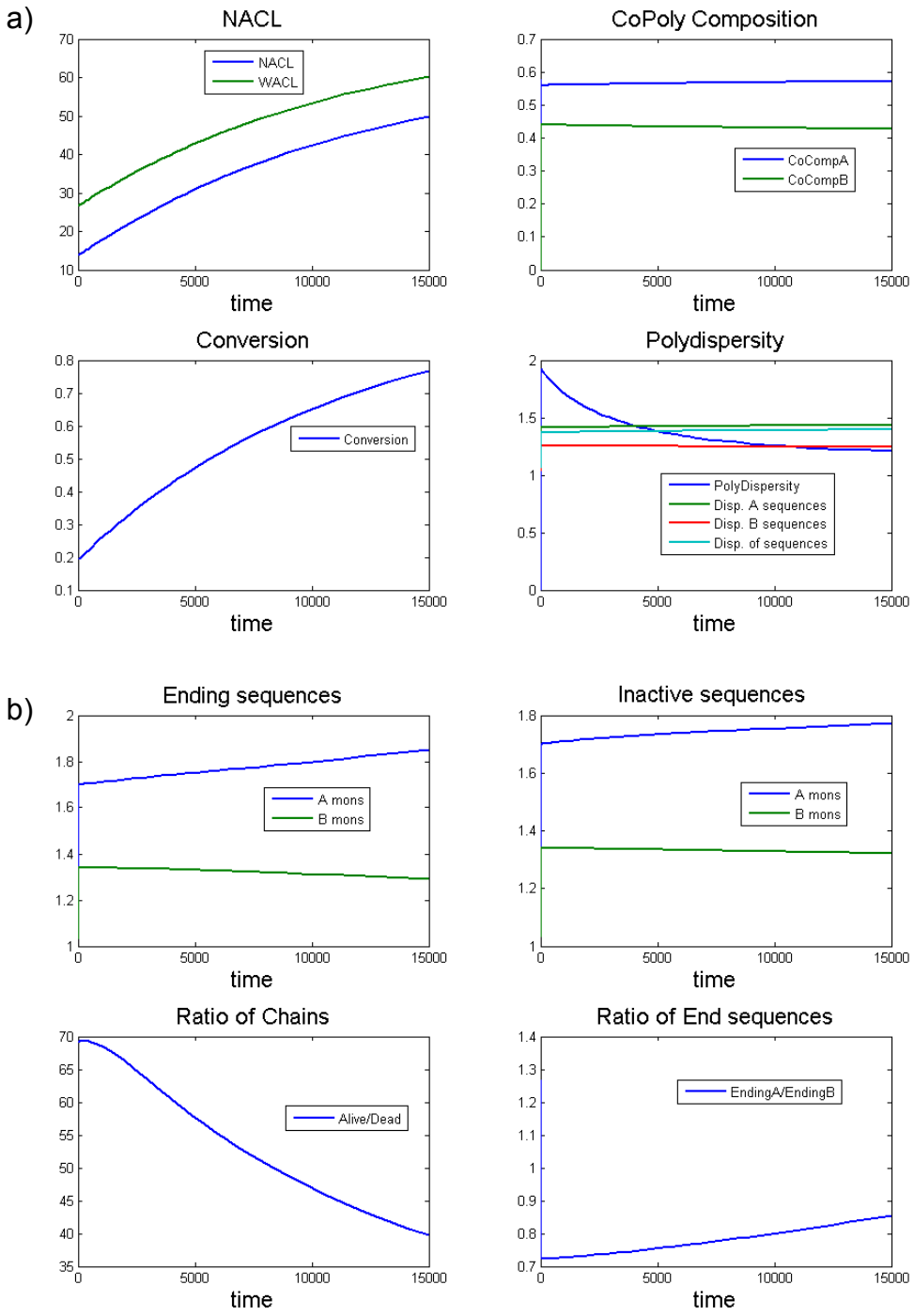

Figure 41: a) NACL, copolymer composition, conversion and dispersity plotted versus time. b) Ending sequences, inactive sequence, ratio of living to dead chains, and ratio of end sequences plotted versus time.

Figure 41 shows that a NACL of 50 with a conversion of 78% is achieved at the end of the PFR. Therefore, the polymer has been elongated by approximately 37

monomers. Polydispersity of the overall polymer is lowered to 1.22, and a high living to dead ratio is still achieved, although it obviously is reduced constantly throughout the reactor. As has been mentioned, the PFR (essentially a batch reactor) has a polydispersity value of one as a purely living system, and since there is some death in this system, values will be obtained slightly above one. Composition drift is very low: this is determined by a fairly constant copolymer composition as well as similar values in end and internal sequence length throughout the reactor time. The ratio between end sequences of 'A' to 'B' is fairly even, at a value of 0.86, with the average end sequence totaling almost 2 monomers. Copolymer composition of 'A' is approximately 55% with low values for the dispersities of the sequences. With the average inactive sequences of 'A' and 'B', an even polymer-blend is clearly determined. Since the dispersities of the sequences in this reactor is lower than in the CSTR, the sequence lengths in this reactor are more uniform. The output of the PFR is added to a CSTR with an additional feed of pure 'B' monomer (2.5M). The sequence model is reset, and Figure 42 illustrates the results of simulation.

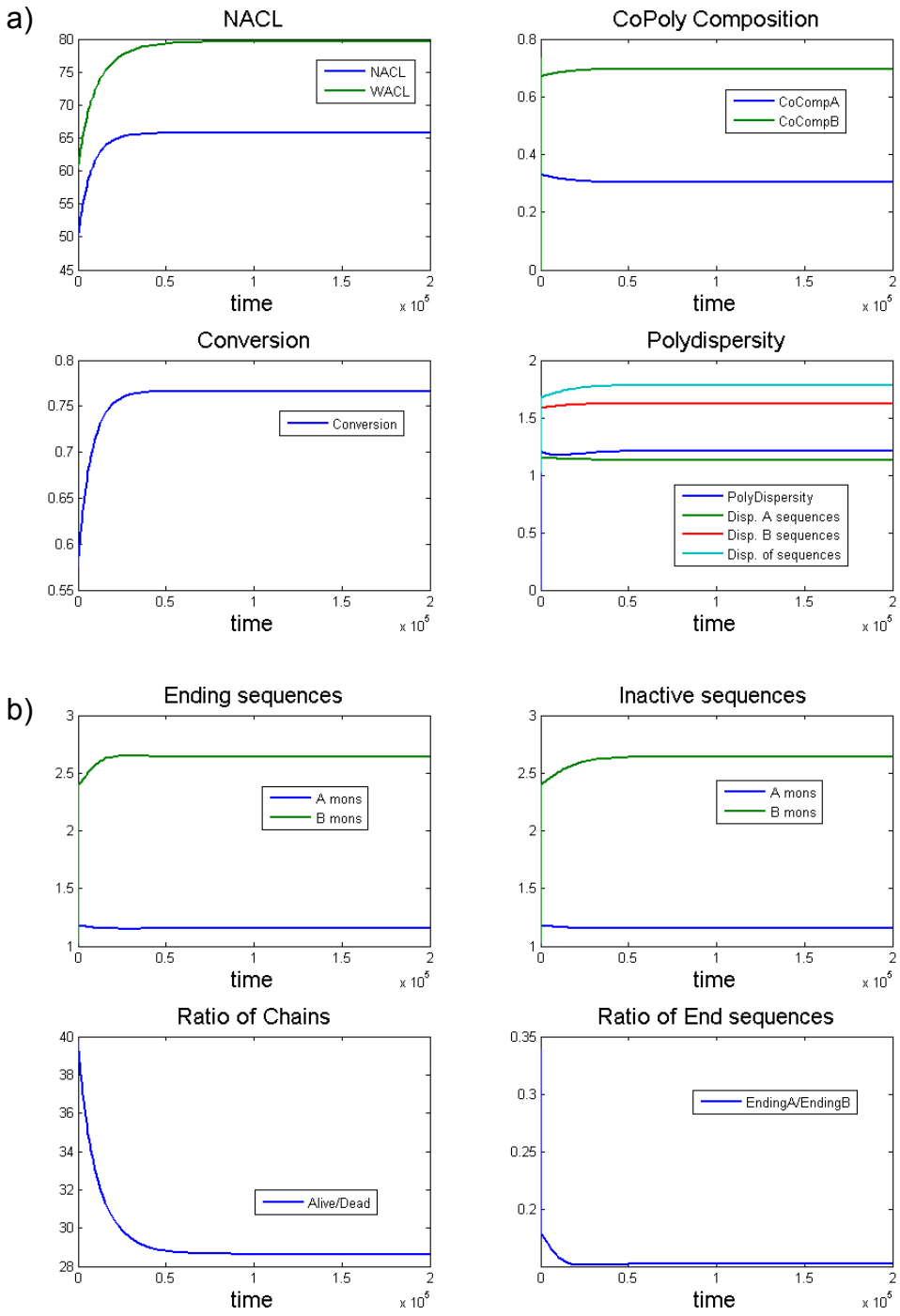

Figure 42: a) NACL, copolymer composition, conversion and dispersity plotted versus time. b) Ending sequences, inactive sequence, ratio of living to dead chains, and ratio of end sequences plotted versus time.

The final CSTR reactor in this series also has a residence time of 15000 seconds. Figure 42 shows that a NACL of 62 with a conversion of 77% is achieved

once the second CSTR reactor reaches steady-state. Therefore, the polymer has been elongated by approximately 12 monomers. The polydispersity rises slightly to a value of 1.25 and a very high living to dead ratio is maintained. However, the dispersities of the sequences is fairly high; therefore despite the lack of composition drift (constant copolymer composition is maintained), sequence lengths are not uniform. The average internal and ending sequence of each monomer is equivalent, which underscores the lack of composition drift in this polymer segment. The ratio of 'A' to 'B' end sequences is 0.16 with a calculated average ending of 'B' of 2.58. With the average inactive sequences of 'A' and 'B', the compositional analysis of the last polymer segment is obtained. The 43% copolymer composition of 'A' monomer highlights an overall polymer that gradually decreases in the concentration of 'A' monomer from the head of the polymer to the tail. With this information, a cartoon snapshot is once again presented in Figure 43 to highlight the aspects of this polymerization.

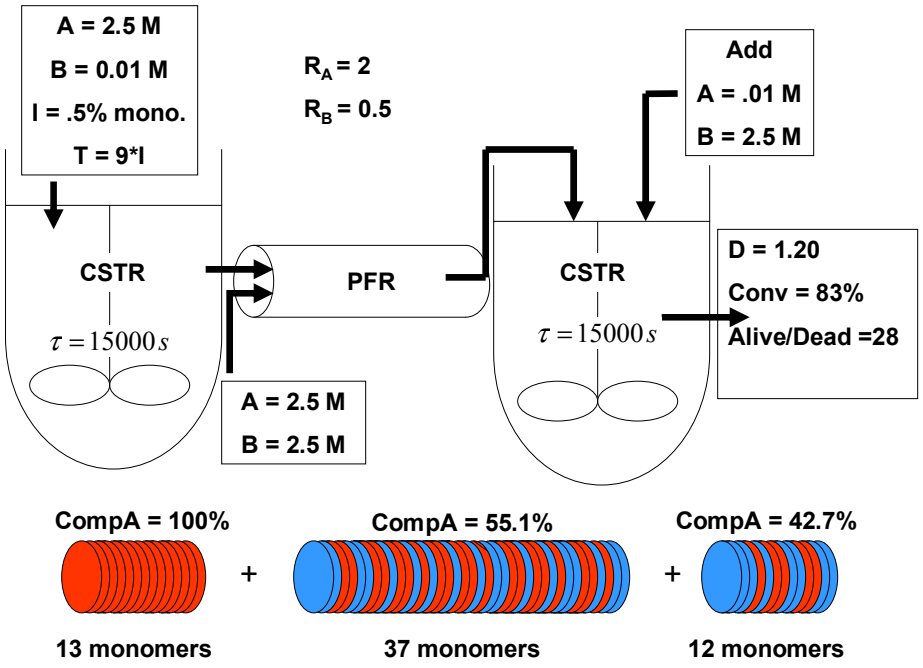

Figure 43: Flow diagram of process with cartoon "snapshot" of simulated polymer

2nd Scenario

The fourth scenario inverts the reactor sequence of the third scenario: a PFR reactor is fed to a CSTR which is fed to another PFR. The goal is to create a monodisperse polymer that is rich in A at the end and tail of the copolymer with a blend in the middle. Reactivity ratios are set at 0.6 and 0.4, respectively, and each reactor has a residence time of 15000 seconds. The first PFR reactor has a feed concentration of 2.5 M and 1.5 M of 'A' and 'B' monomer, respectively. As the initial reactor is a PFR, the amount of initiator is reduced to 3% of the total concentration of monomers with a RAFT agent concentration nine times greater than the initiator. The characteristics of the simulation as a function of time are shown in Figure 44.

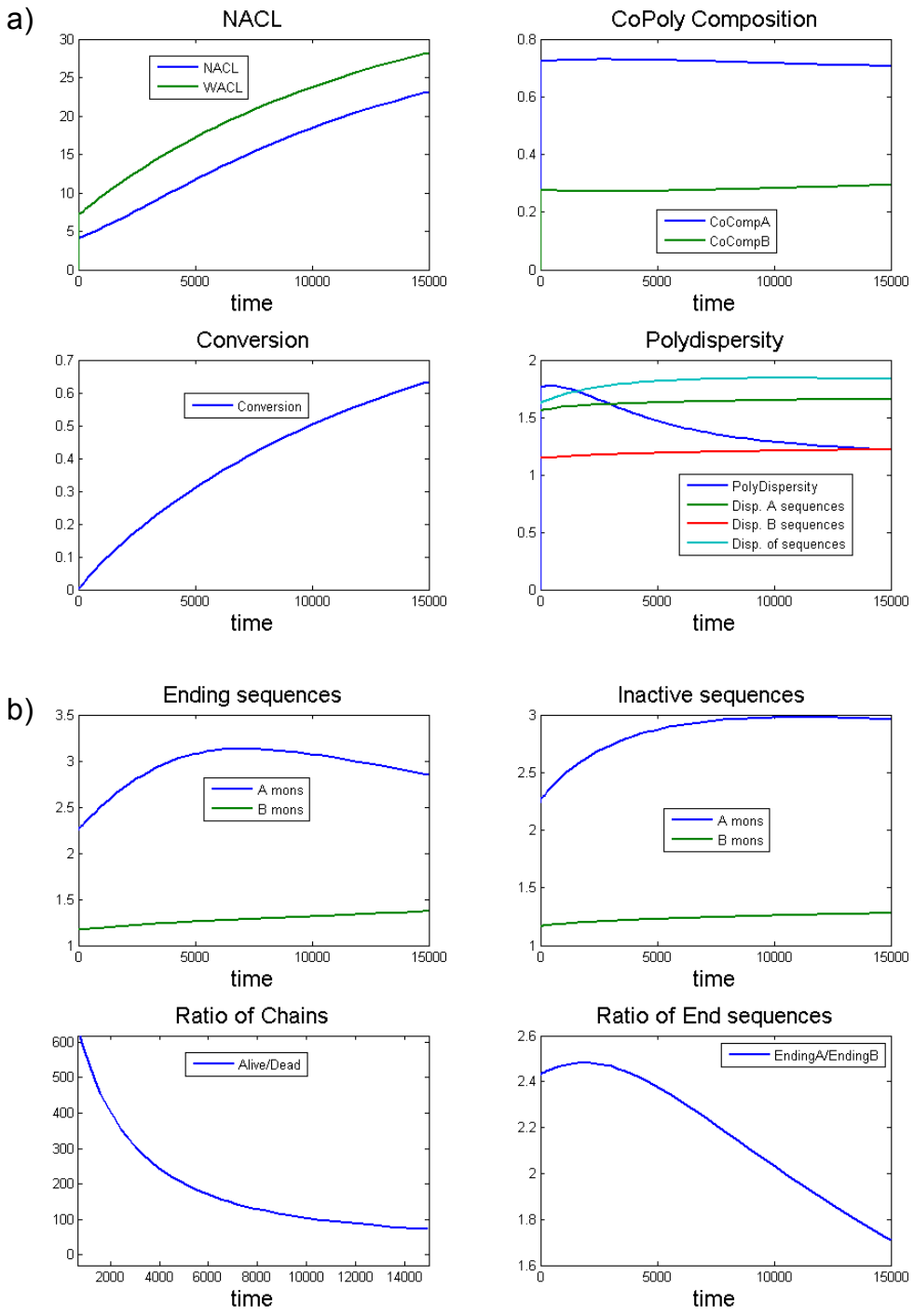

Figure 44: a) NACL, copolymer composition, conversion and dispersity plotted versus time. b) Ending sequences, inactive sequence, ratio of living to dead chains, and ratio of end sequences plotted versus time.

Figure 44 shows that a NACL of 23 with a conversion of 63% is achieved at the end of the PFR. A low polydispersity of 1.22 is achieved with the ratio of living to dead chains totaling 71.8. Composition drift is very low: this is determined by a fairly constant copolymer composition as well as similar values in end and internal sequence length throughout the reactor time. The copolymer composition of 'A' begins at 72.4% at the beginning of the polymerization and lowers slightly to 70.6% at the end of the polymerization. This indicates that a disproportionately higher concentration of 'B' monomers to 'A' monomers did not polymerize, and if the residence time was increased, further composition drift would have been realized. At the end of the reactor, the average end and internal sequence of 'A' monomer totaled 2.85 and 2.96, respectively, while the average end and internal sequence of 'B' monomer totaled 1.28 and 1.37, respectively. The ratio between end sequences of 'A' to 'B' is 1.73, with the average end sequence totaling almost 3 monomers. The dispersity of the 'B' monomer sequences is much lower than the 'A' monomer, primarily due to the higher concentration of 'A' monomer. The output of the PFR is a continuous feed to a CSTR with the reverse ratio of monomer added: 1.5 M of 'A' monomer, and 2.5 M of 'B' monomer. The sequence model is reset, and Figure 45 illustrates the results of the CSTR simulation.

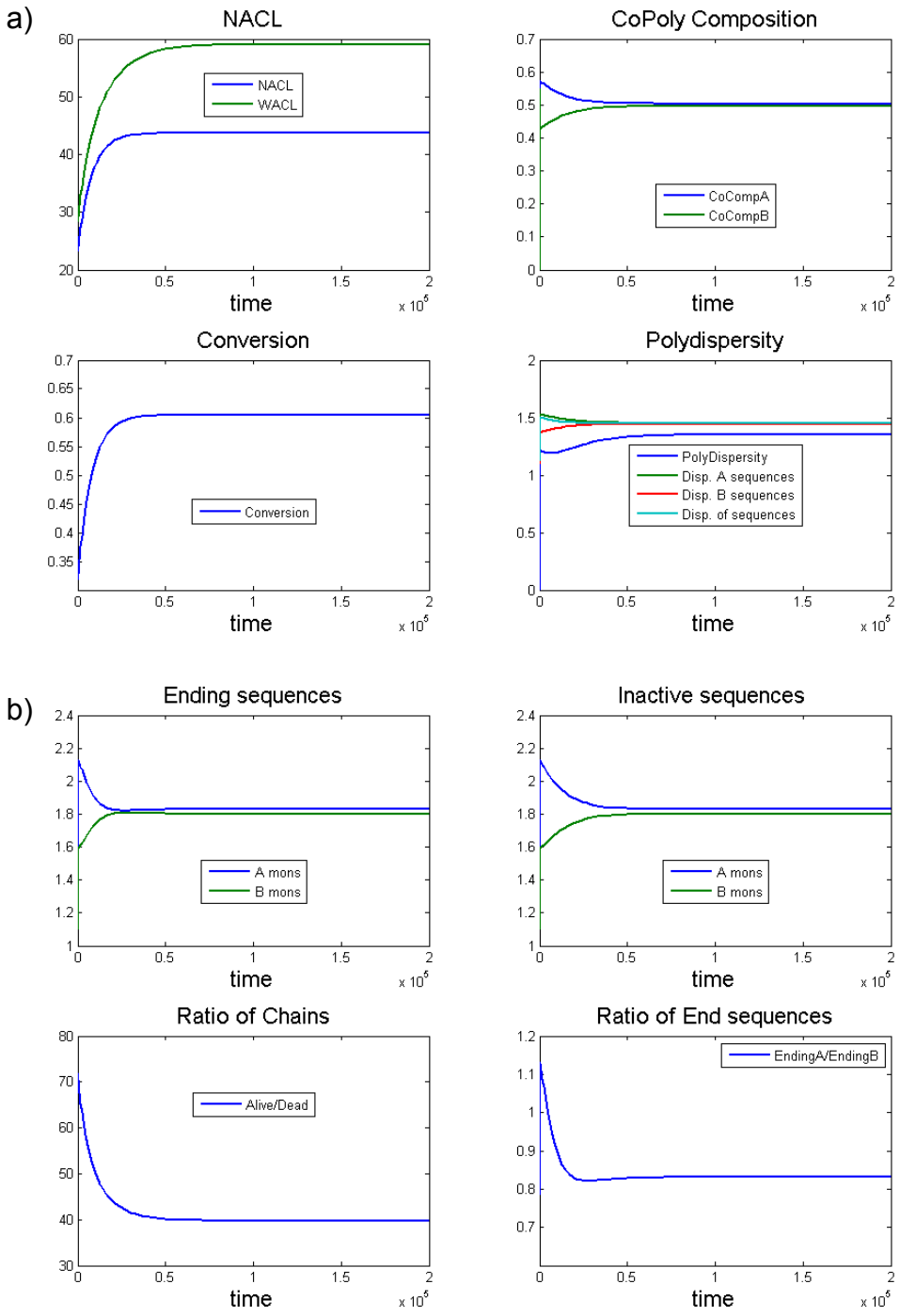

Figure 45: a) NACL, copolymer composition, conversion and dispersity plotted versus time. b) Ending sequences, inactive sequence, ratio of living to dead chains, and ratio of end sequences plotted versus time.

The CSTR reactor in this series also has a residence time of 15000 seconds.

Figure 45 shows that a NACL of 44 with a conversion of 60.5% is achieved once the

second CSTR reactor reaches steady-state. Therefore, the polymer has been elongated by approximately 21 monomers. The polydispersity rises slightly to a value of 1.35 and a very high living to dead ratio of 39.8 is maintained. Once again for a CSTR, the average internal and ending sequence for each monomer is equivalent, which is a result of the lack of composition drift in this polymer segment. The average sequence length of 'A' monomer is 1.83, which is almost equivalent to the average sequence length of 1.80 for the 'B' monomer. This indicates a very even distribution of the copolymer composition of 50.5% for the 'A' monomer. The dispersities of all of sequences are around the modest value of 1.45; therefore composition drift does not occur (constant copolymer composition is maintained), and the sequence lengths are fairly uniform. The ratio of 'A' to 'B' end sequences is fairly even at 0.83 with a calculated average ending of 'B' of 1.80. The output of this CSTR is added to a final PFR with an additional feed of 2.5 M and 0.5 M of monomer 'A' and 'B', respectively. The sequence model is reset, and Figure 46 illustrates the results of this PFR simulation.

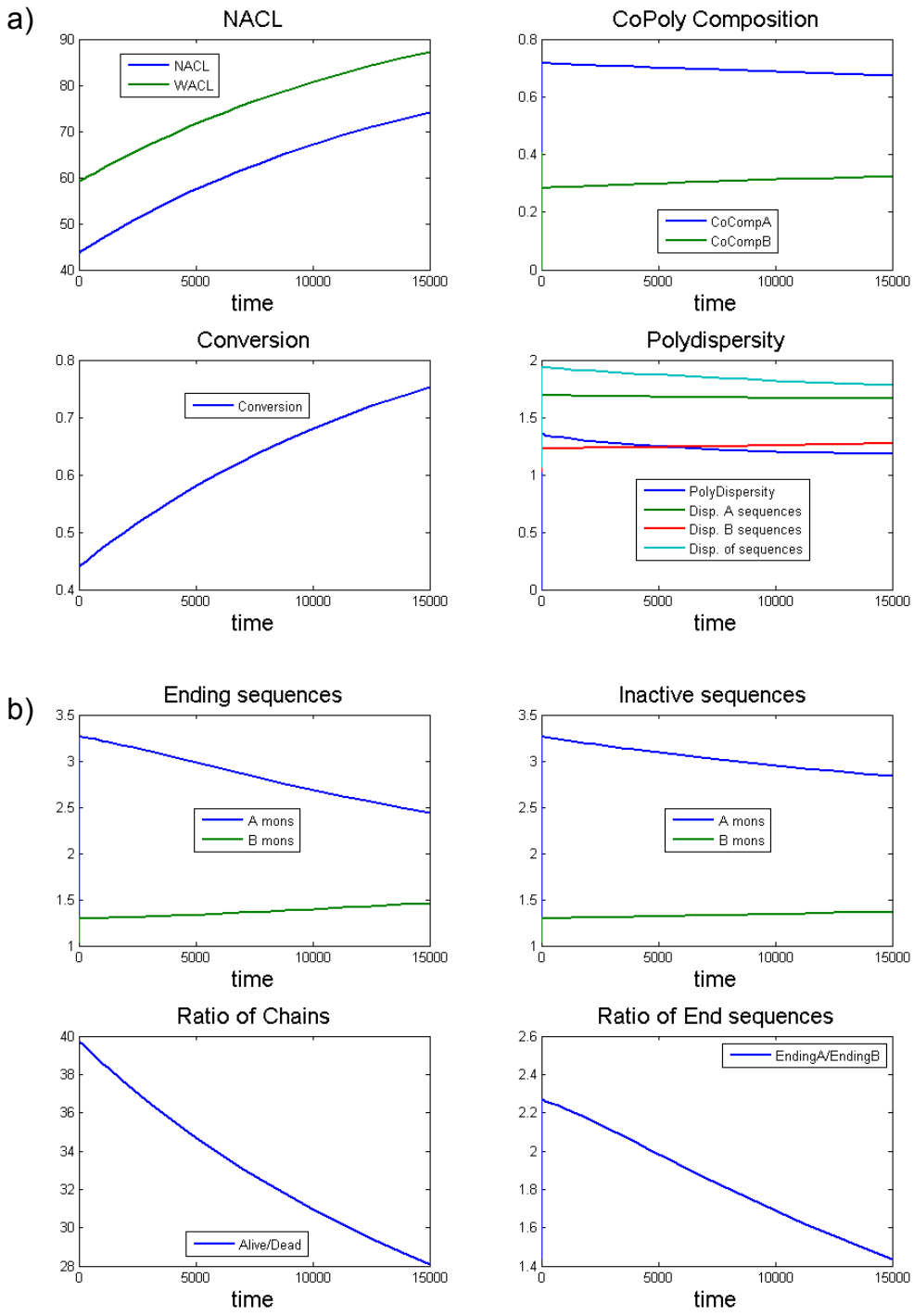

Figure 46: a) NACL, copolymer composition, conversion and dispersity plotted versus time. b) Ending sequences, inactive sequence, ratio of living to dead chains, and ratio of end sequences plotted versus time.

The final PFR reactor in this series also has a residence time of 15000 seconds. Figure 46 shows that a NACL of 74 with a conversion of 75.3% is achieved at the end of the PFR. Therefore, the polymer has been elongated by approximately 30 monomers. Polydispersity of the overall polymer is lowered to 1.18, and a high living to dead ratio is still achieved, although it obviously is reduced constantly throughout the reactor. Composition drift is more significant than the first PFR reactor: copolymer composition of 'A' monomer begins at 72.4% and lowers to 67.5% at the end of the reactor. The sequence model highlights the path of composition drift in the end sequence reduction from 3.26 to 2.4 for the 'A' monomer and the rise in the end sequences of 'B' monomer from 1.26 to 1.49. The ratio between end sequences of 'A' to 'B' is begins at 2.28 and reduces to 1.44, with the average end sequence totaling over 3 monomers at the head of the segment and over 2 monomers at the tail. The dispersity of 'A', 'B' and all sequences total 1.27, 1.66, and 1.78, respectively. The 43% copolymer composition of 'A' monomer highlights an overall polymer that is rich in 'A' monomer at the head and tail of the polymer with a blend in the center. With the above information taken from the graphs produced, a cartoon snapshot of the entire process is once again presented in Figure 47 to highlight the aspects of this polymerization.

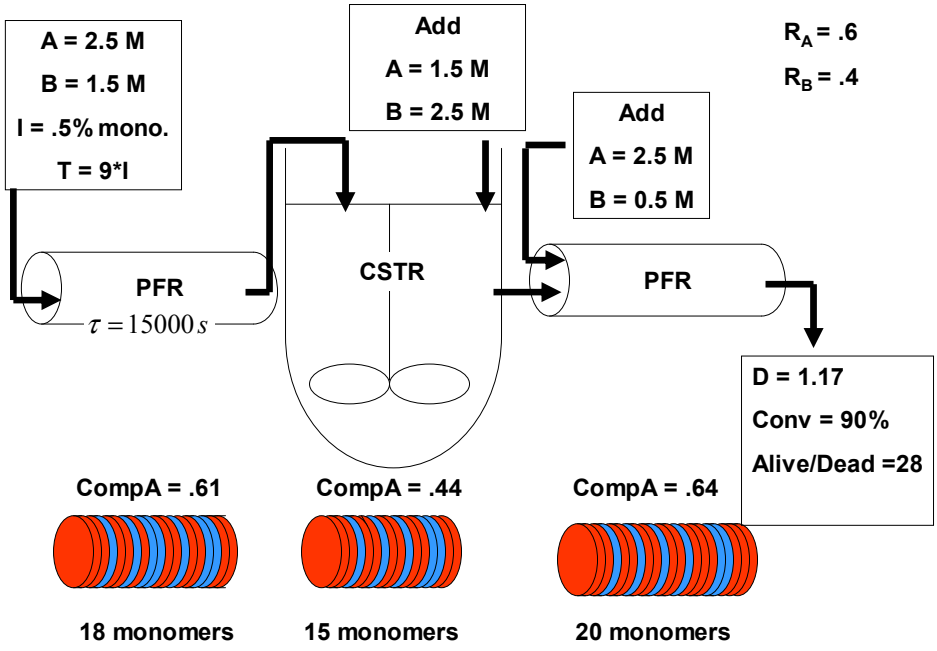

Figure 47: Flow diagram of process with cartoon "snapshot" of simulated polymer

3rd Scenario

The fifth scenario is a repeat of the fourth scenario in reactor sequence: a PFR followed by CSTR ending with a PFR. Reactivity ratios are set at 2.0 and 05, respectively, and each reactor has a residence time of 15000 seconds. The goal of the simulation is to create a long copolymer that gradually decreases in 'A' monomer, essentially creating a long gradient copolymer. To accomplish this, higher concentrations of monomer will be used with feed concentrations of 'A' monomer decreasing at each reactor. The first PFR reactor has a feed concentration of 4 M and 2 M of 'A' and 'B' monomer, respectively. As the initial reactor is a PFR, the amount of initiator is 3% of the total concentration of monomers with a RAFT agent concentration nine times greater than the initiator. The characteristics of the simulation as a function of time are shown in Figure 48.

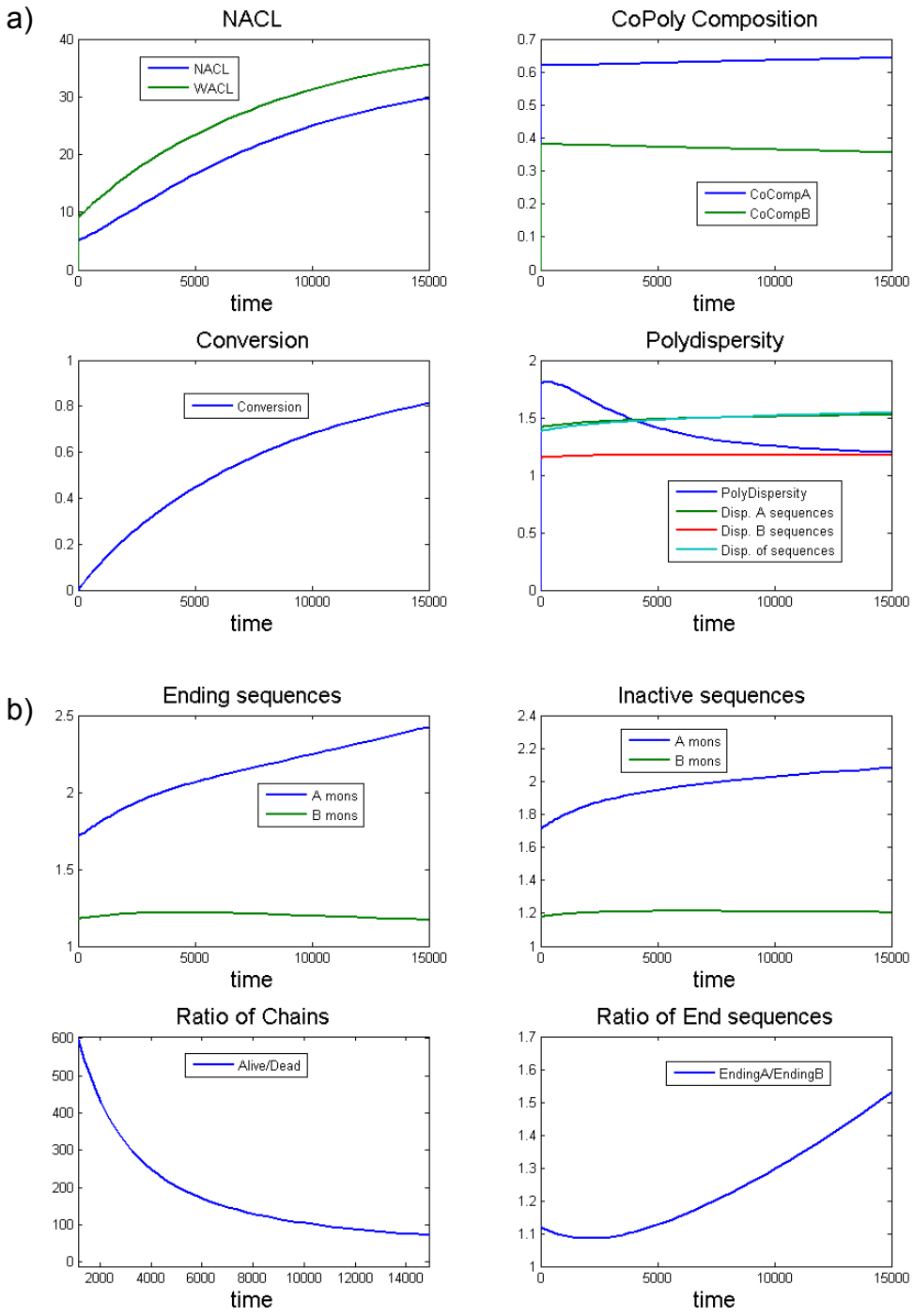

Figure 48: a) NACL, copolymer composition, conversion and dispersity plotted versus time. b) Ending sequences, inactive sequence, ratio of living to dead chains, and ratio of end sequences plotted versus time.

Figure 48 shows that a NACL of 29.7 with a conversion of 81.2% is achieved at the end of the PFR. A low polydispersity of 1.17 is achieved with a very high ratio of living to dead chains. Composition drift is very low: this is determined by a fairly constant copolymer composition as well as similar values in end and internal sequence length throughout the reactor time. The copolymer composition of 'A' begins at 61.8% at the beginning of the polymerization and increases slightly to 64.3% at the end of the polymerization. This indicates that a disproportionately higher concentration of 'A' monomers to 'B' monomers did not polymerize, and if the residence time was increased, further composition drift would have resulted in a final copolymer composition of 66.7%. At the end of the reactor, the average end and internal sequence of 'A' monomer totaled 2.43 and 2..08, respectively, while the average end and internal sequence of 'B' monomer totaled 1.17 and 1.28, respectively. The ratio between end sequences of 'A' to 'B' rises to 1.53 at the end of the reactor from a value of 1.12. The dispersity of the 'B' monomer sequences is much lower than the 'A' monomer, primarily due to the higher concentration of 'A' monomer. The output of the PFR is a continuous feed to a CSTR with the reverse ratio of monomer added: 1.5 M of 'A' monomer, and 2.5 M of 'B' monomer. The sequence model is reset, and Figure 49 illustrates the results of the CSTR simulation.

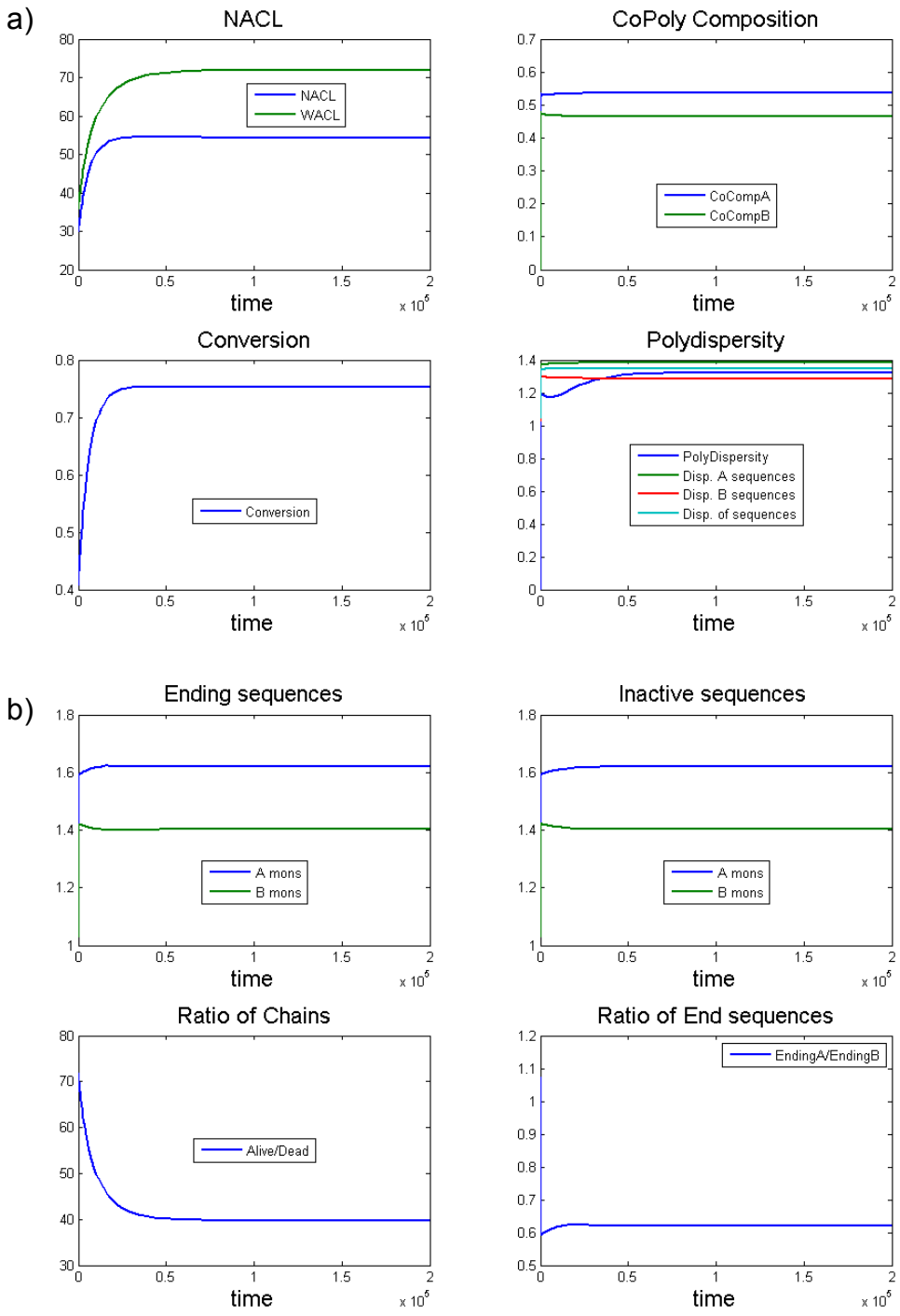

Figure 49: a) NACL, copolymer composition, conversion and dispersity plotted versus time. b) Ending sequences, inactive sequence, ratio of living to dead chains, and ratio of end sequences plotted versus time.

Figure 49 shows that a NACL of 54.4 with a conversion of 75.3% is achieved once the second CSTR reactor reaches steady-state. Therefore, the polymer has been

elongated by approximately 24 monomers. The polydispersity rises slightly to a value of 1.32 and a very high living to dead ratio of 39.7 is maintained. Once again for a CSTR, the average internal and ending sequence for each monomer is equivalent, which is a result of the lack of composition drift in this polymer segment. The average sequence length of 'A' monomer is 1.62, which is slightly higher to the average sequence length of 1.40 for the 'B' monomer. This indicates a very even distribution of the copolymer composition of 53.6% for the 'A' monomer. The dispersities of all of sequences are around the modest value of 1.45; therefore composition drift does not occur (constant copolymer composition is maintained), and the sequence lengths are fairly uniform. The ratio of 'A' to 'B' end sequences is fairly even at 0.62. The output of this CSTR is added to a final PFR with an additional feed of 2.5 M and 0.5 M of monomer 'A' and 'B', respectively. The sequence model is reset, and Figure 50 illustrates the results of this PFR simulation.

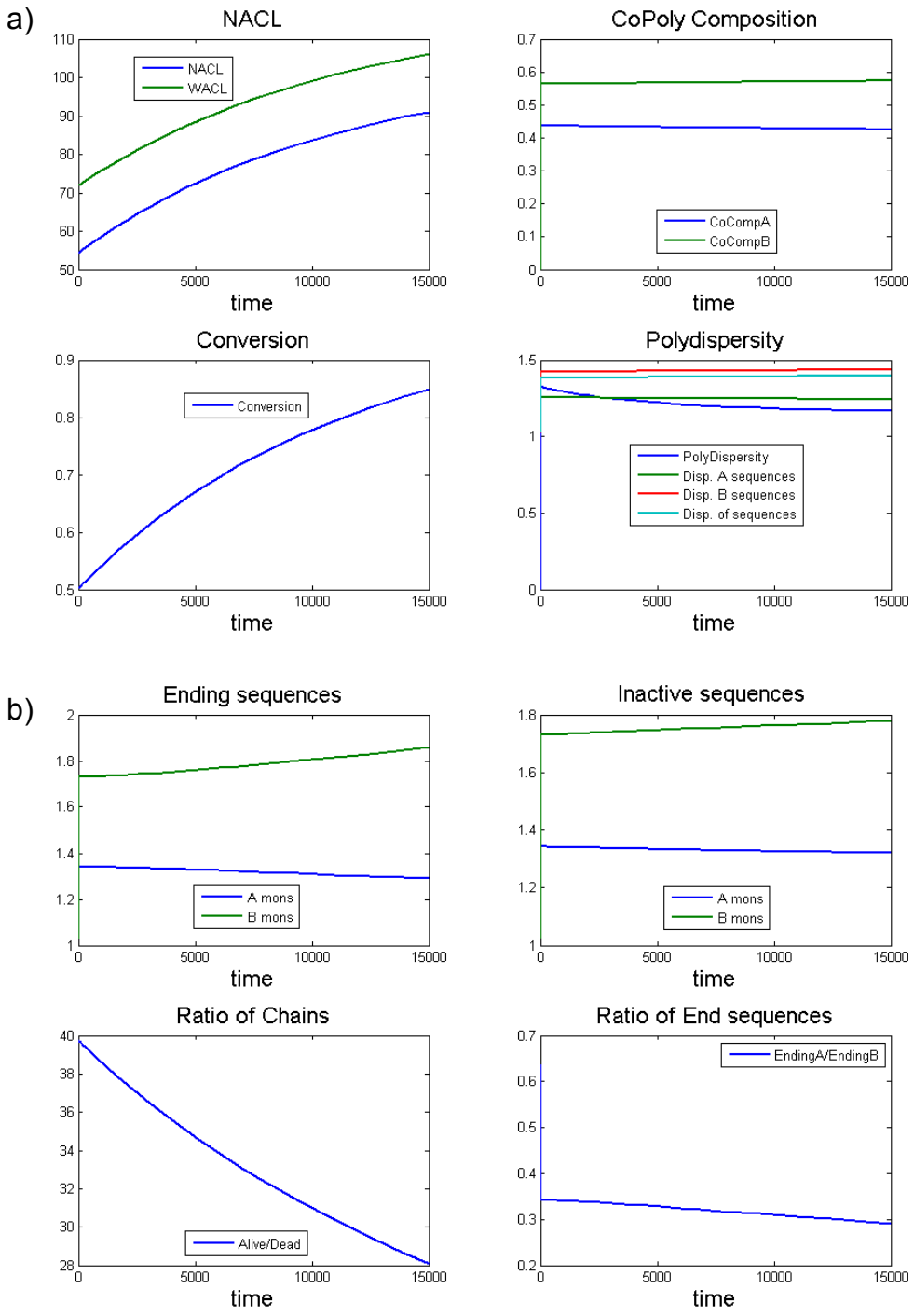

Figure 50: a) NACL, copolymer composition, conversion and dispersity plotted versus time. b) Ending sequences, inactive sequence, ratio of living to dead chains, and ratio of end sequences plotted versus time.

Figure 50 shows that a NACL of 90.9 with an overall conversion of 84.8% is achieved at the end of the PFR. Therefore, the polymer has been elongated by

approximately 37 monomers. Polydispersity of the overall polymer is lowered to 1.17, and a high living to dead ratio of 28.1 is still achieved, although it obviously is reduced constantly throughout the reactor. Composition drift is very low as the copolymer composition of 'A' monomer begins at 44.1% and lowers to 42.6% at the end of the reactor. The composition would have continued to gradually drift towards a final value of 40% if the residence time was increased to allow 100% conversion. The ratio between end sequences of 'A' to 'B' strongly favors B, with the average end sequence totaling close to 2 monomers at the head and tail of the polymer segment. The dispersity of 'A', 'B' and all sequences total 1.24, 1.44, and 1.40, respectively, indicating fairly uniform sequences. The 42.6% copolymer composition of 'A' monomer ends an overall gradient copolymer that is slightly more rich in 'A' monomer at the head and slightly more rich in 'B' monomer at the tail. With the above information taken from the graphs produced, a cartoon snapshot of the entire snapshot is once again presented in Figure 51 to highlight aspects of this polymerization.

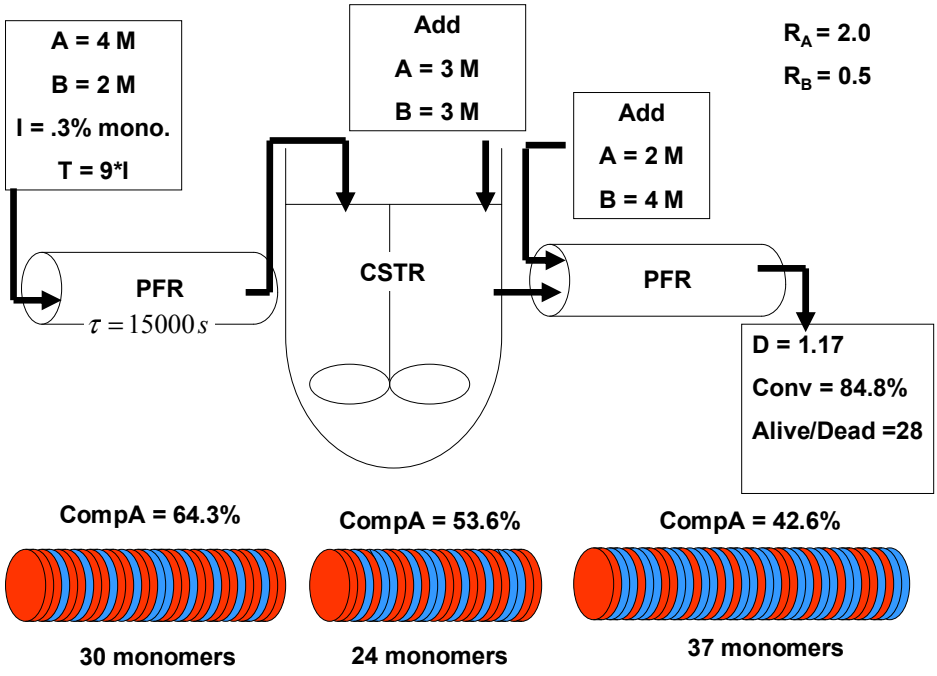

Figure 51: Flow diagram of process with cartoon "snapshot" of simulated polymer

Summary

The first scenario is a proof of concept to illustrate the power of the sequence model to accurately predict the important characteristics of the simulated polymer, including the sequence structure. More scenarios were done to vary reactor conditions as tools to simulate defined copolymer segments in a single copolymer. Copolymers with composition drifting in one segment and without in others were simulated. CSTRs and PFRs were used in tandem to create monodisperse polymers with segments that had compositional uniformity and sequence uniformity. The scenarios were only shown as examples; theoretically, with the development of the sequence model, kinetic parameters and manipulation of reactor conditions, through iteration, a copolymer of any length with polymer segments of varying compositional and sequence structure could be simulated.

Chapter 5: Future Applications

The widespread method of population balances has been used to determine sequence distribution in this work. As has been mentioned, the work on mathematically modeling sequence structure in copolymers used probabilistic functions[25]. The drawbacks to this method are that it only provides a probabilistic representation of what chains are in which state at each degree of polymerization. This provides a much murkier analysis of the overall polymer, and it is only convenient when the probabilities stay constant (i.e. constant monomer composition throughout the reaction). These probabilistic models must be created, manipulated, and interpreted specifically to obtain sequence parameters in addition to the determination of MWD, conversion, and other key characteristics.

While, the chain model was the physical model that simulated the changes in the polymerization, the sequence model had no physical effect on the system, but merely tracked the sequence parameters. The sequence structure determined from the sequence model requires no further manipulation to determine. The key to this method is to treat all inactive sequences equally without regard to orientation on the polymer. Active sequences are by virtue of CRP, always at the end of the copolymer. Geometric inferences on the copolymer could be made from tracking these inactive (internal) sequences or active (end) sequences. Chapter 3 has shown that sequence distributions can be tracked using the sequence model and that series of reactions can be used to model different segments of the overall polymer. Chapter 4 has shown that iteratively, you can vary reactor schemes and conditions to balance dispersity of sequences, constant copolymer composition and polydispersity. Copolymers with

polymer segments varying in size, copolymer composition, sequence structure, and composition drift were simulated.

The nature of CSTRs produce copolymers with a lower dispersity of sequences, and no composition drift (active and inactive sequences that are equivalent) with drawbacks of a low degree of polymerization, low conversion, and high polydispersity. PFRs have high conversion, a high degree of polymerization, low polydispersity with drawbacks of composition drift and a higher dispersity of sequences. Their complementary strengths and weaknesses are the reason they are coupled together. However, Wang et al.[23] have shown through semi-batch operations to control copolymer composition using a simulation derived from the method of moments. This manipulation of the feed to control composition can be used to control sequences. Reactor series would be unnecessary as at any point feed conditions could be changed to alter sequence structure, and the nature of a semi-batch sensitive to composition drift could produce copolymers with a high degree of polymerization, high conversion, low polydispersity.

Also an open-trajectory loop using a PDI controller could be a further application of our model to control sequence structure, MWD, conversion, and polydispersity in the field. Degree of freedom analysis would be needed to determine which parameters, or all of them, could be controlled varying the monomer feed.

Branching was not considered in the model developed because the goal was to illustrate that the sequence model could be used model sequence structure in varying reactors with controlled copolymer composition. The increased complexity in including branching was not deemed justifiable to achieve the primary goal of this

work. Hyperbranched models have been developed using population balances[43], and through additional tracking parameters, branched sequences could also be tracked to theoretically simulate an entire web of copolymers.

In short, the premise of sequence distributions using population balances that has been developed in this work has a multitude of applications. Varying levels of complexity could be added to the model to track sequence distributions more accurately. Pre-defined sequences can be determined iteratively to enhance needed copolymer properties in each section of a polymer. Rate constants, particularly for RAFT transfer, need to be better understood for each copolymer system to obtain more accurate mathematical models to use in industry. Constancy of sequence distributions could very well replace copolymer compositions: maintaining sequences with defined sequence structure may be obtainable with constant copolymer compositions being a result of maintaining those defined sequences. Population balances have been a popular source of mathematical modeling, and this work has added a powerful, new tool.

Appendices

Chain Model Mass Balances

$$\frac{dP_1}{dt} = k_{i1}[R^*][A] \qquad R^* + A \xrightarrow{ki1} P_1$$

$$+ k_{r11}[R^*][TP_1] - k_{r12}[T][P_1] \qquad R^* + TP_1 \underset{kr12}{\overset{kr11}{\leftrightarrow}} T + P_1$$

$$- k_{raft31}\left(\sum_{r=0}^{\infty} TQ_r\right)[P_1] + k_{raft32}\left(\sum_{r=0}^{\infty} Q_r\right)[TP_1] \qquad P_1 + TQ_r \underset{kraft32}{\overset{kraft31}{\leftrightarrow}} TP_1 + Q_r$$

$$+ k_{raft51}\left(\sum_{r=0}^{\infty} P_r\right)[TP_1] - k_{raft52}\left(\sum_{r=0}^{\infty} TP_r\right)[P_1] \qquad P_r + TP_1 \underset{kraft52}{\overset{kraft51}{\leftrightarrow}} TP_r + P_1$$

$$- k_{p1}[A][P_1] - k_{p2}[B][P_1] \qquad P_1 + A \xrightarrow{kp1} P_2 \qquad P_1 + B \xrightarrow{kp2} Q_2$$

$$- k_{tc1}\left(\sum_{r=0}^{\infty} Q_r\right)[P_{1,0}] \qquad P_1 + Q_r \xrightarrow{ktc1} M_{(r+1)}$$

$$- k_{td1}\left(\sum_{r=0}^{\infty} Q_r\right)[P_{1,0}] \qquad P_1 + Q_r \xrightarrow{ktd1} M_1 + M_r$$

$$- k_{tc2}\left(\sum_{r=0}^{\infty} P_r\right)[P_{1,0}] \qquad P_1 + P_r \xrightarrow{ktc2} M_{(1+r)}$$

$$- k_{td2}\left(\sum_{r=0}^{\infty} P_r\right)[P_{1,0}] \qquad P_1 + P_r \xrightarrow{ktd2} M_1 + M_r$$

$n \geq 2$

$$\frac{dP_n}{dt} = k_{r11}[R^*][TP_n] - k_{r12}[T][P_n] \qquad R^* + TP_n \underset{kr12}{\overset{kr11}{\leftrightarrow}} T + P_n$$

$$- k_{raft31}\left(\sum_{r=0}^{\infty} TQ_r\right)[P_n] + k_{raft32}\left(\sum_{r=0}^{\infty} Q_r\right)[TP_n] \qquad P_n + TQ_r \underset{kraft32}{\overset{kraft31}{\leftrightarrow}} TP_n + Q_r$$

$+\ k_{raft51}\left(\sum_{r=0}^{\infty} P_r\right)[TP_n] - k_{raft52}\left(\sum_{r=0}^{\infty} TP_r\right)[P_n]$ $\qquad P_r + TP_n \underset{kraft52}{\overset{kraft51}{\leftrightarrow}} TP_r + P_n$

$-\ k_{p1}[A][P_n]\ -\ k_{p2}[B][P_n]$ $\qquad P_n + A \xrightarrow{kp1} P_{n+1}$ $\qquad P_n + B \xrightarrow{kp2} Q_{n+1}$

$+\ k_{p5}[A][P_{n-1}]\ +\ k_{p7}[A][Q_{n-1}]$ $\qquad P_{n-1} + A \xrightarrow{kp5} P_n$ $\qquad Q_{n-1} + A \xrightarrow{kp7} P_n$

$-\ k_{tc1}\left(\sum_{r=0}^{\infty} Q_r\right)[P_n]$ $\qquad P_n + Q_r \xrightarrow{ktc1} M_{(r+n)}$

$-\ k_{td1}\left(\sum_{r=0}^{\infty} Q_r\right)[P_n]$ $\qquad P_n + Q_r \xrightarrow{ktd1} M_n + M_r$

$-\ k_{tc2}\left(\sum_{r=0}^{\infty} P_r\right)[P_n]$ $\qquad P_n + P_r \xrightarrow{ktc2} M_{(n+r)}$

$-\ k_{td2}\left(\sum_{r=0}^{\infty} P_r\right)[P_n]$ $\qquad P_n + P_r \xrightarrow{ktd2} M_n + M_r$

$\frac{dP_1}{dt} + \frac{dP_n}{dt} = k_{i1}[R^*][A]$ $\qquad R^* + A \xrightarrow{ki1} P_{1,0}$

$+\ k_{r11}[R^*][TP_n] - k_{r12}[T][P_n]$ $\qquad R^* + TP_n \underset{kr12}{\overset{kr11}{\leftrightarrow}} T + P_n$

$-\ k_{raft31}\left(\sum_{r=0}^{\infty} TQ_r\right)[P_n]\ + k_{raft32}\left(\sum_{r=0}^{\infty} Q_r\right)[TP_n]$ $\qquad P_n + TQ_r \underset{kraft32}{\overset{kraft31}{\leftrightarrow}} TP_n + Q_r$

$+\ k_{raft51}\left(\sum_{r=0}^{\infty} P_r\right)[TP_n] - k_{raft52}\left(\sum_{r=0}^{\infty} TP_r\right)[P_n]$ $\qquad P_r + TP_n \underset{kraft52}{\overset{kraft51}{\leftrightarrow}} TP_r + P_n$

$-\ k_{p1}[A][P_n]\ -\ k_{p2}[B][P_n]$ $\qquad P_n + A \xrightarrow{kp1} P_{n+1}$ $\qquad P_n + B \xrightarrow{kp2} Q_{n+1}$

$+\ k_{p5}[A][P_{n-1}]\ +\ k_{p7}[A][Q_{n-1}]$ $\qquad P_{n-1} + A \xrightarrow{kp5} P_n$ $\qquad Q_{n-1} + A \xrightarrow{kp7} P_n$

$-\ k_{tc1}\left(\sum_{r=0}^{\infty} Q_r\right)[P_n]$ $\qquad P_n + Q_r \xrightarrow{ktc1} M_{(r+n)}$

$$- k_{td1}\left(\sum_{r=0}^{\infty} Q_r\right)[P_n] \qquad P_n + Q_r \xrightarrow{ktd1} M_n + M_r$$

$$- k_{tc2}\left(\sum_{r=0}^{\infty} P_r\right)[P_n] \qquad P_n + P_r \xrightarrow{ktc2} M_{(n+r)}$$

$$- k_{td2}\left(\sum_{r=0}^{\infty} P_r\right)[P_n] \qquad P_n + P_r \xrightarrow{ktd2} M_n + M_r$$

$$\frac{dQ_1}{dt} = k_{i2}[R^*][B] \qquad R^* + B \xrightarrow{ki2} Q_1$$

$$+ k_{r21}[R^*][TQ_1] - k_{r22}[T][Q_1] \qquad R^* + TQ_1 \underset{kr22}{\overset{kr21}{\leftrightarrow}} T + Q_1$$

$$- k_{raft61}\left(\sum_{r=0}^{\infty} TP_r\right)[Q_1] + k_{raft62}\left(\sum_{r=0}^{\infty} P_r\right)[TQ_1] \qquad Q_1 + TP_r \underset{kraft62}{\overset{kraft61}{\leftrightarrow}} TQ_1 + P_r$$

$$+ k_{raft41}\left(\sum_{r=0}^{\infty} Q_r\right)[TQ_1] - k_{raft42}\left(\sum_{r=0}^{\infty} TQ_r\right)[Q_1] \qquad Q_r + TQ_1 \underset{kraft42}{\overset{kraft41}{\leftrightarrow}} TQ_r + Q_1$$

$$- k_{p3}[A][Q_1] - k_{p4}[B][Q_1] \qquad Q_1 + A \xrightarrow{kp3} P_2 \qquad Q_1 + B \xrightarrow{kp4} Q_2$$

$$- k_{tc4}\left(\sum_{r=0}^{\infty} P_r\right)[Q_1] \qquad Q_1 + P_r \xrightarrow{ktc4} M_{(r+1)}$$

$$- k_{td4}\left(\sum_{r=0}^{\infty} P_r\right)[Q_1] \qquad Q_1 + P_r \xrightarrow{ktd4} M_1 + M_r$$

$$- k_{tc3}\left(\sum_{r=0}^{\infty} Q_r\right)[Q_1] \qquad Q_1 + Q_r \xrightarrow{ktc3} M_{(r+1)}$$

$$- k_{td3}\left(\sum_{r=0}^{\infty} Q_r\right)[Q_1] \qquad Q_1 + Q_r \xrightarrow{ktd3} M_1 + M_r$$

$$n \geq 2$$

$$\frac{dQ_n}{dt} = k_{r21}[R^*]\,[TQ_n] - k_{r22}\,[T]\,[Q_n] \qquad R^* + TQ_n \underset{kr22}{\overset{kr21}{\leftrightarrow}} T + Q_n$$

$$- k_{raft61}\left(\sum_{r=0}^{\infty} TP_r\right)[Q_n] + k_{raft62}\left(\sum_{r=0}^{\infty} P_r\right)[TQ_n] \qquad Q_n + TP_r \underset{kraft62}{\overset{kraft61}{\leftrightarrow}} TQ_n + P_r$$

$$+ k_{raft41}\left(\sum_{r=0}^{\infty} Q_r\right)[TQ_n] - k_{raft42}\left(\sum_{r=0}^{\infty} TQ_r\right)[Q_n] \qquad Q_r + TQ_n \underset{kraft42}{\overset{kraft41}{\leftrightarrow}} TQ_r + Q_n$$

$$- k_{p3}\,[A]\,[Q_n] - k_{p4}\,[B]\,[Q_n] \qquad Q_n + A \overset{kp3}{\rightarrow} P_{n+1} \qquad Q_n + B \overset{kp4}{\rightarrow} Q_{n+1}$$

$$+ k_{p6}[B]\,[P_{n-1}] + k_{p8}\,[B]\,[Q_{n-1}] \qquad P_{n-1} + B \overset{kp6}{\rightarrow} Q_n \qquad Q_{n-1} + B \overset{kp8}{\rightarrow} Q_n$$

$$- k_{tc4}\left(\sum_{r=0}^{\infty} P_r\right)[Q_n] \qquad Q_n + P_r \overset{ktc4}{\rightarrow} M_{(r+n)}$$

$$- k_{td4}\left(\sum_{r=0}^{\infty} P_r\right)[Q_n] \qquad Q_n + P_r \overset{ktd4}{\rightarrow} M_n + M_r$$

$$- k_{tc3}\left(\sum_{r=0}^{\infty} Q_r\right)[Q_n] \qquad Q_n + Q_r \overset{ktc3}{\rightarrow} M_{(n+r)}$$

$$- k_{td3}\left(\sum_{r=0}^{\infty} Q_r\right)[Q_n] \qquad Q_n + Q_r \overset{ktd3}{\rightarrow} M_n + M_r$$

$n \geq 0, m \geq 1$

$$\frac{dQ_n}{dt} + \frac{dQ_1}{dt} = k_{i2}[R^*][B] \qquad R^* + B \overset{ki2}{\rightarrow} Q_1$$

$$+ k_{r21}[R^*]\,[TQ_n] - k_{r22}\,[T]\,[Q_n] \qquad R^* + TQ_n \underset{kr22}{\overset{kr21}{\leftrightarrow}} T + Q_n$$

$$- k_{raft61}\left(\sum_{r=0}^{\infty} TP_r\right)[Q_n] + k_{raft62}\left(\sum_{r=0}^{\infty} P_r\right)[TQ_n] \qquad Q_n + TP_r \underset{kraft62}{\overset{kraft61}{\leftrightarrow}} TQ_n + P_r$$

$$+ k_{raft41}\left(\sum_{r=0}^{\infty} Q_r\right)[TQ_n] - k_{raft42}\left(\sum_{r=0}^{\infty} TQ_r\right)[Q_n] \qquad Q_r + TQ_n \underset{kraft42}{\overset{kraft41}{\leftrightarrow}} TQ_r + Q_n$$

$-k_{p3}[A][Q_n] - k_{p4}[B][Q_n]$	$Q_n + A \xrightarrow{kp3} P_{n+1}$	$Q_n + B \xrightarrow{kp4} Q_{n+1}$
$+ k_{p6}[B][P_{n-1}] + k_{p8}[B][Q_{n-1}]$	$P_{n-1} + B \xrightarrow{kp6} Q_n$	$Q_{n-1} + B \xrightarrow{kp8} Q_n$
$-k_{tc4}\left(\sum_{r=0}^{\infty} P_r\right)[Q_n]$		$Q_n + P_r \xrightarrow{ktc4} M_{(r+n)}$
$-k_{td4}\left(\sum_{r=0}^{\infty} P_r\right)[Q_n]$		$Q_n + P_r \xrightarrow{ktd4} M_n + M_r$
$-k_{tc3}\left(\sum_{r=0}^{\infty} Q_r\right)[Q_n]$		$Q_n + Q_r \xrightarrow{ktc3} M_{(n+r)}$
$-k_{td3}\left(\sum_{r=0}^{\infty} Q_r\right)[Q_n]$		$Q_n + Q_r \xrightarrow{ktd3} M_n + M_r$

$n \geq 1$

$\frac{dTP_n}{dt} = -k_{r11}[R^*][TP_n] + k_{r12}[T][P_n]$	$R^* + TP_n \underset{kr12}{\overset{kr11}{\leftrightarrow}} T + P_n$
$+ k_{raft31}\left(\sum_{r=0}^{\infty} TQ_r\right)[P_n] - k_{raft32}\left(\sum_{r=0}^{\infty} Q_r\right)[TP_n]$	$P_n + TQ_r \underset{kraft32}{\overset{kraft31}{\leftrightarrow}} TP_n + Q_r$
$-k_{raft51}\left(\sum_{r=0}^{\infty} P_r\right)[TP_n] + k_{raft52}\left(\sum_{r=0}^{\infty} TP_r\right)[P_n]$	$P_r + TP_n \underset{kraft52}{\overset{kraft51}{\leftrightarrow}} TP_r + P_n$

$n \geq 1$

$\frac{dTQ_n}{dt} = -k_{r21}[R^*][TQ_n] + k_{r22}[T][Q_n]$	$R^* + TQ_n \underset{kr22}{\overset{kr21}{\leftrightarrow}} T + Q_n$
$+ k_{raft61}\left(\sum_{r=0}^{\infty} TP_r\right)[Q_n] - k_{raft62}\left(\sum_{r=0}^{\infty} P_r\right)[TQ_n]$	$Q_n + TP_r \underset{kraft62}{\overset{kraft61}{\leftrightarrow}} TQ_n + P_r$
$-k_{raft41}\left(\sum_{r=0}^{\infty} Q_r\right)[TQ_n] + k_{raft42}\left(\sum_{r=0}^{\infty} TQ_r\right)[Q_n]$	$Q_r + TQ_n \underset{kraft42}{\overset{kraft41}{\leftrightarrow}} TQ_r + Q_n$

$$\frac{dM_1}{dt} = + k_{td1}\left(\sum_{r=0}^{\infty} Q_r\right)[P_1] \qquad P_1 + Q_r \xrightarrow{ktd1} M_1 + M_r$$

$$+ k_{td2}\left(\sum_{r=0}^{\infty} P_r\right)[P_1] \qquad P_1 + P_r \xrightarrow{ktd2} M_1 + M_r$$

$$+ k_{td3}\left(\sum_{r=0}^{\infty} Q_r\right)[Q_1] \qquad Q_1 + Q_r \xrightarrow{ktd3} M_1 + M_r$$

$$+ k_{td4}\left(\sum_{r=0}^{\infty} P_r\right)[Q_1] \qquad Q_1 + P_r \xrightarrow{ktd4} M_1 + M_r$$

$n \geq 2$

$$\frac{dM_n}{dt} = \tfrac{1}{2}\, k_{tc1}\left(\sum_{a=0}^{n} P_a Q_{n-a}\right) \qquad P_s + Q_r \xrightarrow{ktc1} M_n$$

$$+ \tfrac{1}{2}\, k_{tc4}\left(\sum_{a=0}^{n} P_a Q_{n-a}\right) \qquad Q_s + P_r \xrightarrow{ktc4} M_n$$

$$+ \tfrac{1}{2}\, k_{tc2}\left(\sum_{a=0}^{n} P_a P_{n-a}\right) \qquad P_s + P_r \xrightarrow{ktc2} M_n$$

$$+ \tfrac{1}{2}\, k_{tc3}\left(\sum_{a=0}^{n} Q_a Q_{n-a}\right) \qquad Q_s + Q_r \xrightarrow{ktc3} M_n$$

$$+ k_{td1}\left(\sum_{r=0}^{\infty} Q_r\right)[P_n] \qquad P_n + Q_r \xrightarrow{ktd1} M_n + M_r$$

$$+ k_{td2}\left(\sum_{r=0}^{\infty} P_r\right)[P_n] \qquad P_n + P_r \xrightarrow{ktd2} M_n + M_r$$

$$+ k_{td3}\left(\sum_{r=0}^{\infty} Q_r\right)[Q_n] \qquad Q_n + Q_r \xrightarrow{ktd3} M_n + M_r$$

$$+ k_{td4}\left(\sum_{r=0}^{\infty} P_r\right)[Q_n] \qquad Q_n + P_r \xrightarrow{ktd4} M_n + M_r$$

$$\frac{dM_1}{dt}+\frac{dM_n}{dt} = \tfrac{1}{2}\, k_{tc1}\left(\sum_{a=0}^{n} P_a Q_{n-a}\right) \qquad P_s + Q_r \xrightarrow{ktc1} M_n$$

$$+ \tfrac{1}{2}\, k_{tc4}\left(\sum_{a=0}^{n} P_a Q_{n-a}\right) \qquad Q_s + P_r \xrightarrow{ktc4} M_n$$

$$+ \tfrac{1}{2}\, k_{tc2}\left(\sum_{a=0}^{n} P_a P_{n-a}\right) \qquad P_s + P_r \xrightarrow{ktc2} M_n$$

$$+ \tfrac{1}{2}\, k_{tc3}\left(\sum_{a=0}^{n} Q_a Q_{n-a}\right) \qquad Q_s + Q_r \xrightarrow{ktc3} M_n$$

$$+ k_{td1}\left(\sum_{r=0}^{\infty} Q_r\right)[P_n] \qquad P_n + Q_r \xrightarrow{ktd1} M_n + M_r$$

$$+ k_{td2}\left(\sum_{r=0}^{\infty} P_r\right)[P_n] \qquad P_n + P_r \xrightarrow{ktd2} M_n + M_r$$

$$+ k_{td3}\left(\sum_{r=0}^{\infty} Q_r\right)[Q_n] \qquad Q_n + Q_r \xrightarrow{ktd3} M_n + M_r$$

$$+ k_{td4}\left(\sum_{r=0}^{\infty} P_r\right)[Q_n] \qquad Q_n + P_r \xrightarrow{ktd4} M_n + M_r$$

Sequence Distribution Mass Balances

g = 1

$$\frac{dL_1^*}{dt} = k_{i1}[R^*][A] \qquad R^* + A \xrightarrow{ki1} L_1^*$$

$$- k_{p1}[A][L_1^*] - k_{p2}[B][L_1^*] \qquad L_1^* + A \xrightarrow{kp1} L_2^* \qquad L_1^* + B \xrightarrow{kp2} O_1$$

$$- k_{r11}[T][L_1^*] + k_{r12}[TL_1^*][R^*] \qquad L_1^* + T \underset{kr12}{\overset{kr11}{\leftrightarrow}} TL_1^* + R^*$$

$$- k_{raft31}[TO_s^*][L_1^*] + k_{raft32}[O_s^*][TL_1^*] \qquad L_1^* + TO_s^* \underset{kraft32}{\overset{kraft31}{\leftrightarrow}} TL_1^* + O_s^*$$

$$+ k_{raft51}[L_s^*][TL_1^*] - k_{raft52}[TL_s^*][L_1^*] \qquad L_s^* + TL_1^* \underset{kraft52}{\overset{kraft51}{\leftrightarrow}} TL_s^* + L_1^*$$

$$- k_{tc1}\left(\sum_{s=0}^{\infty} L_s^*\right)[L_1^*] - k_{td1}\left(\sum_{s=0}^{\infty} L_s^*\right)[L_1^*] \qquad L_1^* + L_s^* \xrightarrow{ktc1} L_1 \qquad L_1^* + L_s^* \xrightarrow{ktd1} L_1$$

$$- k_{tc2}\left(\sum_{s=0}^{\infty} O_s^*\right)[L_1^*] - k_{tc2}\left(\sum_{s=0}^{\infty} O_s^*\right)[L_1^*] \qquad L_1^* + O_s^* \xrightarrow{ktc2} L_1 \qquad L_1^* + O_s^* \xrightarrow{ktd2} L_1$$

$$\frac{dO_1^*}{dt} = k_{i2}[R^*][B] \qquad R^* + A \xrightarrow{ki2} O_1^*$$

$$- k_{p3}[A][O_1^*] - k_{p4}[B][O_1^*] \qquad O_1^* + A \xrightarrow{kp3} L_1^* \qquad O_1^* + B \xrightarrow{kp4} O_2^*$$

$$- k_{r11}[T][O_1^*] + k_{r12}[TO_1^*][R^*] \qquad O_1^* + T \underset{kr12}{\overset{kr11}{\leftrightarrow}} TO_1^* + R^*$$

$$- k_{raft61}[TL_s^*][O_1^*] + k_{raft62}[L_s^*][TO_1^*] \qquad O_1^* + TL_s^* \underset{kraft62}{\overset{kraft61}{\leftrightarrow}} TO_1^* + L_s^*$$

$$+ k_{raft41}[O_s^*][TO_1^*] - k_{raft42}[TO_s^*][O_1^*] \qquad O_s^* + TO_1^* \underset{kraft42}{\overset{kraft41}{\leftrightarrow}} TO_s^* + O_1^*$$

$$-k_{tc4}\left(\sum_{s=0}^{\infty} L_s^*\right)[O_1^*] - k_{td4}\left(\sum_{s=0}^{\infty} L_s^*\right)[O_1^*] \qquad O_1^* + L_s^* \xrightarrow{ktc4} O_1 \qquad O_1^* + L_s^* \xrightarrow{ktd4} O_1$$

$$-k_{tc3}\left(\sum_{s=0}^{\infty} O_s^*\right)[O_1^*] - k_{td3}\left(\sum_{s=0}^{\infty} O_s^*\right)[O_1^*] \qquad O_1^* + O_s^* \xrightarrow{ktc3} O_1 \qquad O_1^* + O_s^* \xrightarrow{ktd3} O_1$$

g > 1

$$\frac{dL_g^*}{dt} = -k_{p1}[A][L_g^*] - k_{p2}[B][L_g^*] \qquad L_g^* + A \xrightarrow{kp1} L_{g+1}^* \qquad L_g^* + B \xrightarrow{kp2} O_1$$

$$+k_{p5}[A][L_{g-1}^*] \qquad L_{g-1}^* + A \xrightarrow{kp5} L_g^*$$

$$-k_{r11}[T][L_g^*] + k_{r12}[TL_g^*][R^*] \qquad L_g^* + T \underset{kr12}{\overset{kr11}{\leftrightarrow}} TL_g^* + R^*$$

$$-k_{raft31}[TO_s^*][L_g^*] + k_{raft32}[O_s^*][TL_g^*] \qquad L_g^* + TO_s^* \underset{kraft32}{\overset{kraft31}{\leftrightarrow}} TL_g^* + O_s^*$$

$$+k_{raft51}[L_s^*][TL_g^*] - k_{raft52}[TL_s^*][L_g^*] \qquad L_s^* + TL_g^* \underset{kraft52}{\overset{kraft51}{\leftrightarrow}} TL_s^* + L_g^*$$

$$-k_{tc1}\left(\sum_{s=0}^{\infty} L_s^*\right)[L_g^*] - k_{td1}\left(\sum_{s=0}^{\infty} L_s^*\right)[L_g^*] \qquad L_g^* + L_s^* \xrightarrow{ktc1} L_g \qquad L_g^* + L_s^* \xrightarrow{ktd1} L_g$$

$$-k_{tc2}\left(\sum_{s=0}^{\infty} O_s^*\right)[L_g^*] - k_{tc2}\left(\sum_{s=0}^{\infty} O_s^*\right)[L_g^*] \qquad L_g^* + O_s^* \xrightarrow{ktc2} L_g \qquad L_g^* + O_s^* \xrightarrow{ktd2} L_g$$

$$\frac{dO_g^*}{dt} = -k_{p3}[A][O_g^*] - k_{p4}[B][O_g^*] \qquad O_g^* + A \xrightarrow{kp3} L_1^* \quad O_g^* + B \xrightarrow{kp4} O_{g+1}^*$$

$$+k_{p8}[B][O_{g-1}^*] \qquad O_{g-1}^* + B \xrightarrow{kp8} O_g^*$$

$$-k_{r11}[T][O_g^*] + k_{r12}[TO_g^*][R^*] \qquad O_g^* + T \underset{kr12}{\overset{kr11}{\leftrightarrow}} TO_g^* + R^*$$

$$-k_{raft61}[TL_s^*][O_g^*] + k_{raft62}[L_s^*][TO_g^*] \qquad O_g^* + TL_s^* \underset{kraft62}{\overset{kraft61}{\leftrightarrow}} TO_g^* + L_s^*$$

$+ k_{raft41}[O_s^*]\,[TO^*_g] - k_{raft42}[TO_s^*][O^*_g]$ $\quad O^*_s + TO^*_g \underset{kraft42}{\overset{kraft41}{\leftrightarrow}} TO^*_s + O^*_g$

$-k_{tc4}\left(\sum_{s=0}^{\infty} L_s^*\right)[O_g^*] - k_{td4}\left(\sum_{s=0}^{\infty} L_s^*\right)[O_g^*]$ $\quad O_g^* + L_s^* \xrightarrow{ktc4} O_g$ $\quad O_g^* + L_s^* \xrightarrow{ktd4} O_g$

$-k_{tc3}\left(\sum_{s=0}^{\infty} O_s^*\right)[O_g^*] - k_{td3}\left(\sum_{s=0}^{\infty} O_s^*\right)[O_g^*]$ $\quad O_g^* + O_s^* \xrightarrow{ktc3} O_g$ $\quad O_g^* + O_s^* \xrightarrow{ktd3} O_g$

$\frac{dL_1^*}{dt} + \frac{dL_g^*}{dt} = k_{i1}[R^*][A]$ $\quad R^* + A \xrightarrow{ki1} L_1^*$

$-k_{p1}[A]\,[L_g^*] - k_{p2}[B]\,[L_g^*]$ $\quad L_g^* + A \xrightarrow{kp1} L_{g+1}^*$ $\quad L_g^* + B \xrightarrow{kp2} O_1$

$+ k_{p5}[A]\,[L_{g-1}^*]$ $\quad L_{g-1}^* + A \xrightarrow{kp5} L_g^*$

$-k_{r11}[T]\,[L_g^*] + k_{r12}[TL_g^*][R^*]$ $\quad L_g^* + T \underset{kr12}{\overset{kr11}{\leftrightarrow}} TL^*_g + R^*$

$-k_{raft31}[TO^*_s]\,[L_g^*] + k_{raft32}[O^*_s]\,[TL_g^*]$ $\quad L^*_g + TO^*_s \underset{kraft32}{\overset{kraft31}{\leftrightarrow}} TL^*_g + O^*_s$

$+ k_{raft51}[L_s^*]\,[TL^*_g] - k_{raft52}[TL_s^*]\,[L^*_g]$ $\quad L^*_s + TL^*_g \underset{kraft52}{\overset{kraft51}{\leftrightarrow}} TL^*_s + L^*_g$

$-k_{tc1}\left(\sum_{s=0}^{\infty} L_s^*\right)[L_g^*] - k_{td1}\left(\sum_{s=0}^{\infty} L_s^*\right)[L_g^*]$ $\quad L_g^* + L^*_s \xrightarrow{ktc1} L_g$ $\quad L_g^* + L^*_s \xrightarrow{ktd1} L_g$

$-k_{tc2}\left(\sum_{s=0}^{\infty} O_s^*\right)[L_g^*] - k_{tc2}\left(\sum_{s=0}^{\infty} O_s^*\right)[L_g^*]$ $\quad L_g^* + O^*_s \xrightarrow{ktc2} L_g$ $\quad L_g^* + O^*_s \xrightarrow{ktd2} L_g$

$\frac{dO_1^*}{dt} + \frac{dO_g^*}{dt} = k_{i2}[R^*][B]$ $\quad R^* + A \xrightarrow{ki2} O_1^*$

$-k_{p3}[A]\,[O_g^*] - k_{p4}[B]\,[O_g^*]$ $\quad O_g^* + A \xrightarrow{kp3} L_1^*$ $\quad O_g^* + B \xrightarrow{kp4} O_{g+1}^*$

$+ k_{p8}[B]\,[O_{g-1}^*]$ $\quad O_{g-1}^* + B \xrightarrow{kp8} O_g^*$

$$- k_{r11}[T]\,[O_g^*] + k_{r12}[TO_g^*][R^*] \qquad O_g^* + T \underset{kr12}{\overset{kr11}{\leftrightarrow}} TO^*_g + R^*$$

$$- k_{raft61}[TL^*_s]\,[O_g^*] + k_{raft62}\,[L^*_s]\,[TO_g^*] \qquad O^*_g + TL^*_s \underset{kraft62}{\overset{kraft61}{\leftrightarrow}} TO^*_g + L^*_s$$

$$+ k_{raft41}[O_s^*]\,[TO^*_g] - k_{raft42}[TO_s^*]\,[O^*_g] \qquad O^*_s + TO^*_g \underset{kraft42}{\overset{kraft41}{\leftrightarrow}} TO^*_s + O^*_g$$

$$- k_{tc4}\left(\sum_{s=0}^{\infty} L_s^*\right)[O_g^*] - k_{td4}\left(\sum_{s=0}^{\infty} L_s^*\right)[O_g^*] \qquad O_g^* + L_s^* \xrightarrow{ktc4} O_g \qquad O_g^* + L_s^* \xrightarrow{ktd4} O_g$$

$$- k_{tc3}\left(\sum_{s=0}^{\infty} O_s^*\right)[O_g^*] - k_{td3}\left(\sum_{s=0}^{\infty} O_s^*\right)[O_g^*] \qquad O_g^* + O_s^* \xrightarrow{ktc3} O_g \qquad O_g^* + O_s^* \xrightarrow{ktd3} O_g$$

$$\frac{dTL_g^*}{dt} = k_{r11}[T]\,[L_g^*] - k_{r12}[TL_g^*][R^*] \qquad L_g^* + T \underset{kr12}{\overset{kr11}{\leftrightarrow}} TL^*_g + R^*$$

$$+ k_{raft31}[TO^*_s]\,[L_g^*] - k_{raft32}[TL_g^*][O^*_s] \qquad L^*_g + TO^*_s \underset{kraft32}{\overset{kraft31}{\leftrightarrow}} TL^*_g + O^*_s$$

$$- k_{raft51}[TL^*_g]\,[L_s^*] + k_{raft52}[TL_s^*][L^*_g] \qquad L^*_s + TL^*_g \underset{kraft52}{\overset{kraft51}{\leftrightarrow}} TL^*_s + L^*_g$$

$$\frac{dTO_g^*}{dt} = k_{r11}[T]\,[O_g^*] - k_{r12}[TO_g^*][R^*] \qquad O_g^* + T \underset{kr12}{\overset{kr11}{\leftrightarrow}} TO^*_g + R^*$$

$$+ k_{raft61}[TL^*_s]\,[O_g^*] - k_{raft62}[TO_g^*][L^*_s] \qquad O^*_g + TL^*_s \underset{kraft62}{\overset{kraft61}{\leftrightarrow}} TO^*_g + L^*_s$$

$$- k_{raft41}[TO^*_g]\,[O_s^*] + k_{raft42}[TO_s^*][O^*_g] \qquad O^*_s + TO^*_g \underset{kraft42}{\overset{kraft41}{\leftrightarrow}} TO^*_s + O^*_g$$

Internal Sequence

$$\frac{dL_g}{dt} = k_{p2}\,[B]\,[L_g^*] \qquad L^*_g + B \xrightarrow{kp2} L_g$$

$$-k_{tc1}\left(\sum_{s=0}^{\infty} L_s^*\right)[L_g^*] - k_{td1}\left(\sum_{s=0}^{\infty} L_s^*\right)[L_g^*] \qquad L_g^* + L^*_s \xrightarrow{ktc1} L_g \qquad L_g^* + L^*_s \xrightarrow{ktd1} L_g$$

$$-k_{tc2}\left(\sum_{s=0}^{\infty} O_s^*\right)[L_g^*] - k_{tc2}\left(\sum_{s=0}^{\infty} O_s^*\right)[L_g^*] \qquad L_g^* + O^*_s \xrightarrow{ktc2} L_g \qquad L_g^* + O^*_s \xrightarrow{ktd2} L_g$$

$$\frac{dO_g}{dt} = k_{p3}\,[A]\,[O_g^*] \qquad O^*_g + A \xrightarrow{kp3} O_g$$

$$-k_{tc4}\left(\sum_{s=0}^{\infty} L_s^*\right)[O_g^*] - k_{td4}\left(\sum_{s=0}^{\infty} L_s^*\right)[O_g^*] \qquad O_g^* + L_s^* \xrightarrow{ktc4} O_g \qquad O_g^* + L_s^* \xrightarrow{ktd4} O_g$$

$$-k_{tc3}\left(\sum_{s=0}^{\infty} O_s^*\right)[O_g^*] - k_{td3}\left(\sum_{s=0}^{\infty} O_s^*\right)[O_g^*] \qquad O_g^* + O_s^* \xrightarrow{ktc3} O_g \qquad O_g^* + O_s^* \xrightarrow{ktd3} O_g$$

MATLAB CODE

The code is available upon request to Dr. Joseph Schork.

Bibliography

1. Braunecker, Wade A. and Krzysztof Matyjaszewski, *Controlled/living radical polymerization: Features, developments, and perspectives.* Progress in Polymer Science, 2007. **32**(1): p. 93-146.
2. Feldermann, Achim, Andrew Ah Toy, Hong Phan, Martina H. Stenzel, Thomas P. Davis, and Christopher Barner-Kowollik, *Reversible addition fragmentation chain transfer copolymerization: influence of the RAFT process on the copolymer composition.* Polymer, 2004. **45**(12): p. 3997-4007.
3. Szwarc, M., */`Living/' Polymers.* Nature, 1956. **178**(4543): p. 1168-1169.
4. Butte, Alessandro, Giuseppe Storti, and Massimo Morbidelli, *Kinetics of "living" free radical polymerization.* Chemical Engineering Science, 1999. **54**(15-16): p. 3225-3231.
5. Goto, Atsushi and Takeshi Fukuda, *Kinetics of living radical polymerization.* Progress in Polymer Science, 2004. **29**(4): p. 329-385.
6. Solomon DH, Rizzardo E, Cacioli P, European Patent Application EP 135280, 1985.
7. Georges MK, Moffat KA, Veregin RPN, Kazmaier PM, Hamer GK, Polym Mater Sci Eng, 1993. **69**(305).
8. Schork, F. Joseph, Yingwu Luo, Wilfred Smulders,James P. Russum,Alessandro Butté ,Kevin Fontenot, *Miniemulstion Polymerization.* Polymer Particles, Advances in Polymer Science, 2005: p. 129-256.
9. Wang, Jin-Shan and Krzysztof Matyjaszewski, *Controlled/"living" radical polymerization. atom transfer radical polymerization in the presence of transition-metal complexes.* J. Am. Chem. Soc., 1995. **117**(20): p. 5614-5615.
10. Patten, Timothy E., Jianhui Xia, Teresa Abernathy, and Krzysztof Matyjaszewski, *Polymers with Very Low Polydispersities from Atom Transfer Radical Polymerization.* Science, 1996. **272**(5263): p. 866-868.
11. Wang, Jin-Shan and Krzysztof Matyjaszewski, *Controlled/"Living" Radical Polymerization. Halogen Atom Transfer Radical Polymerization Promoted by a Cu(I)/Cu(II) Redox Process.* Macromolecules, 1995. **28**(23): p. 7901-7910.
12. Uegaki, H., Y. Kotani, M. Kamigaito, and M. Sawamoto, *NiBr2(Pn-Bu3)2-Mediated Living Radical Polymerization of Methacrylates and Acrylates and Their Block or Random Copolymerizations1.* Macromolecules, 1998. **31**(20): p. 6756-6761.
13. Kato, Mitsuru, Masami Kamigaito, Mitsuo Sawamoto, and Toshinobu Higashimura, *Polymerization of Methyl Methacrylate with the Carbon Tetrachloride/Dichlorotris-(triphenylphosphine)ruthenium(II)/Methylaluminum Bis(2,6-di-tert-butylphenoxide) Initiating System: Possibility of Living Radical Polymerization.* Macromolecules, 1995. **28**(5): p. 1721-1723.
14. Kotani, Y., M. Kato, M. Kamigaito, and M. Sawamoto, *Living Radical Polymerization of Alkyl Methacrylates with Ruthenium Complex and Synthesis of Their Block Copolymers1.* Macromolecules, 1996. **29**(22): p. 6979-6982.

15. Moineau, G., M. Minet, Ph Dubois, Ph Teyssie, T. Senninger, and R. Jerome, *Controlled Radical Polymerization of (Meth)acrylates by ATRP with NiBr2(PPh3)2 as Catalyst.* Macromolecules, 1999. **32**(1): p. 27-35.
16. Lecomte, Ph, I. Drapier, Ph Dubois, Ph Teyssie, and R. Jerome, *Controlled Radical Polymerization of Methyl Methacrylate in the Presence of Palladium Acetate, Triphenylphosphine, and Carbon Tetrachloride.* Macromolecules, 1997. **30**(24): p. 7631-7633.
17. Brandts, Jim A. M., Patrick van de Geijn, Ernst E. van Faassen, Jaap Boersma, and Gerard van Koten, *Controlled radical polymerization of styrene in the presence of lithium molybdate(V) complexes and benzylic halides.* Journal of Organometallic Chemistry, 1999. **584**(2): p. 246-253.
18. Krstina, Julia, Graeme Moad, Ezio Rizzardo, Catherine L. Winzor, Charles T. Berge, and Michael Fryd, *Narrow Polydispersity Block Copolymers by Free-Radical Polymerization in the Presence of Macromonomers.* Macromolecules, 1995. **28**(15): p. 5381-5385.
19. Le TP, Moad G, Rizzardo E, Thang SH, PCT Interational Application, 1998: p. 40.
20. Rizzardo E, Thang SH, Moad G, PCT Interational Application, 1999: p. 88.
21. Goto, A., K. Sato, Y. Tsujii, T. Fukuda, G. Moad, E. Rizzardo, and S. H. Thang, *Mechanism and Kinetics of RAFT-Based Living Radical Polymerizations of Styrene and Methyl Methacrylate.* Macromolecules, 2001. **34**(3): p. 402-408.
22. Wang, Aileen R., Shiping Zhu, *Modeling the reversible addition-fragmentation transfer polymerization process.* Journal of Polymer Science Part A: Polymer Chemistry, 2003. **41**(11): p. 1553-1566.
23. Wang, Rui, Yingwu Luo Bogeng Li Xiaoying Sun Shiping Zhu, *Design and Control of Copolymer Composition Distribution in Living Radical Polymerization Using Semi-Batch Feeding Policies: A Model Simulation.* Macromolecular Theory and Simulations, 2006. **15**(4): p. 356-368.
24. Mayo, Frank R. and Frederick M. Lewis, *Copolymerization. I. A Basis for Comparing the Behavior of Monomers in Copolymerization; The Copolymerization of Styrene and Methyl Methacrylate.* J. Am. Chem. Soc., 1944. **66**(9): p. 1594-1601.
25. Ray, W. Harmon, *On the Mathematical Modeling of Polymerization Reactors.* Polymer Reviews, 1972. **8**(1): p. 1 - 56.
26. Lefebvre, M. D., C. M. Dettmer, R. L. McSwain, C. Xu, J. R. Davila, R. J. Composto, S. T. Nguyen, and K. R. Shull, *Effect of Sequence Distribution on Copolymer Interfacial Activity.* Macromolecules, 2005. **38**(25): p. 10494-10502.
27. Lin, Chen-Lung, Wan-Chun Chen, Shiao-Wei Kuo, and Feng-Chih Chang, *Sequence distribution affect the phase behavior and hydrogen bonding strength in blends of poly(vinylphenol-co-methyl methacrylate) with poly(ethylene oxide).* Polymer, 2006. **47**(10): p. 3436-3447.
28. Chernikova, Elena, Polina Terpugova, Chuong Bui, and Bernadette Charleux, *Effect of comonomer composition on the controlled free-radical*

copolymerization of styrene and maleic anhydride by reversible addition-fragmentation chain transfer (RAFT). Polymer, 2003. **44**(15): p. 4101-4107.
29. Theis, Alexander, Achim Feldermann, Nathalie Charton, Thomas P. Davis, Martina H. Stenzel, and Christopher Barner-Kowollik, *Living free radical polymerization (RAFT) of dodecyl acrylate: Chain length dependent termination, mid-chain radicals and monomer reaction order.* Polymer, 2005. **46**(18): p. 6797-6809.
30. McLeary, J. B., F. M. Calitz, J. M. McKenzie, M. P. Tonge, R. D. Sanderson, and B. Klumperman, *Beyond Inhibition: A ¹H NMR Investigation of the Early Kinetics of RAFT-Mediated Polymerization with the Same Initiating and Leaving Groups.* Macromolecules, 2004. **37**(7): p. 2383-2394.
31. Prescott, S. W., *Chain-Length Dependence in Living/Controlled Free-Radical Polymerizations: Physical Manifestation and Monte Carlo Simulation of Reversible Transfer Agents.* Macromolecules, 2003. **36**(25): p. 9608-9621.
32. Chernikova, E., A. Morozov, E. Leonova, E. Garina, V. Golubev, C. Bui, and B. Charleux, *Controlled Free-Radical Polymerization of n-Butyl Acrylate by Reversible Addition-Fragmentation Chain Transfer in the Presence of tert-Butyl Dithiobenzoate. A Kinetic Study.* Macromolecules, 2004. **37**(17): p. 6329-6339.
33. Perrier, S., C. Barner-Kowollik, J. F. Quinn, P. Vana, and T. P. Davis, *Origin of Inhibition Effects in the Reversible Addition Fragmentation Chain Transfer (RAFT) Polymerization of Methyl Acrylate.* Macromolecules, 2002. **35**(22): p. 8300-8306.
34. Calitz, F. M., J. B. McLeary, J. M. McKenzie, M. P. Tonge, B. Klumperman, and R. D. Sanderson, *Evidence for Termination of Intermediate Radical Species in RAFT-Mediated Polymerization.* Macromolecules, 2003. **36**(26): p. 9687-9690.
35. Monteiro, M. J. and H. de Brouwer, *Intermediate Radical Termination as the Mechanism for Retardation in Reversible Addition-Fragmentation Chain Transfer Polymerization.* Macromolecules, 2001. **34**(3): p. 349-352.
36. Barner-Kowollik, Christopher, Michelle L. Coote Thomas P. Davis Leo Radom Philipp Vana, *The reversible addition-fragmentation chain transfer process and the strength and limitations of modeling: Comment on ?the magnitude of the fragmentation rate coefficient?* Journal of Polymer Science Part A: Polymer Chemistry, 2003. **41**(18): p. 2828-2832.
37. Wang, Aileen R., Shiping Zhu Yungwan Kwak Atsushi Goto Takeshi Fukuda Michael S. Monteiro, *A difference of six orders of magnitude: A reply to ?the magnitude of the fragmentation rate coefficient?* Journal of Polymer Science Part A: Polymer Chemistry, 2003. **41**(18): p. 2833-2839.
38. McLeary, James B. Matthew P. Tonge Bert Klumperman, *A Mechanistic Interpretation of Initialization Processes in RAFT-Mediated Polymerization.* Macromolecular Rapid Communications, 2006. **27**(15): p. 1233-1240.
39. Charleux, B., J. Nicolas, and O. Guerret, *Theoretical Expression of the Average Activation-Deactivation Equilibrium Constant in Controlled/Living Free-Radical Copolymerization Operating via Reversible Termination.*

Application to a Strongly Improved Control in Nitroxide-Mediated Polymerization of Methyl Methacrylate. Macromolecules, 2005. **38**(13): p. 5485-5492.
40. Pinto, M. A., R. Li, C. D. Immanuel, P. A. Lovell, and F. J. Schork, *Effects of Reversible Addition Fragmentation Transfer (RAFT) on Branching in Vinyl Acetate Bulk Polymerization.* Ind. Eng. Chem. Res., 2008. **47**(3): p. 509-523.
41. Schork, F. Joseph, Wilfred Smulders, *On the molecular weight distribution polydispersity of continuous living-radical polymerization.* Journal of Applied Polymer Science, 2004. **92**(1): p. 539-542.
42. Smulders, Wilfred W., Christopher W. Jones F. Joseph Schork, *Continuous RAFT miniemulsion polymerization of styrene in a train of CSTRs.* AIChE Journal, 2005. **51**(3): p. 1009-1021.
43. Smagala, Thomas G. and Benjamin J. McCoy, *Population balance modeling of polymer branching and hyperbranching.* Chemical Engineering Science, 2006. **61**(1): p. 3-17.